Integrated Photonic Quantum Walks in Complex Lattice Structures

Dissertation

zur Erlangung des akademischen Grades
doctor rerum naturalium (Dr. rer. nat.)

vorgelegt dem Rat der Physikalisch-Astronomischen Fakultät
der Friedrich-Schiller-Universität Jena

von Dipl. Phys. Markus Gräfe,
geboren am 26.11.1986 in Reichenbach im Vogtland

1. Gutachter: Prof. Dr. Alexander Szameit (Friedrich-Schiller-Universität Jena)

2. Gutachter: Prof. Dr. Philip Walther (Universität Wien)

3. Gutachter: Prof. Dr. Antonio Ancona (CNR-IFN Sede Secondaria di Bari)

Tag der Disputation: 13. Juni 2017

»Our job in physics is to see things simply, to understand a great many complicated phenomena in a unified way, in terms of a few simple principles.«

Steven Weinberg (Nobel Lecture 1979)

Contents

1. Introduction **7**

2. Fundamentals **13**

2.1. Integrated photonic discrete-time quantum walks 13

2.2. Continuous-time quantum walks in waveguide arrays 19

2.3. Two-photon quantum walks 21

2.4. Direct laser inscription of waveguides 26

2.5. Generating and detecting indistinguishable photon pairs 28

3. High-order single-photon W-states on-chip **33**

3.1. Generation of single-photon W-states 34

3.2. Multi-partite entanglement verification 39

3.3. Random number generation 42

4. Multiplexed detection for characterization of light states **45**

4.1. Photon number statistics vs. click statistics 46

4.2. Divide and conquer: characterization of light states by on-off detectors 50

5. Bloch oscillations of N00N states **55**

5.1. On-chip generation of path-entangled states with tailored symmetry 56

5.2. Two-photon N00N states in a photonic Bloch oscillator lattices . . 62

6. Conclusion & Outlook **73**

A. Coherent states **79**

References **81**

Acknowledgements **93**

Zusammenfassung **95**

List of own publications

Conference Contributions

Ehrenwörtliche Erklärung

Lebenslauf

CHAPTER 1

Introduction

What is the connection between the who-to-follow suggestion offered by Twitter [1], the paths of foraging animals [2], and fixational eye movements [3]? It is the statistical concept of random walks [4], the underlying principle to mathematically describe these phenomena. First introduced by Pearson in 1905 in a challenge to the readers of *Nature* seeking for a solution for the following problem [5]:

> »A man starts from a point O and walks l yards in a straight line; he then turns through any angle whatever and walks another l yards in a second straight line. He repeats this process n times. I require the probability that after these n stretches he is at a distance between r and $r + \mathrm{d}r$ from his starting point, O.«

His request was promptly answered by Lord Rayleigh, who had already discovered a solution for very large n [6]. Surprisingly, in the same year Einstein and Smoluchowski also indirectly answered Pearson's question using the very concept of random walks to explain the phenomenon of Brownian motion [7–9].

Both revealed that the path of a molecule suspended in a liquid follows a random trajectory as a result of repeated collisions with molecules of the liquid. These seminal works not only described diffusive transport, but rather catalyzed the widespread acceptance that matter is indeed composed of atoms and molecules. Hence, the experimental verification of this theory by Perrin was recognized with the Nobel Prize in physics in 1926 [10]. Nowadays random walks are a ubiquitous tool for all kinds of processes ranging from estimating the size of the world wide web [11] to population statistics of species [12], and even the fluctuation of dollar bills throughout the united states [13]. One of the simplest and yet very fundamental random walk system is the Galton board, where a classical walker hops to one *or* another side with ideally one-half probability at each step. This arrangement demonstrates the diffusive propagation of the walker through the board: The variance of its localization distribution increases linearly with the number of steps, and the characteristic Gaussian distribution emerges at the output.

A fundamentally different situation arises when introducing a quantum particle as walker. Founded on the Copenhagen interpretation of quantum mechanics, the coherent spreading of the particle's wavefunction can be understood as the hopping of the quantum walker at each step to one *and* another side with a certain probability amplitude, and thus, inhabiting superposition states [14,15]. This inevitably leads to interference between the different possible paths, and yields a ballistic spreading where the variance grows quadratically with the number of steps. While Feynman and Hibbs were the first to elaborate on this concept in 1965 [16]; it took almost 30 years until it was reconsidered by Aharanov, Davidovich and Zagury, who coined the terminology of a quantum (random) walk (QW) [14]. This revival of the field continues to this day, where QWs are the fundamental concept behind Grover's superior search algorithm [17] and are in principle capable of universal quantum computing [18,19]. Notably, billions of years before scientists discovered the potential of QWs for quantum technology, the blind watchmaker of evolution harnessed this mechanism for the most essential biochemical process found in nature: discrete QW-like energy transport in photosynthesis enabled the development of all higher forms

of life on this planet [20,21].

In principle, one can distinguish two different types of QWs: discrete-time QWs like the quantum version of the Galton board, where the walker evolves in discrete steps determined by random events, and continuous-time QWs, in which a time-independent lattice Hamiltonian governs the walker's dynamics. As such the latter describes the coherent evolution of quantum states on a lattice. For both regimes one finds numerous physical systems for implementation such as ultra-cold atoms and Bose-Einstein condensates [22, 23], trapped ions [24, 25], nuclear magnetic resonance spin-chains [26, 27], superconducting quantum interference devices [28], optical fiber loops [29], bulk-optical beam displacers [30], or photonic waveguide networks [31,32].

Photons offer the unique combination of large coherence length required for multi-path interference and insensitivity to environmental influences. Moreover, they benefit from an extremely long lifetime and their linearity. Another advantage are additional degrees of freedom such as polarization and wavelength that comes along with the use of single photons. Furthermore, photon generation and detection is well-established and relies on cost-efficient and resource saving approaches.

The implementation of photonic QWs in waveguide lattices on-chip brings the advantages of high robustness, ultra-stability, and miniaturization. The necessary interaction between waveguides is provided by their evanescent light fields leaking into the neighboring guides, thus, allowing a tunneling from site to site. Consequently, both QW regimes, discrete- and continuous-time, can be implemented in a straightforward fashion. Naturally, the evolution is not in time but along the longitudinal waveguide coordinate. Hence, a three-dimensional (3D) fabrication technique like the direct laser-writing allows to observe photonic QWs in two spatial dimensions [33,34].

It is worth mentioning that based on the coherent evolution, single-photon QW dynamics are indistinguishable from the evolution of classical laser light when intensities are substituted by probabilities. However, this drastically changes when considering two or more indistinguishable photons. In such multi-photon

QWs the coherent addition of the probability amplitudes leads to multi-photon interference and genuinely non-classical correlations as it was first proposed in 2009 and experimentally verified shortly afterwards [35, 36]. Since then, integrated photonic QWs have been employed in various scenarios including Shor's factorization [37], on-chip quantum teleportation [38], or demonstrating Boson sampling [39–41]. Clearly, this fledgling field holds great promise for future discoveries and innovative applications.

Similarly, photonic waveguide lattices are an ideal systems for quantum simulation. Along these lines, the evolution of quantum correlations through complex lattices and the emergence, survival or destruction of entanglement is of crucial interest. Moreover, it is challenging to investigate whether even single-photon QWs can offer physics beyond classical coherent laser light evolution and whether multi-path interference is a necessary ingredient to this end? Furthermore, despite the technical endeavor to fully miniaturize quantum optical settings by integration of single-photon sources and detectors on-chip, till now, interfacing between source, operative chip and detection unit is necessary. This naturally limits the performance of all applications. In addition to this, one may ask: Is there any difference between the photons counted by the detectors and the photons actually leaving the sample? And if so, does this difference matter?

In this thesis new applications of QWs of single photons are discovered and explored. To this end discrete waveguide networks are utilized to synthesize exotic states and harness them for genuine random number generation. Further, by means of a multiplexing structure it is demonstrated how to exploit photon click statistics provided by standard on-off detectors instead of the notoriously inaccessible photon number statistics for evaluating the non-classicality of any unknown light state, in particular as outcome of a QW. Aside from that, special interest is paid in the experimental investigation of two-photon correlations of path-entangled photon pairs in Bloch oscillator lattices revealing striking effects of the wavefunction's symmetry.

The fundamentals in integrated photonic discrete- and continuous-time QWs of single- and two-photon states as well as the waveguide fabrication technique and the experimental settings are the elements of Chapter 2 that is followed by three chapters presenting the achievements of this work. Chapter 3 demonstrates the capability to generate single-photon W-states of high-order by use of a discrete-time QW network. The multipartite entanglement is verified and a new application in the form of random number generation is presented. The application of the same QW network as a tool to deploy click statistics provided by *non*-number resolving single-photon detectors to distinct classical and quantum light is the topic of Chapter 4. In Chapter 5 the investigations are extended to the QW dynamics of entangled photon pairs and how their correlations evolve within a Bloch oscillator lattice. The thesis is concluded by a brief summary of the obtained results and an outlook on promising further developments of this field.

CHAPTER 2

Fundamentals

This chapter is opened by a brief introduction to the theory of discrete- and continuous-time QWs for one and two particles. These approaches are discussed within the framework of integrated optics. Afterwards the fabrication process of the underlying waveguide structures is explained. This is followed by a description of the single photon and photon pair generation scheme as well as the detection setting.

2.1. Integrated photonic discrete-time quantum walks

Like its classical counterpart, a discrete-time QW is governed by the stepwise evolution of the walker based on the outcome of a random event. Albeit such events can have a manifold of simultaneous outcomes the most fundamental case is tossing a two-sided "quantum coin", which will be considered in the following. Such a quantum coin can be implemented by any physical systems

endowed with a binary degree of freedom, like spin-1/2, polarization, or a two-level atomic system. Each of the two possibilities represents one side of the quantum coin and corresponds to the basis states. Considering a quantum walker moving on a one-dimensional lattice the quantum coin has the basis state vectors $|\mathrm{L}\rangle$ causing the walker to move one step to the left and $|\mathrm{R}\rangle$ letting the walker move one step to the right. In general both states appear with the probability amplitudes α_L and α_R, respectively ($|\alpha_\mathrm{L}|^2 + |\alpha_\mathrm{R}|^2 = 1$). After tossing the coin a classical walker will move one step to the left *or* right with the probabilities $|\alpha_\mathrm{L}|^2$, respectively $|\alpha_\mathrm{R}|^2$. In stark contrast, a quantum walker will move simultaneously in sense of superposition to the left *and* right, ending in the state $|\psi\rangle = \alpha_\mathrm{L}|\mathrm{L}\rangle + \alpha_\mathrm{R}|\mathrm{R}\rangle$. Flipping the coin multiple times will cause the walker to evolve into a complex superposition of states depending on how the probability amplitudes of subsequent steps interfere with each other.

This concept can be implemented in the context of integrated photonics by employing 50:50 directional couplers (DCs) and single photons as quantum walkers (see Fig. 2.1). Such couplers are essentially formed by two evanescently coupled waveguides (see Sec. 2.2). They are the integrated version of a beam splitter and work as such in both the classical and the quantum regime. Realizing different splitting ratios is possible by different coupling strengths or interaction lengths and would correspond to an unbalanced coin. It is important to note that in this physical system the time coordinate is replaced by a spatial (z-) propagation coordinate of the photons. The evolution of quantized light in waveguides is conveniently described by means of the photonic creation and annihilation operators $\hat{a}_q^\dagger$ and $\hat{a}_q$, respectively, which literally create, respectively destroy a photon in waveguide mode q* [42, 43]. In a DC their evolution is governed by the Heisenberg equation [35, 42–45] (see also Sec. 2.2):

$$\frac{\mathrm{d}}{\mathrm{d}z}\begin{pmatrix}\hat{a}_1^\dagger(z)\\ \hat{a}_2^\dagger(z)\end{pmatrix} = \mathrm{i}\begin{pmatrix}\beta_1 & \kappa\\ \kappa & \beta_2\end{pmatrix}\begin{pmatrix}\hat{a}_1^\dagger(z)\\ \hat{a}_2^\dagger(z)\end{pmatrix}. \tag{2.1}$$

*Here, the word "mode" refers to the spatial modes in the waveguide lattice bound to each of the (single-mode) guides and should not be confused with any eigenmodes of the lattice. Hence, $\hat{a}_q^\dagger$ creates a photon in waveguide number q.

Here, β_1 and β_2 represent the propagation constants of the waveguides and κ is the evanescent coupling coefficient between the two spatial modes. Assuming identical waveguides with $\beta_1 = \beta_2 = \beta$ one can directly integrate Eq. 2.1 and obtain the transformation of the input to the output modes

$$\begin{pmatrix} \hat{a}_1^\dagger(z) \\ \hat{a}_2^\dagger(z) \end{pmatrix} = \begin{pmatrix} \cos(\kappa z) & \mathrm{i}\sin(\kappa z) \\ \mathrm{i}\sin(\kappa z) & \cos(\kappa z) \end{pmatrix} \begin{pmatrix} \hat{a}_1^\dagger(0) \\ \hat{a}_2^\dagger(0) \end{pmatrix}, \tag{2.2}$$

where the global phase factor $\mathrm{e}^{\mathrm{i}\beta z}$ has been omitted. By choosing a propagation distance of $z = \pi/4\kappa$ a 50:50 splitting behavior will be achieved and Eq. 2.2 becomes

$$\begin{pmatrix} \hat{a}_1^\dagger \\ \hat{a}_2^\dagger \end{pmatrix}_{\text{out}} = \frac{1}{\sqrt{2}} \begin{pmatrix} 1 & \mathrm{i} \\ \mathrm{i} & 1 \end{pmatrix} \begin{pmatrix} \hat{a}_1^\dagger \\ \hat{a}_2^\dagger \end{pmatrix}_{\text{in}}, \tag{2.3}$$

where the arguments of the creation operators were replaced by the labels "in" and "out". As long as it is unambiguous the arguments will stay omitted throughout the following. Consequently, exciting port 1 of a (50:50) DC by a single photon will transform the input state to (see Fig. 2.1)

$$\hat{a}_1^\dagger |0\rangle \xrightarrow{\text{DC}} \frac{1}{\sqrt{2}} \left(\hat{a}_1^\dagger + \mathrm{i}\, \hat{a}_2^\dagger \right) |0\rangle, \tag{2.4}$$

which is a two-mode path-entangled state. It means that a single photon will emerge from either port of the DC with exactly the same probability of $1/2$ and that there is a phase difference of $\pi/2$ between the two output channels. Typically, the waveguide, in which the light couples over, is referred to as reflection channel whereas the other one is called transmission channel. This notation is in agreement with the commonly used one from bulk beam splitters, where the reflection channel carries a $\pi/2$ phase shift, too.

One can now realize discrete-time QWs of single photons by utilizing 50:50 DCs as a fundamental building block and cascading several stages to a mesh as illustrated in Fig. 2.2. Such grids can be understood as the quantum optical version of a Galton board. For illustration of the operation principle of these photonic

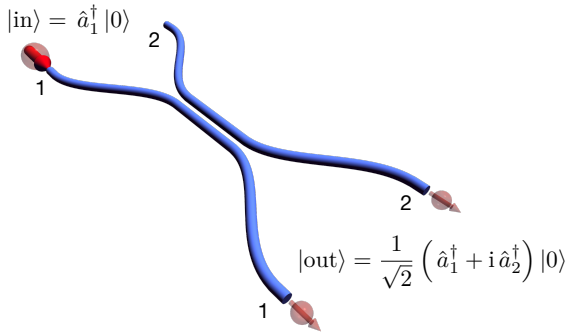

Figure 2.1.: Sketch of an integrated photonic waveguide coupler known as directional coupler (DC) with 50:50 splitting ratio. The device transforms the input state $|\text{in}\rangle$ into the path-entangled output state $|\text{out}\rangle$. Figure taken from [32].

based QWs a large system of 31 splitting stages (corresponding to $\binom{31+1}{2} = 496$ DCs) will be considered. Sending a single photon into one of the input guides, after two steps the input state $|\psi_1\rangle = \hat{a}_1^\dagger |0\rangle$ transforms to

$$\hat{a}_1^\dagger |0\rangle \overset{\text{two steps}}{\longrightarrow} \frac{1}{2} \left(\mathrm{i}\, \hat{a}_1^\dagger + \hat{a}_2^\dagger + \mathrm{i}\, \hat{a}_3^\dagger - \hat{a}_4^\dagger \right) |0\rangle \ . \tag{2.5}$$

Thus, the walker is coherently distributed among the four modes with equal probability amplitudes but again a phase shift of $\pi/2$ between them. So far, the walker has not experienced any quantum interference. This changes already when going one step further. After the third step the walker will be in the state (see Fig. 2.2)

$$\hat{a}_1^\dagger |0\rangle \overset{\text{three steps}}{\longrightarrow} \frac{1}{2\sqrt{2}} \left(-\hat{a}_1^\dagger + \mathrm{i}\, \hat{a}_2^\dagger + 2\mathrm{i}\, \hat{a}_4^\dagger - \hat{a}_5^\dagger - \mathrm{i}\, \hat{a}_6^\dagger \right) |0\rangle \ . \tag{2.6}$$

Evidently, the probability to find a photon in channel three vanishes due to destructive interference. Letting the photon evolve over the whole system such quantum interference forms an intricate probability pattern as shown in Fig. 2.3(a). In strong contrast to its classical counterpart, the Galton board with a binomial probability distribution centered around the initial site, the photon can be most likely found on the opposite side with respect to the input port.

Turning now towards another input state $|\psi_2\rangle = \frac{1}{\sqrt{2}} (\hat{a}_1^\dagger + \hat{a}_2^\dagger) |0\rangle$, where a single

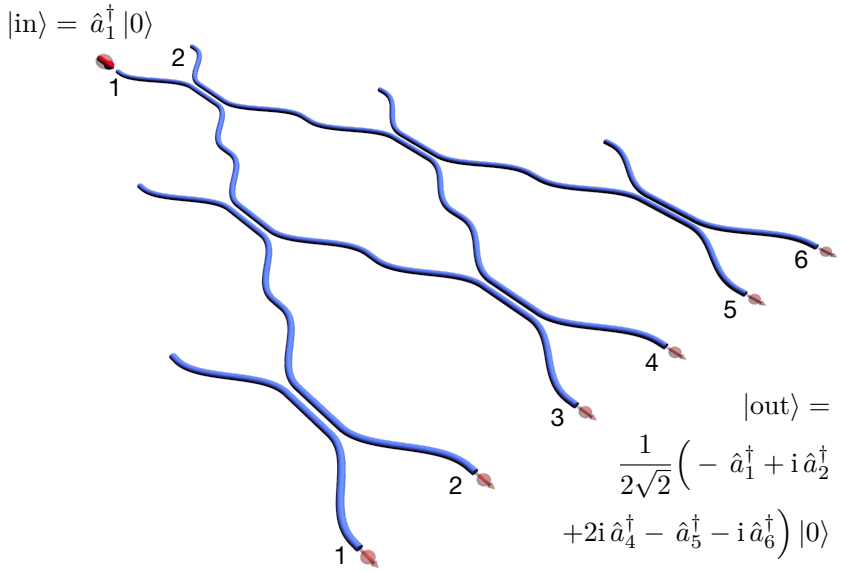

Figure 2.2.: Mesh of directional couplers as the first three steps of a discrete-time QW of a single photon. Figure taken from [32].

photon enters simultaneously at the two input channels. Since this state forms a superposition of modes it is possible to analyze the walker dynamics separately for each state and add the corresponding probability amplitudes. Accordingly, the results obtained in the previous case can be used to calculate the state of the walker after two and three steps

$$\frac{1}{\sqrt{2}}\left(\hat{a}_1^\dagger + \hat{a}_2^\dagger\right)|0\rangle \overset{\text{two steps}}{\longrightarrow} \frac{1+\mathrm{i}}{2\sqrt{2}}\left(\mathrm{i}\,\hat{a}_1^\dagger + \hat{a}_2^\dagger + \hat{a}_3^\dagger + \mathrm{i}\,\hat{a}_4^\dagger\right)|0\rangle\ , \tag{2.7}$$

and

$$\frac{1}{\sqrt{2}}\left(\hat{a}_1^\dagger + \hat{a}_2^\dagger\right)|0\rangle \overset{\text{three steps}}{\longrightarrow} \frac{1+\mathrm{i}}{4}\left(-\hat{a}_1^\dagger + \mathrm{i}\hat{a}_2^\dagger + (1+\mathrm{i})(\hat{a}_3^\dagger + \hat{a}_4^\dagger) + \mathrm{i}\hat{a}_5^\dagger - \hat{a}_6^\dagger\right)|0\rangle\ , \tag{2.8}$$

respectively. Clearly, the mirror-symmetry of the input state must be conserved during evolution through the symmetric structure. Therefore, the output state exhibits a highly symmetric probability distribution as clearly indicated by the two counter-propagating ballistic lobes in Fig. 2.3(b).

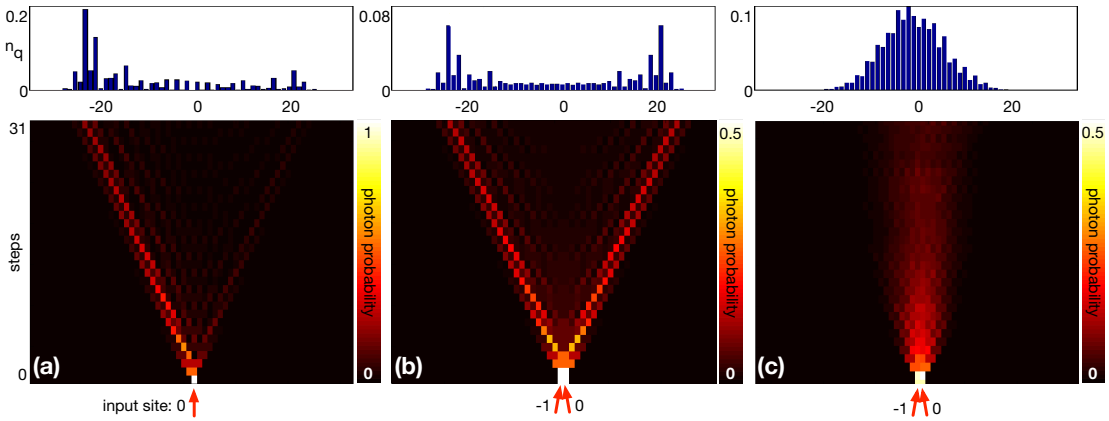

Figure 2.3.: Single-photon evolution in discrete-time quantum walk of 31 steps provided by a mesh of directional couplers. (a) Evolution of a single photon launched into one (right) input channel of a directional coupler. (b) Evolution of a single photon prepared in a superposition of states exciting both input ports of the first directional coupler. (c) Same input state as in (b) but now the mesh is endowed with random phase shifts after each DC. This dynamical disorder leads to a diffusive evolution of the walker, corresponding to the classical random walk. The top row presents the corresponding probability distributions to find a photon at the output. Figure reproduced from [32].

Intriguingly, integrated photonic architectures are also capable of demonstrating the transition from a QW towards a classical random walk. In general, dephasing and decoherence cause a quantum walker to become a classical walker. In fact, such dephasing will prevent the ballistic spreading, rather inducing a binomial (in limit of many lattice sites Gaussian) diffusive evolution that is directly linked to classical random walks. A possible implementation is the introduction of random phase shifts after each DC. Fig. 2.3(c) shows the average probability evolution of the input state $|\psi_2\rangle$ evolving in a system of 31 splitting steps, where the phases after each DC are randomly changed. They obey a uniform distribution with values from $[0, \pi]$ and the results are averaged over 20,000 realizations. By comparing Figs. 2.3(b) & (c) one can directly obverse the impact of dephasing as it washes out the two ballistic lobes and leads to a binomial probability distribution centered around the origin.

Instead of having discrete splitting structures, one can "melt" together the interaction regions of subsequent DCs resulting in a continuous coupling during propagation. Such kind of lattices allow the investigation of all kinds of lat-

tice dynamics in the tight-binding regime. For instance, the time evolution of a certain wavefunction in a tight-binding modeled solid state is equivalent to the photon state propagation along the longitudinal lattice direction. As a result waveguide arrays are well-suited to simulate continuous-time quantum transport phenomena. It will be discussed in the next section.

2.2. Continuous-time quantum walks in waveguide arrays

The step from a discrete system towards a continuous one can be conveniently understood in the field of integrated photonics. In contrast to the former section, single photons as quantum walkers are now propagating through continuously evanescently coupled waveguide arrays [46, 47] instead of discrete DC stages. To create this kind of photonic lattices single-mode waveguides are placed next to each other in such a way that their evanescent mode fields overlap with the neighboring guides. In consequence, every guide becomes coupled with its neighbors. Thus, light can tunnel from one site to another during propagation through the lattice. The Hamiltonian of a system of M evanescently coupled single-mode waveguides is

$$\hat{H} = \hbar \sum_{m=1}^{M} \left\{ \beta_m \, \hat{a}_m^\dagger \, \hat{a}_m + \sum_{m \neq j=1}^{M} \kappa_{j,m} \, \hat{a}_j^\dagger \, \hat{a}_m \right\} . \tag{2.9}$$

In agreement with the description of the DCs β_m is the propagation constant of guide m and $\kappa_{j,m} = \kappa_{m,j}$ is the hopping rate between channels j and m. Most settings imply coupling to adjacent sites only ($j = m \pm 1$). However, for the sake of generality the coupling between all waveguides will be included in the following description. Note that losses, which are equal in all guides contribute only via a global loss factor to the Hamiltonian. If the individual waveguides exhibit different losses the particular loss rates manifest themselves in the imaginary parts of the then complex propagation constants. Naturally, the evolution of such a system is more intricate due to its non-Hermiticity [48]. Since all systems

throughout this thesis are Hermitian this can be disregarded. In accordance with the previous section, the system dynamics is described by the Heisenberg equation of motion for the photonic creation operators [35,36]:

$$\frac{\mathrm{d}\,\hat{a}_q^\dagger}{\mathrm{d}z} = -\frac{\mathrm{i}}{\hbar}\left[\hat{a}_q^\dagger(z),\,\hat{H}\right] = \mathrm{i}\left(\beta_q\,\hat{a}_q^\dagger(z) + \sum_{q\neq j=1}^{M}\kappa_{q,j}\,\hat{a}_j^\dagger(z)\right). \tag{2.10}$$

It is important to emphasize again, that the time evolution coordinate is replaced by the spatial propagation coordinate z. The special case of $M = 2$ results in Eq. 2.1 for describing the DC. Formal integration of Eq. 2.10 yields

$$\hat{a}_q^\dagger(z) = \sum_{j=1}^{M} U_{q,j}(z)\,\hat{a}_j^\dagger(0)\,, \tag{2.11}$$

where $U_{q,j}(z) = \left(\mathrm{e}^{\frac{\mathrm{i}}{\hbar}\hat{H}z}\right)_{q,j}$ are the matrix elements of the unitary linear z-evolution operator $\hat{U}$. Intuitively, $U_{q,j}(z)$ can be understood as the probability amplitude to find a photon after the propagation length z at lattice site q when initially injected into site j. This becomes even more clear when considering the average photon number (or photon density) $n_q(z) = \langle\psi(0)|\,\hat{a}_q^\dagger(z)\,\hat{a}_q(z)|\psi(0)\rangle$ in channel q. For the input state $|\psi(0)\rangle = \hat{a}_m^\dagger(0)\,|0\rangle$, meaning that one photon is launched into waveguide m, the average photon number becomes $n_q(z) = |U_{q,m}(z)|^2$. Hence, it directly corresponds to the classical intensity distribution when injecting laser light into channel m as one can see in Fig. 2.4. Since, the distribution of the output probability amplitudes for a certain excitation (at site m) is given by the system's impulse response, $U_{q,m}(z)$ can also be understood as Green's function of the system.

For the special case of a uniform waveguide lattice one has $\beta_q = \beta$ and adjacent coupling with $\kappa_{q,q\pm1} = \kappa$. Sending now a single photon into site j one can find that the probability amplitude at site q is analytically described by [35,46,49]

$$U_{q,j}(z) = \mathrm{i}^{q-j}\mathrm{e}^{\mathrm{i}\beta z}J_{q-j}(2\kappa z)\,, \tag{2.12}$$

where J_{q-j} is a Bessel function of the first kind and order $(q-j)$.

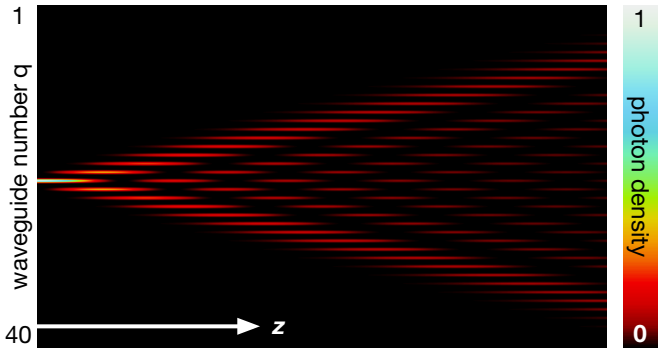

Figure 2.4.: Evolution of the average photon number n_q when sending a single photon into the central channel of an array of 40 identical evanescently coupled waveguides. The photon density evolves likewise as the intensity when shining in laser light of the same wavelength. The typical two ballistic lobes can be clearly seen.

Evidently, the complexity of single-photon QWs increases with the number lattice sites, that is, the number of spatial modes. For further enhancement one needs to harness all feasible degrees of freedom, like spin, polarization, frequency, or orbital angular momentum. Obviously, high-dimensional degrees of freedom are of advantage. Interestingly, in contrast to single photons, multiphoton quantum states inherently live in a high-dimensional Hilbert space, which will be the content of the next section.

2.3. Two-photon quantum walks

If one considers two indistinguishable photons propagating through a waveguide array of M ports, the corresponding wave function will have $M(M+1)/2$ elements. More generally, N photons traversing waveguide lattices of M channels inhabit a Hilbert space of $\binom{N+M-1}{N}$ dimensions.

In the following this fact is illustrated for QWs in integrated photonic lattices performed by quantum states of two photons, which feature non-classical dynamics. Beginning with the simplest case one can study a system of two indistinguishable photons, one launched into each waveguide of a DC described by

Eq. 2.2. It is readily clear that the input and output modes are related according to

$$\begin{aligned}\hat{a}_1^\dagger \hat{a}_2^\dagger |0\rangle \xrightarrow{\text{DC}} & \left[\cos(\kappa z)\, \hat{a}_1^\dagger + \mathrm{i}\sin(\kappa z)\, \hat{a}_2^\dagger\right] \times \left[\mathrm{i}\sin(\kappa z)\, \hat{a}_1^\dagger + \cos(\kappa z)\, \hat{a}_2^\dagger\right] |0\rangle \\ & = \mathrm{i}\cos(\kappa z)\sin(\kappa z) \left[\left(\hat{a}_1^\dagger\right)^2 + \left(\hat{a}_2^\dagger\right)^2\right] |0\rangle \\ & + \left[\cos^2(\kappa z) - \sin^2(\kappa z)\right] \hat{a}_1^\dagger \hat{a}_2^\dagger |0\rangle \ . \end{aligned} \tag{2.13}$$

As a result a DC will transform a separable two-photon state into a superposition of four states. Moreover, for 50:50 splitting at exactly $z = \pi/4\kappa$, the amplitudes $\cos^2(\kappa z)$ and $\sin^2(\kappa z)$ interfere destructively. Therefore, the output state becomes

$$\hat{a}_1^\dagger \hat{a}_2^\dagger |0\rangle \xrightarrow{\text{DC}} \frac{\mathrm{i}}{2} \left[\left(\hat{a}_1^\dagger\right)^2 + \left(\hat{a}_2^\dagger\right)^2\right] |0\rangle \ . \tag{2.14}$$

It describes the physical situation where both photons emerge together from one of the output ports with the same probability of $1/2$ and never occur in different ones. This phenomenon is called Hong-Ou-Mandel (HOM) effect and was first observed in 1987 at a bulk beam splitter [50, 51]. The photon behavior is also referred to as (spatial) photon *bunching*. In fact, the two indistinguishable photons at the input are transformed into a path-entangled pair as a direct result of the quantum (path) interference of the two-photon amplitudes. The generalization of such type of states are called N00N state $\sim \left[\left(\hat{a}_1^\dagger\right)^N + \left(\hat{a}_2^\dagger\right)^N\right] |0\rangle$ or in other notation $\sim |N0\rangle + |0N\rangle$, meaning that N photons are in either of the two modes.

The observation of the HOM effect can be performed by coincidence measurements of the photons. In doing so, photon detectors placed at the output of a 50:50 DC should register simultaneous photon counts as long as both channels are slightly delayed, meaning that there is no temporal overlap of both photons, hence, they are distinguishable in their arrival time. In contrast, there are *no* coincidences for zero delay. An experimentally obtained example is shown in Fig. 2.5, where a time delay between the two input ports was tuned via a translation stage and joint clicks were registered. Clearly, the two-photon count

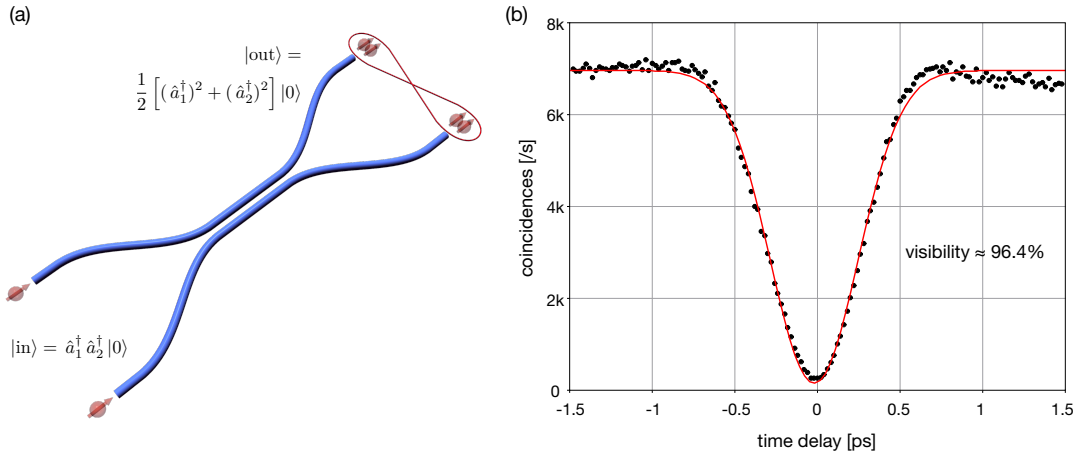

Figure 2.5.: Hong-Ou-Mandel effect in integrated optics. (a) Two photons enter a 50:50 directional coupler and become entangled. (b) Their coincidences at the output are measured. By tuning their (in)distinguishability via their time delay the typical "HOM-dip" is observed, here with a visibility (drop in coincidences per average value) of approximately 96.4%.

rate drops down to a minimum for zero time delay and the "HOM-dip" is visible. In general, such coincidence measurements between channels q and r can be described analytically via the fourth-order correlation function (also known as intensity correlation function or two-photon rate)

$$\Gamma_{q,r}(z) = \langle \psi(0)|\, \hat{a}_q^\dagger(z)\, \hat{a}_r^\dagger(z)\, \hat{a}_r(z)\, \hat{a}_q(z) |\psi(0)\rangle \ . \tag{2.15}$$

It is strongly related to the probability distribution $P_{q,r} = \frac{\Gamma_{q,r}}{1+\delta_{q,r}}$ of detecting simultaneously one photon at site q and the other at r. Additionally, for Hermitian systems the relation $n_q = \sum_r \Gamma_{q,r}$ holds. For the particular case of the 50:50 DC (interaction length $z = \pi/4\kappa$) q and r run from 1 to 2. The probability amplitudes $U_{q,j}$ are given by Eq. 2.3. Hence, sending two photons in the separable state $|\psi(0)\rangle = \hat{a}_1^\dagger(0)\, \hat{a}_2^\dagger(0)\, |0\rangle$ into a 50:50 DC, one finds for the correlation between the outputs $\Gamma_{1,2} = \Gamma_{2,1} = 0$, meaning that there will be no simultaneous photon detection events.

This approach can be easily extended to multi-port waveguide systems. By launching two photons prepared in a separable state into sites m and n of an

array, the corresponding correlation matrix is determined by Eqs. 2.11 & 2.15:

$$\Gamma_{q,r}(z) = |U_{q,m}(z)U_{r,n}(z) + U_{q,n}(z)U_{r,m}(z)|^2\,, \tag{2.16}$$

where $U_{q,m}$ is still the probability amplitude to find a photon at channel q when originally started in m. Fig. 2.6(b) shows the correlation matrix of this particular case with $m = 20$ and $n = 21$ in a lattice of 40 waveguides. The map exhibits clear bunching behavior of the photons, since they tend to occupy the same sites. Another interesting scenario arises when changing the input state to the path-entangled state $\frac{1}{2}\left[\left(\hat{a}_m^\dagger\right)^2 + \mathrm{e}^{\mathrm{i}\theta}\left(\hat{a}_n^\dagger\right)^2\right]|0\rangle$. In that case the correlation function can be written as

$$\Gamma_{q,r}(z) = |U_{q,m}(z)U_{r,m}(z) + \mathrm{e}^{-\mathrm{i}\theta}U_{q,n}(z)U_{r,n}(z)|^2\,. \tag{2.17}$$

An exemplary pattern can be observed in Fig. 2.6(c) for $\theta = 0$. In this scenario both photons are almost never found together in the same channel. Thus, they show anti-bunching. As comparison, considering two *distinguishable* photons the correlations are given by

$$\Gamma_{q,r}(z) = |U_{q,m}(z)U_{r,n}(z)|^2 + |U_{q,n}(z)U_{r,m}(z)|^2\,, \tag{2.18}$$

which leads to the four characteristic peaks in Fig. 2.6(d) and directly corresponds to the intensity correlation when injecting coherent laser light in the input ports m and n. Interestingly, although the correlation matrices for the three input states are very different the average photon number is identical for all of them since it is determined by the incoherent sum of the single site excitations: $n_q(z) = |U_{q,m}(z)|^2 + |U_{q,n}(z)|^2$ (see Fig. 2.6(a)). Therefore, it carries no signature of photon indistinguishability, which is in strong contrast to the correlations exhibited by indistinguishable photons. As it turns out, elements of the correlation matrix from distinguishable photons obey the Bell-like inequality $\sqrt{\Gamma_{q,q}\Gamma_{r,r}} - \Gamma_{q,r} < 0$ [52]. It becomes more stringent for phase averaged

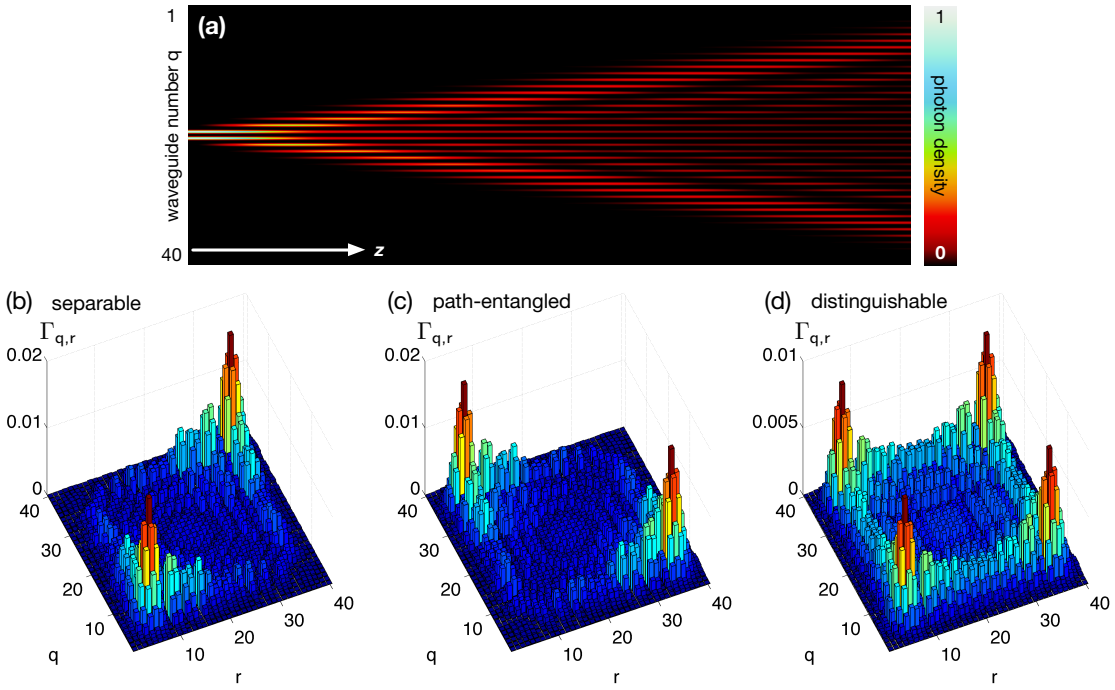

Figure 2.6.: Quantum correlations in a homogeneously coupled array of 40 waveguides with centered two-photon excitation at sites $m = 20$ and $n = 21$. (a) Evolution of the average photon number $n_q(z)$. (b) Correlation map $\Gamma_{q,r}$ at the output for the case of both photons being indistinguishable and prepared in a separable state and (c) both photons enter in the path-entangled state $\frac{1}{2}\left[(\hat{a}_{20}^{\dagger})^2 + (\hat{a}_{21}^{\dagger})^2\right]|0\rangle$. The patterns clearly show photon bunching and anti-bunching, respectively. (d) Correlation map for two distinguishable photons exhibiting the characteristic four peaks.

coherent laser light [35,36]:

$$V_{q,r} = \frac{1}{3}\sqrt{\Gamma_{q,q}\Gamma_{r,r}} - \Gamma_{q,r} < 0\,. \tag{2.19}$$

This case represents the upper limit that can be achieved without multi-photon interference. Hence, violations with $V_{q,r} > 0$ are an unambiguous sign of non-classical two-photon correlations caused by interference of indistinguishable photons. It is worth to mention that a HOM-dip visibility of 50% corresponds to $V_{1,2} = \frac{1}{3}\sqrt{\frac{3}{4}\times\frac{3}{4}} - \frac{1}{4} = 0$, which is exactly the reason the visibility needs to be above this limit to ensure non-classical behavior of indistinguishable photons.

Summarized, when two or more indistinguishable photons propagate in waveguide arrays, even without any interaction, their intensity correlations shed light onto the non-classical QW behavior.

As outlined in the Introduction (Chapter 1) QWs in waveguide lattices with intricate geometry will be an important subject of investigation in this work. Such systems are for instance implemented via detunings in the propagation constants of the waveguides or by exploiting the second transverse spatial dimension. These strategies necessitate a method that is capable of fabricating waveguides in a 3D geometry and further allows a precise control of their parameters. The direct inscription by ultrashort laser pulses into glass is such a technique and will be explained in the next section.

2.4. Direct laser inscription of waveguides

Fused silica glass is a commonly used material for integrated photonics. Since its energy gap between its valance and conduction band is much larger than the energy of a photon from the visible or near-infrared range it is transparent to these wavelengths. Furthermore, it matches the refractive index of standard optical fibers [53, 54]. However, its transparency to a broad wavelength range makes it also hard to optically process the material. Nonetheless in the focal volume of ultrashort laser pulses very high light intensities are reached causing both field ionization and multi-photon absorption processes. As a result, the refractive index of the material can be permanently increased in the focal region, thus, building a light guiding core [33]. By moving the glass sample through the laser focus one can literally write waveguides as sketched in Fig. 2.7. Due to the fact that the modification occurs in the focal volume only, one can move the glass sample on 3D trajectories, and thus, create 3D waveguide structures. This is one of the main advantages of this technique compared to lithographic approaches. However, due to the refractive index increase in the order of $\sim 10^{-3}$ the bending radii of curved waveguides are limited to the centimeter regime. In straight guides losses are in the range of $0.3 \ldots 0.9\,\mathrm{dB/cm}$. Moreover, the prop-

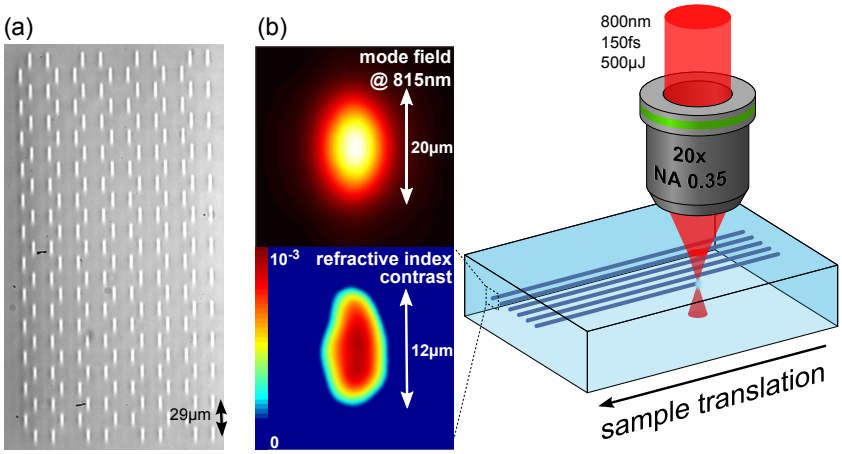

Figure 2.7.: Direct laser writing. (a) Microscopic image of a cross section of a laser written waveguide structure. (b) Waveguides are inscribed by focusing ultrashort laser pulses into a glass sample and moving the sample through the incident beam. This causes a permanent refractive index increase in the focal volume. Accordingly, light is guided in these structures.

agation constant β of a waveguide (defined by it refractive index increase) can be precisely controlled by both the inscription power and velocity. The slower the inscription the more energy is deposited per unit length and the larger is β and vice versa. Even though this has also an impact on the coupling strengths the effect is much weaker than the influence on the propagation constant and can be neglected in most cases. As mentioned in Sec. 2.2 the coupling is governed by the evanescent field overlap of the waveguide modes with adjacent guides. Accordingly it depends on the distance between two waveguides in an exponential manner.

All waveguide structures in this work were inscribed either in *Corning® HPFS® 7980 Standard Grade* or in *Corning® HPFS® 7980 ArF Grade* by a laser system from *Coherent* (pump *Verdi V18*, oscillator *Mira 900*, and amplifier *RegA 9000*). This laser systems provides ultrashort pulses at 800 nm center wavelength and 100 kHz repetition rate with a pulse length of approximately 150 fs at full width half maximum (FWHM) and pulse energy of roughly 500 nJ. The laser pulses are focused using a 20×-objective (numerical aperture $NA = 0.35$). The samples are moved by a three-axis translation stage (*Aerotech ANT130*) with a maximum processing length of 15 cm at an inscription velocity typically between

60 mm/min and 100 mm/min. This way, waveguides with an elliptical cross section of around 2 µm × 10 µm are created as it is exemplary shown in Fig. 2.7(a). Hence, the waveguide modes are elliptical as well as one can see from Fig. 2.7(b). Their size depends on the refractive index increase defined by the amount of energy deposited per unit length and varies from 10 µm × 15 µm to 15 µm × 20 µm (FWHM) at 815 nm. To send in and couple out single photons, fiber arrays are used (see also next Sec. 2.5). In these structures eight fibers are horizontally aligned with a core-to-core distance of 127 µm. This necessitates a fan-in and fan-out structure before and after the actual waveguide interaction region, since considerable coupling dynamics take place in the range of 18…35 µm (corresponding to coupling strengths $\kappa \approx 1.5 \ldots 0.1\,\mathrm{cm}^{-1}$). In addition, the fiber array at the input side consists of polarization-maintaining single-mode fibers, which typically feature a mode size of approximately 5.5 µm × 5.5 µm. In consequence, the mode fields of the inscribed waveguides have to be as small as possible to minimize in- and out-coupling losses with the fiber arrays. As it turned out recently, inscribing the first and last few millimeters of a waveguide multiple times can shrink the modes sizes down to approximately 6 µm × 12 µm at the input and output facet. In doing so the power is linearly changed along this few millimeters from slightly beneath the threshold, where glass modification just starts, to a value above, but below the inscription power used in the main part of the waveguide lattice.

In summary, direct laser-writing with ultrashort laser pulses allows the fabrication of sophisticated waveguide structures. The fast single step prototyping together with highly controllable parameters and especially the 3D capability renders it to a convenient technique for quantum photonic applications.

2.5. Generating and detecting indistinguishable photon pairs

As shown in the previous section, waveguides in glass samples are ideally suited to study photonic QWs. In addition, expedient photon sources as well as

reliable single photon detectors are required to perform such experiments.

The most commonly used source for indistinguishable or entangled photon pairs* is based on spontaneous parametric down-conversion (SPDC) [55, 56]. In this process, a pump photon at frequency ω_p is (down-)converted into signal and idler photons at frequencies ω_s and ω_i, respectively in a second-order non-linear crystal. Naturally, the conservation of both energy ($\omega_p = \omega_s + \omega_i$) and momentum (phase matching of the wavevectors $\mathbf{k}_p = \mathbf{k}_s + \mathbf{k}_i$) holds. Consequently, the down-converted photon pair is emitted in certain directions only, determined by the photon frequencies, refractive indices, polarization, and the orientation of the non-linear crystal. For homogeneous crystals, one distinguishes between two types of phase matching. While for type-I phase matching signal and idler photons are identically polarized (and orthogonally to the pump photon) they show orthogonal polarization for the type-II phase matching [55]. The photon source used for all experiments presented in this work is based on type-I phase matching condition. As indicated in Fig. 2.8(a) signal and idler photons have a certain angle θ_s and θ_i, respectively, with respect to the pump direction. Depending on the angle Θ between the pump beam and the optical axis orientation in the crystal, the generation of identical photon pairs is possible by a degenerate type-I phase matched SPDC (same polarization for signal and idler). That means, $\omega_s = \omega_i = \omega_p/2$ and thus, $\theta_s = \theta_i$. As a result, photons emerge pairwise on opposite sites of a cone with an opening angle of $2\theta_s$ (see Fig. 2.8(b)). By collecting photons at two opposite points of the cone, pairs of indistinguishable photons can be used for further investigations. This way, different photon states can be prepared from these pairs to provide various QW input states.

In the visible and the near-infrared regime single photon detection is conveniently done via silicon avalanche photo diodes. In these semiconductor devices a large voltage is applied against the current transmitting direction of their pn-junction. An incoming photon is absorbed by generating an electron-hole

*SPDC also generates photon states containing multiple pairs. However, their probability in the continuous pump regime and in the context of the experimental setting in this work is negligible.

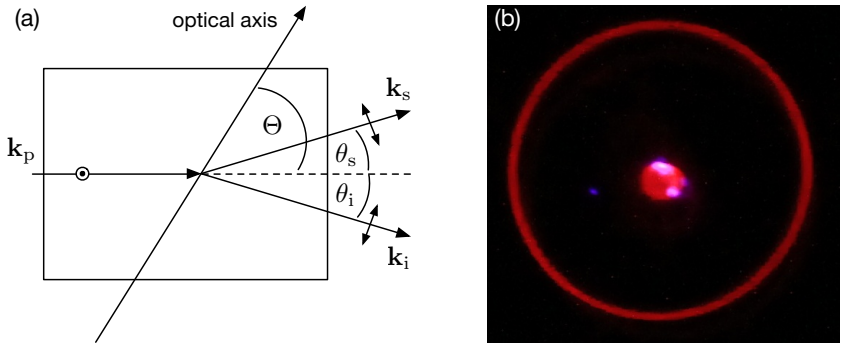

Figure 2.8.: Spontaneous parametric down conversion in a non-linear crystal. (a) A pump photon with wavevector $\mathbf{k}_\mathrm{p}$ is converted into signal and idler photon with $\mathbf{k}_\mathrm{s}$ and $\mathbf{k}_\mathrm{i}$, respectively. Both photons emerge under a certain angle θ_s and θ_i, respectively. (b) In the degenerate case of $\theta_\mathrm{s} = \theta_\mathrm{i}$ photons leave the crystal in a cone geometry, which can be observed at a certain distance as a ring on a CCD. The bright spot in the middle is the strongly damped pump beam.

pair. Both charge carriers are separated and accelerated so strongly that they generate more carriers by impact ionization. This leads to an avalanche of carriers, which are detected as macroscopic current. Typically their dead time is around a few tens of nanoseconds (the time the detector remains "blind" after a detection event). Naturally, based on their working principle, it is not possible to distinguish whether there have been one, two, or even more photons impinging on the detector within the dead time window. For that reasons such detectors are often called "click" or on-off detectors. In contrast, recently developed superconducting transitions edge sensors (TES) are capable of photon-number resolution [57, 58]. There, an absorbed photon electro-thermally increases the resistance and thus, leads to a decreasing TES current, which is measurable and most importantly proportional to the number of absorbed photons. Evidently, these sophisticated devices with a detection efficiency of almost one offer many new possibilities and advantages but also go hand in hand with some disadvantages: They have a jitter four orders of magnitudes longer than in avalanche photo diodes and a dead time in the range of a few microseconds [59]. Further, the capacity for photon number resolution is limited to a few photons only, since the linear correspondence to the TES current breaks down for larger photon numbers. Additionally, the discrimination between N and $N+1$ photons becomes less efficient for higher photon numbers N. Another drawback is the

cryogenic environment needed for TES, which makes them thoroughly expensive. Therefore, all experimental photon detection in this work was performed via avalanche photo diode based single photon counting modules of type *SPCM CD 3398 H* from *Excelitas*, which operate at room temperature and are commercially available. They offer a detection efficiency above 50%, a dark count rate below 50 counts per second and a dead time of 20 ns.

As it will be demonstrated in Chapter 4 standard on-off detectors are capable of collecting click distributions likewise meaningful as the genuine photon statistics. For that purpose the state of light to be analyzed has to undergo a QW on a tailored multiplexing lattice before impinging on the detectors.

The full setup for QW experiments discussed in this work is depicted in Fig. 2.9. The type I SPDC is driven by a 407.5 nm diode laser (*Coherent OBIS 405*) at 70…100 mW optical power. The non-linear bismuth borate crystal is 1 mm thick and orientated such that signal and idler photons at 815 nm emerge with an opening angle (after refraction at the crystal-air surface) of $2\theta_s = 14.4^\circ$. Since SPDC yields a rather broad spectrum, proper filtering of signal and idler is needed to increase their indistinguishability. This is done by 3 nm bandpass filters (*Semrock 830nm MaxLine®*; allow 815 nm center wavelength under a certain angle). By coupling the photons into polarization maintaining single-mode fibers two opposite points of the photon cone are selected. These fibers can be connected to any of the eight polarization maintaining single-mode fibers of the input fiber array. There, the fibers are directly butt coupled to the waveguides within the glass sample. Hence, the waveguide structures need a fan-in and fan-out structure. In the glass chip the photons undergo a QW in the inscribed waveguide lattice. Note, further state preparation can be either done externally, with e.g. a fiber beam splitter, or on-chip by tailored waveguide structures. At the fan-out side a fiber array of eight multi-mode (not polarization maintaining) fibers is attached and routes out-coming photons to the single photon detectors described above. Using multi-mode fibers at the output side bears the advantage of maximized coupling efficiency, whereas the polarization state of the photons does not need to be maintained at this stage. A 16-channel correlation card (*Becker & Hickel DPC 230*) allows to not only collect the single count

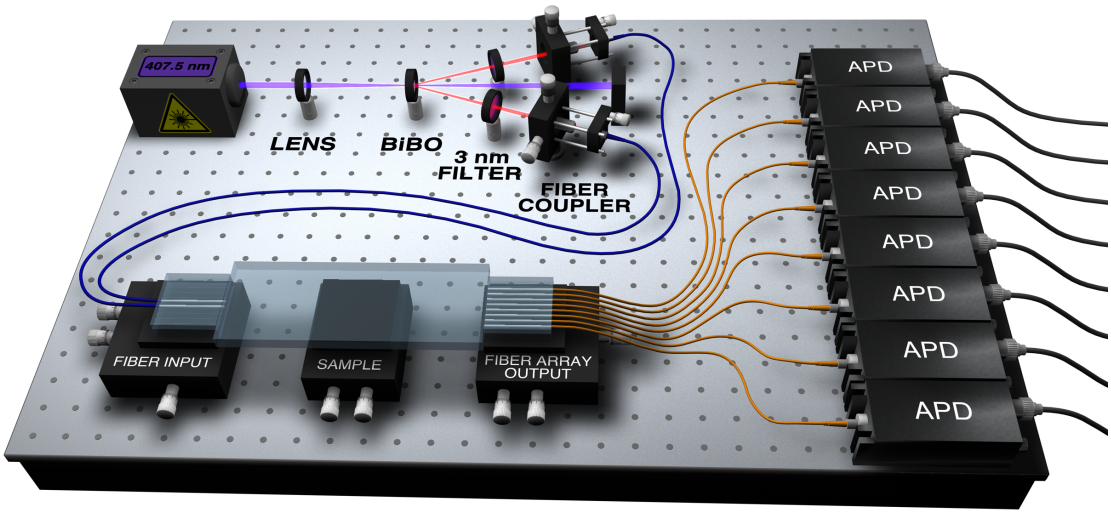

Figure 2.9.: Schematic image of the quantum setup used for measurements presented in this thesis. Optional, one of the blue input fibers can be directly connected to another (ninth) single-photon detector (APD) such that photons from there can trigger the measurements.

rates but also to register joint detector clicks (coincidences) within a minimum time window of 165 ps.

The description of the theoretical concepts as well as the experimental techniques can be partially found in [34] and [32].

CHAPTER 3

High-order single-photon W-states on-chip

As extension of Sec. 2.3 one can consider the entanglement of more than only two physical systems. Such multipartite entanglement plays a key role in a number of counter-intuitive phenomena in quantum mechanics [60–63]. Among the possible types of maximally entangled states are the so-called W-states, which were first introduced as a coherent superposition of three qubit states exhibiting equal probability amplitudes [64]. The entanglement carried by these quantum entities has the remarkable property of being intrinsically robust to decoherence in one of the qubits. This concept can be readily generalized to N qubits. Based on their unique properties, photonic W-states have been proposed as a platform to explore fundamental phenomena linked to the non-locality of single-particle quantum states [65–73]. Photonic W-states of order N means here the situation where a single photon is coherently shared among N

paths or modes [74,75]:

$$\begin{aligned} |\mathrm{W}_N\rangle &= \frac{1}{\sqrt{N}} \sum_{n=1}^{N} \mathrm{e}^{\mathrm{i}\phi_n}\, \hat{a}_n^\dagger\, |0\rangle \\ &= \frac{1}{\sqrt{N}} \left(\mathrm{e}^{\mathrm{i}\phi_1}\, |10\ldots0\rangle + \mathrm{e}^{\mathrm{i}\phi_2}\, |01\ldots0\rangle + \ldots + \mathrm{e}^{\mathrm{i}\phi_N}\, |00\ldots1\rangle \right) , \end{aligned} \tag{3.1}$$

where ϕ_n are arbitrary but fixed relative phases. This intrinsic spatial quantum "parallelism" could be potentially useful in a number of applications ranging from quantum networks to quantum key distribution and communication schemes [75].

To date the preparation of such multipartite entangled states is still a challenging task and has relied on bulk optics [76–79]. This could be an impediment, especially in settings where miniaturization is an issue. Along these lines, two approaches for the efficient generation of singe-photon W-states based on continuous- and discrete-time single-photon QWs are developed and implemented in the first part of this chapter. Subsequently, a verification scheme is presented. The chapter will be closed by introducing a new promising application of W-states, that is, the generation of genuine random numbers.

3.1. Generation of single-photon W-states

The creation of W-states can be realized on the basis of continuous- or discrete-time QWs of single photons in waveguide lattices. The former scheme is predestined for but not limited to odd orders N [80]. At this, single photons are launched into the central waveguide c of a waveguide array of $N = 2c - 1$ identical guides with a tailored coupling distribution. The hopping rates $\kappa_{j,j\pm1}$ are designed such that the probability to find a photon launched at site c is equal for all output channels after a certain propagation length. To elucidate this, one can consider the preparation of a W-state of order $N = 3$ by using a waveguide trimer comprising identical coupling coefficients $\kappa_{1,2} = \kappa_{2,3} = \kappa$. According to

Eqs. 2.10 & 2.11 the Heisenberg equation is given by

$$\frac{\mathrm{d}}{\mathrm{d}z}\begin{pmatrix}\hat{a}_1^\dagger(z)\\ \hat{a}_2^\dagger(z)\\ \hat{a}_3^\dagger(z)\end{pmatrix} = \mathrm{i}\begin{pmatrix}0 & \kappa & 0\\ \kappa & 0 & \kappa\\ 0 & \kappa & 0\end{pmatrix}\begin{pmatrix}\hat{a}_1^\dagger(0)\\ \hat{a}_2^\dagger(0)\\ \hat{a}_3^\dagger(0)\end{pmatrix} \tag{3.2}$$

with the solution

$$\begin{pmatrix}\hat{a}_1^\dagger(z)\\ \hat{a}_2^\dagger(z)\\ \hat{a}_3^\dagger(z)\end{pmatrix} = \begin{pmatrix}\cos^2(\frac{\kappa z}{\sqrt{2}}) & -\frac{\mathrm{i}}{\sqrt{2}}\sin(\sqrt{2}\kappa z) & -\sin^2(\frac{\kappa z}{\sqrt{2}})\\ -\frac{\mathrm{i}}{\sqrt{2}}\sin(\sqrt{2}\kappa z) & \cos^2(\sqrt{2}\kappa z) & -\frac{\mathrm{i}}{\sqrt{2}}\sin(\sqrt{2}\kappa z)\\ -\sin^2(\frac{\kappa z}{\sqrt{2}}) & -\frac{\mathrm{i}}{\sqrt{2}}\sin(\sqrt{2}\kappa z) & \cos^2(\frac{\kappa z}{\sqrt{2}})\end{pmatrix}\begin{pmatrix}\hat{a}_1^\dagger(0)\\ \hat{a}_2^\dagger(0)\\ \hat{a}_3^\dagger(0)\end{pmatrix}. \tag{3.3}$$

Hence, by sending a single photon into the central waveguide the input state $\hat{a}_2^\dagger|0\rangle$ evolves to $|\mathrm{W}_3\rangle = \frac{1}{\sqrt{3}}\left(\mathrm{i}\,\hat{a}_1^\dagger + \hat{a}_2^\dagger + \mathrm{i}\,\hat{a}_3^\dagger\right)|0\rangle$ after the propagation length $z_\mathrm{W} = \arctan\sqrt{2}/\sqrt{2}\kappa$. Thus, the photon is in a coherent superposition with equal probability of $1/3$ to be found in any of the three channels. This is illustrated in Fig. 3.1(a). Going one step further to five guides, the Heisenberg equation becomes

$$\frac{\mathrm{d}}{\mathrm{d}z}\begin{pmatrix}\hat{a}_1^\dagger(z)\\ \hat{a}_2^\dagger(z)\\ \hat{a}_3^\dagger(z)\\ \hat{a}_4^\dagger(z)\\ \hat{a}_5^\dagger(z)\end{pmatrix} = \mathrm{i}\begin{pmatrix}0 & \kappa_1 & 0 & 0 & 0\\ \kappa_1 & 0 & \kappa_2 & 0 & 0\\ 0 & \kappa_2 & 0 & \kappa_2 & 0\\ 0 & 0 & \kappa_2 & 0 & \kappa_1\\ 0 & 0 & 0 & 0 & \kappa_1\end{pmatrix}\begin{pmatrix}\hat{a}_1^\dagger(0)\\ \hat{a}_2^\dagger(0)\\ \hat{a}_3^\dagger(0)\\ \hat{a}_4^\dagger(0)\\ \hat{a}_5^\dagger(0)\end{pmatrix}. \tag{3.4}$$

Here, again symmetric coupling around the central guide is assumed: $\kappa_{1,2} = \kappa_{4,5} = \kappa_1$ and $\kappa_{2,3} = \kappa_{3,4} = \kappa_2$. A simple analytic solution as in the previous case is not possible anymore. However, a straight forward numeric calculation reveals, that for $\kappa_1/\kappa_2 \approx 1.618$ a single photon started in the central guide ($\hat{a}_3^\dagger|0\rangle$) yields the W-state $|\mathrm{W}_5\rangle = \frac{1}{\sqrt{5}}\left(-\hat{a}_1^\dagger + \mathrm{i}\,\hat{a}_2^\dagger + \hat{a}_3^\dagger + \mathrm{i}\,\hat{a}_4^\dagger - \hat{a}_5^\dagger\right)|0\rangle$ at $z_\mathrm{W} \approx 0.861/\kappa_2$, which is displayed in Fig. 3.1(b). In that manner, by engineering the couplings in waveguide arrays one can fabricate various odd ordered W-states. Practically, in direct laser written waveguides one is limited by the

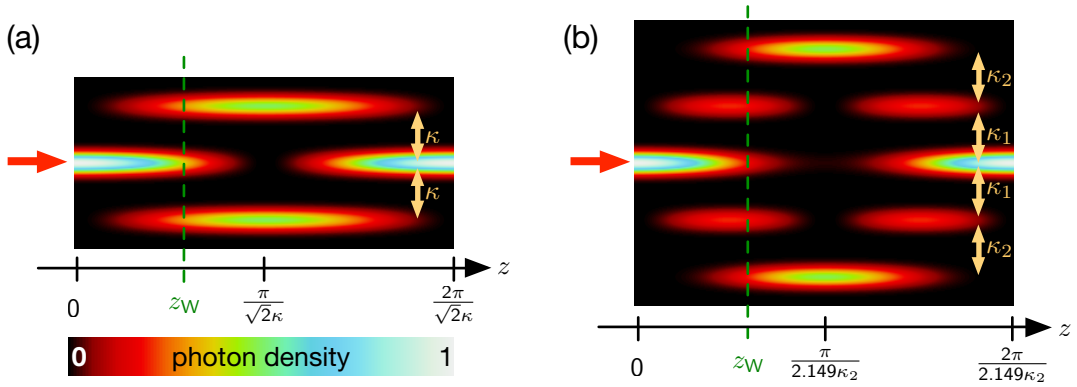

Figure 3.1.: Single-photon evolution in tailored waveguide lattices. (a) Photon density when the central of three waveguides is excited. (b) Same as (a) but with five guides and different coupling strengths κ_1 and κ_2. The propagation distance z_W, at which an equal density distribution is achieved, is marked by a dashed green line.

combination of the waveguide length and their mutual distances, determining the coupling strength. For that reason, a tailored array of $N = 5$ waveguides as shown in Fig. 3.2(a) was experimentally realized. The length of the interaction region was $z_W = 5\,\text{cm}$ and the couplings, respectively the distances, were chosen according to the parameters described above. Single photons, provided by one arm of the SPDC source presented in Sec. 2.5, were sent into the corresponding waveguide structure inscribed into a glass chip. By collecting the output click-statistic one finds a flat probability distribution as presented in Fig. 3.2(c). The probability to detect a photon in one of the five channels is $\overline{P}_{N=5} = 20.0 \pm 0.9$ where the standard deviation is caused by the deviations from a perfectly uniform distribution. Those uncertainties origin on the one hand from fabrication tolerances. In particular the limited precision of the positioning system of approximately 0.2 µm leads to not-perfectly matching coupling constants. On the other hand, the fan-out structure affects the photon probability distribution in a non-uniform way by both slightly different bending losses and non-trivially changing coupling strengths. While the former effect was minimized by sufficient large bending radii the latter one is accounted by a 3D fanning geometry. Bending the waveguides alternating up- and downwards rather rapidly and consecutively bringing them smoothly back in plane

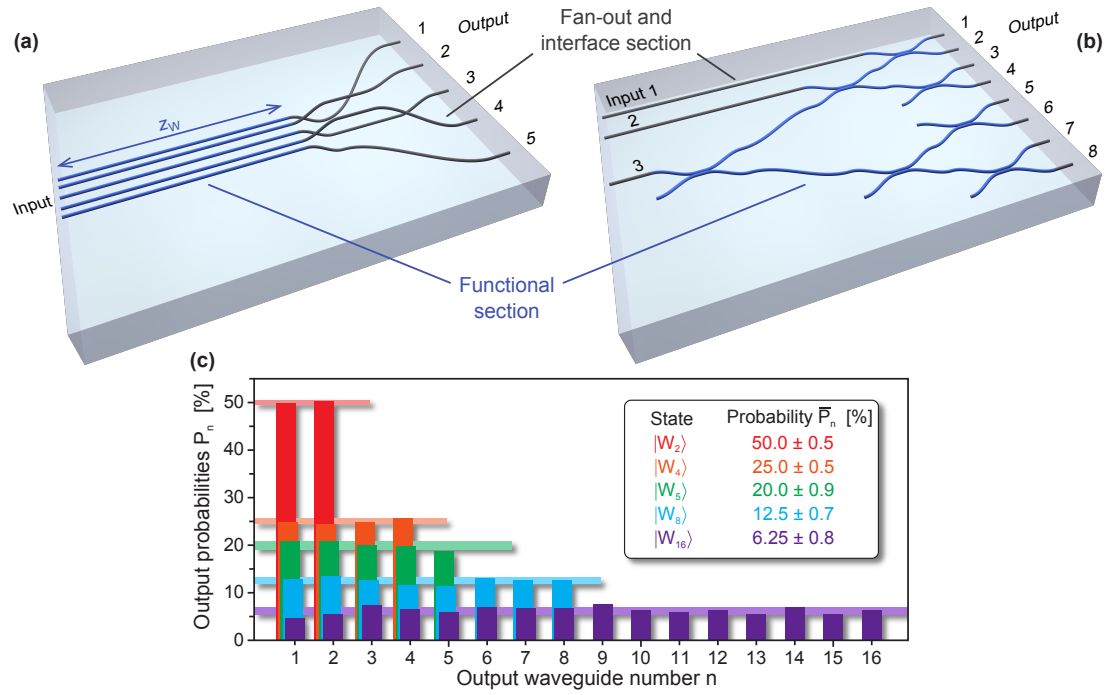

Figure 3.2.: On-chip generation of high-order single-photon W-states. (a) Approach based on continuously coupled waveguides. The coupling strengths are designed such that after the propagation of z_W photons initially launched in the central guide are coherently shared among all five guides with equal probability, thus, forming the state $|W_5\rangle$. A fan-out region is added to collect the photons with fiber arrays. (b) Scheme resting upon discrete splitting steps realized with balanced directional couplers. Depending on the input channel ("1", "2", or "3") single photons will be transformed to the W-states $|W_2\rangle$, $|W_4\rangle$, or $|W_8\rangle$, respectively. (c) Experimentally measured output probability statistics for detecting a photon for W-states of the orders $N = 2, 4, 5, 8, 16$. All distribution are nearly uniform and their standard deviations (compared to ideal uniform distributions) are shown as horizontal bars. Figure taken from [81].

with sufficient horizontal spacing minimizes further coupling in the fan-out region but cannot suppress it entirely. Although the probability distribution is quite close to uniformity, this approach is at the borders of technical feasibility. Already the implementation with seven waveguides considerably deviates from a uniform distribution yielding $\overline{P}_{N=7} = 14.3 \pm 1.9$. Positioning, and hence coupling uncertainties become even more crucial. Nevertheless, with the experimental realization of W-states of order five the hitherto "world record" of $N = 4$ [77] was exceeded.

The second approach to create W-states (of even order) is based on a discrete

network of DCs as imaged in Fig. 3.2(b). Since solely 50:50 DCs are utilized, only one coupling constant has to be matched promising a more viable implementation. The mesh shown in Fig. 3.2(b) enables a discrete-time QW of single photons without the opportunity for path-interference. In this vein, sending a single photon into input 1, it encounters one DC and hence, will be coherently split between the two output ports resulting in the state (see Eq. 2.14) $|\mathrm{W}_2\rangle = \frac{1}{\sqrt{2}}\left(\hat{a}_1^\dagger + \mathrm{i}\,\hat{a}_2^\dagger\right)|0\rangle$. By contrast, choosing input 2, the photon will be split at the first DC and then both outputs will be divided again each at a different DC giving the state $|\mathrm{W}_4\rangle = \frac{1}{2}\left(\mathrm{i}\,\hat{a}_1^\dagger + \hat{a}_2^\dagger + \mathrm{i}\,\hat{a}_3^\dagger - \hat{a}_4^\dagger\right)|0\rangle$ (compare Eq. 2.5). Finally, launching the photon at input 3, it will face three consecutive splitting stages yielding

$$|\mathrm{W}_8\rangle = \frac{1}{\sqrt{8}}\left(-\hat{a}_1^\dagger + \mathrm{i}\,\hat{a}_2^\dagger + \hat{a}_3^\dagger + \mathrm{i}\,\hat{a}_4^\dagger - \hat{a}_5^\dagger + \mathrm{i}\,\hat{a}_6^\dagger - \hat{a}_7^\dagger - \mathrm{i}\,\hat{a}_8^\dagger\right)|0\rangle\ , \tag{3.5}$$

describing the situation where a single photon is shared among eight spatial modes. The structure shown in Fig. 3.2(b) was inscribed in a glass sample and single photons sent into the three different input ports. The experimentally obtained probability statistics for all three cases are presented in Fig. 3.2(c). Again, a very high uniformity can be seen and is validated by the probabilities $\overline{P}_{N=2} = 50.0 \pm 0.5$, $\overline{P}_{N=4} = 25.0 \pm 0.5$, and $\overline{P}_{N=8} = 12.5 \pm 0.7$. This emphasizes the high fidelity of the waveguide structure and indicates the feasibility of the discrete-time QW approach. It is further underpinned by the generation of the state $|\mathrm{W}_{16}\rangle$. To this end, a waveguide lattice consisting of two layers of the structure presented in Fig. 3.2(b) was realized with its input ports (input port 3) connected by an additional vertically aligned DC. The output probability distribution is still flat (see Fig. 3.2(c)), yet the fluctuations naturally slightly increase resulting in $\overline{P}_{N=16} = 6.25 \pm 0.8$. With this, it is successfully demonstrated that a single photon can be coherently split over 16 channels by means of a QW in an integrated waveguide lattice. Evidently, by simply blocking output ports all lower W-state orders, even and odd ones, can be realized. However, this would go hand in hand with a decreased efficiency.

3.2. Multi-partite entanglement verification

The obtained probability distributions from the previous section shown in Fig. 3.2(c) are all flat and close to uniformity, thus strongly indicating the generation of W-states. However, to be entirely sure that a multipartite entangled W-states is created a faithful verification scheme is required. Conventionally, a state tomography of the output states can bring certainty. Due to the tremendous increase in complexity by the number of qubits for this method, it is highly favorable to exploit an alternative characterization approach that exhibits a better scaling. A first attempt would be a coherence test, meaning to check for the coherent superposition of the single photons. In this vein, if a W-state of order N is sent into an interferometer of N channels, the average photon number distribution will be given by the modulus square of the sum of the individual single site excitations (see Sec. 2.2, especially Eq. 2.11). In other words, the output probability distribution will be determined by the coherent sum of the individual single site excitations:

$$\text{coherent W-state: } n_q(z) \sim \left| \sum_{j=1}^{N} U_{q,j}(z) \right|^2 . \tag{3.6}$$

This is in strong contrast to the case when the single photons are separately launched into an optical system. Then, according to Sec. 2.3, the average photon number is given by the incoherent sum of the single site excitations:

$$\text{incoherent single site excitations: } n_q(z) \sim \sum_{j=1}^{N} \left| U_{q,j}(z) \right|^2 . \tag{3.7}$$

Interestingly, when creating $|W_5\rangle$ by a coupled waveguide array of length $z_W = 5\,\text{cm}$ the very same system shows to be highly sensitive to the coherence of the input state. Along these lines, single photons were individually sent into all channels and their corresponding output probabilities were incoherently summed up yielding a nearly uniform distribution as expected theoretically (see Fig. 3.3(b) (right panel)). Now, by doubling the length to $2z_W$ of the $|W_5\rangle$

generating array allows to test the coherent superposition of single photons at z_W (see Fig. 3.3(a)). Fig. 3.3(b) (top left) shows the experimentally obtained single photon output statistics which matches the theoretical calculation (bottom left) very close and is clearly non-uniform. This unequivocally verifies the coherent spreading of the single photon among five waveguides at z_W.

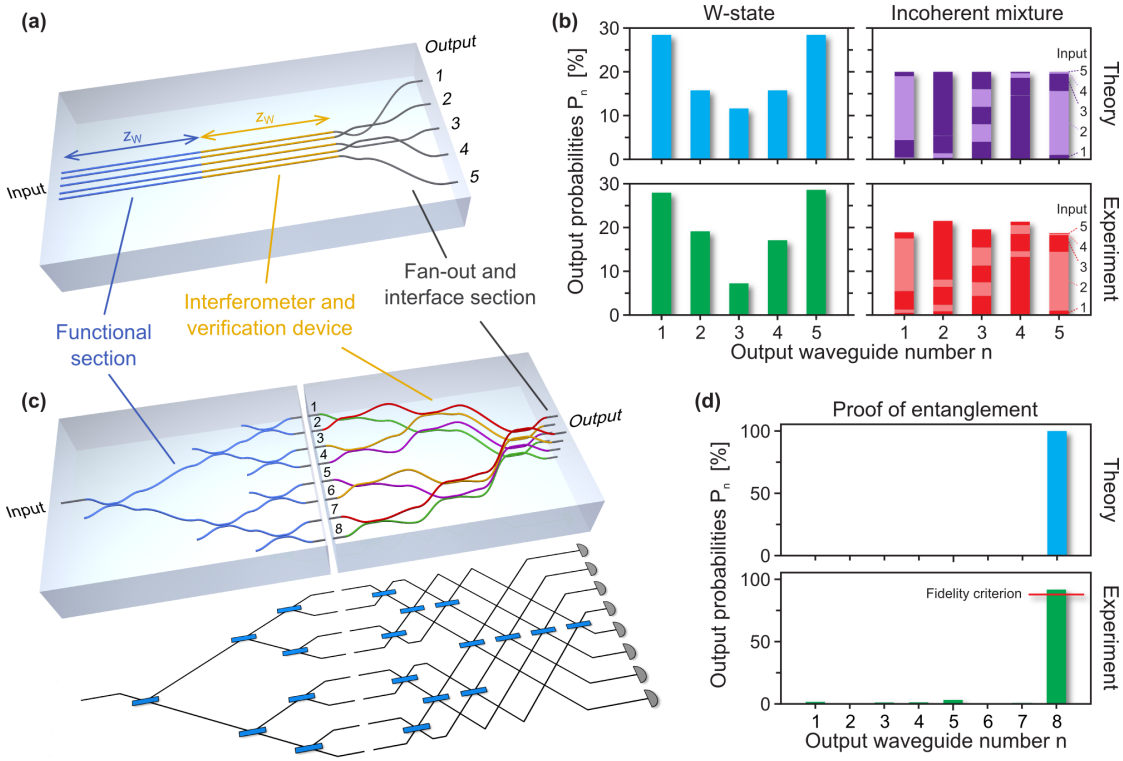

Figure 3.3.: Validation of W-states. (a) Experimental system to verify the coherent single-photon superposition of W-states with order $N = 5$. Injected single photons are expected to inhabit the state $|W_5\rangle$ after the propagation length z_W. For confirmation the created state further propagates until the propagation length $2z_W$ where it shows a specific interference based output probability pattern. (b) Comparison of coherent (left) and incoherent (right) input into the second interferometric array. Theory (top row) and experiments (bottom row) are congruent and reveal the coherent superposition of single photons being in the state $|W_5\rangle$. The incoherent measurements were performed by launching single photons subsequently into the five input channels (alternating colors) of an array of length z_W and incoherently sum up the output probabilities. (c) For the case of $N = 8$ the generated state is sent to an attached eightport-interferometer projecting the desired state $|W_8\rangle$ into one output channel. (d) Theoretical (top) and measured (bottom) output statistics after the verification device proofing the multipartite entanglement of the W-states by exceeding the required fidelity condition of $7/8$. Figure taken from [81].

The coherence of the single photons was also successfully tested for the discrete W-state generation scheme for the case of $N = 4$. Beyond this, a direct proof of the multipartite entanglement for W-states of order $N = 8$ has been implemented. To this end, one can follow the approach by Lougovski *et al.* [82] to project the state onto a basis of N orthogonal W-states $|\mathrm{W}_N^{(k)}\rangle$ $(k = 1 \ldots N)$ that vary in their phase distribution and include the state under consideration in Eq. 3.5. Such a projection is performed by applying a unitary transformation $\hat{V}$ mapping each of the orthogonal W-states onto one particular channel $\hat{V}\,|\mathrm{W}_N^{(k)}\rangle = \hat{a}_k^\dagger\,|0\rangle$. Considering now an unknown state with density matrix $\hat{\rho}$, it will evolve as $\hat{\tilde{\rho}} = \hat{V}^\dagger \hat{\rho} \hat{V}$. Hence, its overlap with the state $|\mathrm{W}_N^{(k)}\rangle$ is given by the probability to find a photon in channel k:

$$\mathcal{F} = \langle \mathrm{W}_N^{(k)}|\hat{\rho}|\mathrm{W}_N^{(k)}\rangle = \langle \mathrm{W}_N^{(k)}|\hat{V}^\dagger\hat{V}\hat{\rho}\hat{V}^\dagger\hat{V}|\mathrm{W}_N^{(k)}\rangle = \langle 0|\,\hat{a}_k\hat{\tilde{\rho}}\,\hat{a}_k^\dagger|0\rangle = \hat{\tilde{\rho}}_{kk}\,. \qquad (3.8)$$

Intriguingly, it holds that the fidelity is always below a certain threshold for all biseparable states: $\mathcal{F} \leq (N-1)/N$ [83, 84]. That way, obtaining a fidelity above the given threshold is a sufficient criterion to verify genuine N-partite entanglement in the state $\hat{\rho}$.

Along these lines the unitary $\hat{V}$ for the case of $N = 8$ is realized by the waveguide structure shown in Fig. 3.3(c). This eight-port interferometer allows coupling between all modes and projects certain single photon W-states at the input to one single output channel depending on the phase distribution of the input state. In doing so, the regarded input state $|\mathrm{W}_8\rangle$ from Eq. 3.5 will be projected to output guide number eight ($k = 8$). To put it another way, if the state, sent into the interferometric QW structure, is $|\mathrm{W}_8\rangle$, photons will emerge only from port eight. In that particular case, if the fidelity of this process is above the threshold of $7/8$, the eightpartite entanglement is indeed confirmed. As depicted in Fig. 3.3(c) such an eight-port interferometer was inscribed into a second glass chip that was attached to the first chip generating the W-states. Measuring the output probability statistics at the end of the verification chip (see Fig. 3.3(d)) yields a fidelity of $\mathcal{F} = 0.981 \pm 0.004 > 7/8$ clearly violating the fidelity criterion. Hence, eight-mode entanglement is experimentally verified for the $|\mathrm{W}_8\rangle$ state. While the deviation of the fidelity from unity is mainly caused by the

non-uniformity of the output probability distribution of $|W_8\rangle$ (see Fig. 3.2(c)), its uncertainty is determined by the Poissonian (or more precisely binomial; see Chapter 4) count statistics in the output waveguide of the verification chip.

By giving evidence of the multipartite entanglement it is possible to demonstrate that single photons, undergoing a discrete-time QW on a cascaded lattice of DCs, form W-states. As a result a very robust and miniaturized generation method for high-order W-states is accomplished not only exceeding the former limit in size by a factor of four but also enabling new applications.

3.3. Random number generation

The generation of random numbers is a key issue to enable (quantum) secure communication. Despite the fact that one can find various algorithms for random number generation on (classical) computers this topic is still crucial since all these algorithms are essentially predictable and thus, often called pseudo-random numbers. Indeed, many applications demand genuine random events, which can only be found in quantum physics. Accordingly, methods exploiting vacuum fluctuations [85], radioactive decay [86], or attenuated light [87] have been realized for providing genuine random numbers. Since the first method is based on Gaussian statistics and the latter two feature a Poissonian one, post-processing of the obtained data by a so-called Hash function, for conversion into a uniform distribution, is compulsory. Another promising technique, making post-processing obsolete, is to send single photons into a 50:50 beam splitter and utilize their random outcome in reflection and transmission channel, respectively, when being detected [88]. In doing so M subsequent photons are feasible to generate a random number out of the range $0 \dots 2^M - 1$. Applying now projective measurements on high-order single photon W-states seems like a natural extension of this basic principle. Their already uniform probability statistics render Hash functions or any other post-processing unnecessary. Moreover, the random number range scales very beneficial with the order N of the W-states: $0 \dots N^M - 1$. In other words: Exploiting the state $|W_N\rangle$ is like

rolling a N-sided (quantum) dice. In order to stress this fact, one can consider the case of three photons consecutively sent on a single beam splitter, which enables the generation of a random number between 0 and 7. In contrast, utilizing three photons in a row, each prepared in, e.g., the state $|W_{16}\rangle$, can yield a random number between 0 and 4095. Additionally, for high photon fluxes the single beam splitter scheme can easily suffer from detector saturation. This is avoided for high-order W-states, where the photon flux is split over many channels.

The principle of efficiently generating genuine random numbers through high-order single-photon W-states is exemplified and demonstrated experimentally for $|W_8\rangle$ states. For that purpose one can associate a random number $m = n - 1 = 0 \ldots 7$ with detecting a photon in channel $n = 1 \ldots 8$. In this way a three-digit number is generated. Through concatenating detection events one can assemble higher-digit random numbers. The experimental setup used here requires only the conversion from photon detection events into the digital format and *no* post-processing. In order to verify the randomness the standard statistical test suit for random numbers from the *National Institute of Standards and Technology* [89] was applied to an arbitrarily chosen sample set of 1 Mbit recorded at an average generation rate of 60 kbit/s. This test suite contains 15 randomness tests. For instance the first test checks the equal distribution of digital "zeros" and "ones". The maximum deviation of the ideal 50:50 ratio was found to be 3.444×10^{-4}. The recorded data successfully passed all 15 test. The names of the tests and their individual outcomes are summarized in Tab. 3.1.

This results unambiguously reveal the good suitability of high-order single photon W-states for random number generation. Though, the bit rates used here are a magnitude lower than in already established schemes [85, 87] but the lack of post-processing is an important advantage of this approach. Besides, the limiting factor is not the photonic system rather than the photon flux and the detection speed and efficiency. Hence, employing brighter photon sources as well as faster and more efficient detectors can give an enormous boost in generation bit rates [90, 91].

In summary, high-order photonic W-states have been efficiently generated by QWs of single photons in integrated waveguide lattices. Their multipartite entanglement was verified and a new application successfully introduced, that is, the generation of genuine random numbers. A compact version of the work discussed in this chapter can be found in [81].

Table 3.1.: Statistical test suite from the *National Institute of Standards and Technology*. All tests were applied to an arbitrarily chosen random bit sequence of 1 Mbit. Note, a given sequence is supposed to be random with a significance level of 0.01 when each P-value is larger than 0.0001. Table reproduced from [81].

statistical test	P-value	outcome
frequency	0.39562	success
block frequency	0.58495	success
cumulative sums	0.47015	success
runs	0.58495	success
longest run	0.30636	success
rank	0.12829	success
FFT	0.61638	success
non-periodic templates	0.82541	success
overlapping templates	0.34230	success
universal	0.04215	success
approximate entropy	0.71287	success
random excursions	0.10208	success
random excursions variants	0.89837	success
serial	0.11428	success
linear complexity	0.43006	success

CHAPTER 4

Multiplexed detection for characterization of light states

To distinguish whether a given light field exhibits quantum features or not is a crucial task in photonic quantum science. It can be achieved by evaluating the photon number statistics in that light field. For this purpose the individual photons can be detected and counted in a photon-number resolving manner. Furthermore, quite recently a very potential application has been demonstrated [92]. Coherent optical communication with a performance above the standard quantum limit has been enabled by means of photon-number resolved detection. As already outlined in Sec. 2.5 superconducting transition edge sensors are capable of resolving the number of detected photons [57,58]. Unfortunately, they require cryogenic cooling, are rather slow and up to now their performance becomes poor for photon numbers higher than ten [57]. On the contrary, standard on-off detectors (also called "click" detectors) based on avalanche photo diodes cannot discriminate between the number of impinging photons. In other words, no matter if one or two or more photons hit the detector at the same time, they will all be registered as *one* click. In this chapter, a possible

solution to this problem will be presented. Based on a QW akin to a divide-and-conquer scheme, the genuine nature of given light states can be unambiguously determined harnessing standard on-off detectors only. The first section will explain the theoretical idea behind this approach, which exploits merely the click statistics provided by on-off detectors instead of the photon statistics. The subsequent section deals with the experimental verification of the proposed scheme and its application to characterize single-photon sources.

4.1. Photon number statistics vs. click statistics

It is well-known that the nature of light is specified by its photon statistics. In this vein, classical fields like thermal light from a candle exhibit a super-Poissonian distribution of the photon number whereas the distribution is sub-Poissonian for quantum light such as photons prepared in a Fock state [42, 43] (see Fig. 4.1). Interestingly, photons in a coherent state follow a Poissonian statistics [42, 43], thus living up to the expectations to be on the border line between the quantum and the classical domain. This is one of the reasons why they are considered as "the most classical quantum states". Supplementary information on coherent states can be found in the Appendix A. By employing the first and second moments of the photon number distribution, more precisely mean value $\langle n \rangle^*$ and variance $\langle (\Delta n)^2 \rangle = \langle n^2 \rangle$ - $\langle n \rangle^2$, Mandel introduced a measure for the non-classicality already in 1979, now called Mandel parameter [93]

$$Q_{\mathrm{M}} = \frac{\langle (\Delta n)^2 \rangle}{\langle n \rangle} - 1 \,. \tag{4.1}$$

It is negative for sub-Poissonian statistics, and hence, for non-classical light fields. In contrast, classical fields with a super-Poissonian statistics yield a positive Q_{M} value and it becomes zero for coherent states (Poissonian). Note that

*In difference to the rest of this thesis the average photon number is indicated by $\langle n \rangle$ (instead of simply n) throughout the hole chapter (and the Appendix A). This step is necessary for better distinction and to emphasize its statistical property as an average. Hence, it holds $\langle n \rangle = \langle \psi | \hat{n} | \psi \rangle = \langle \psi | \hat{a}^\dagger \hat{a} | \psi \rangle$ with the photon number operator $\hat{n} = \hat{a}^\dagger \hat{a}$.

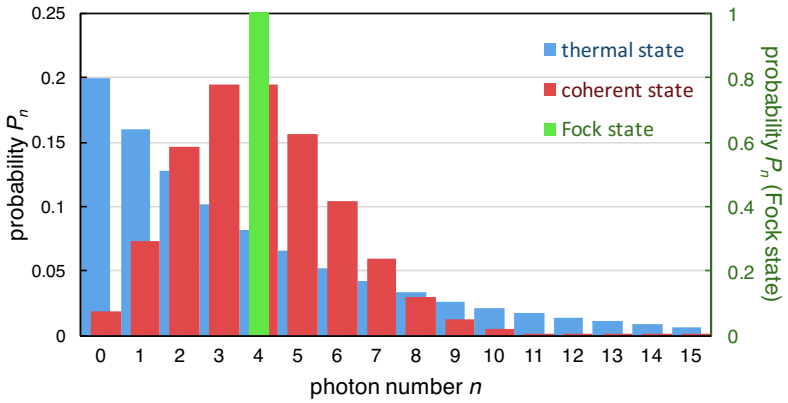

Figure 4.1.: Photon number statistics for different states: thermal, Fock, and coherent state follow a super-, sub-, and Poissonian statistics, respectively. The mean photon number $\langle n \rangle = 4$ is identical in all three cases. The right vertical axis applies to the Fock state distribution only.

a calculation of the Q_{M} requires access to the full photon number statistics. As mentioned in the introduction to this chapter, standard on-off detectors only provide click statistics that is *not* equal to the photon number distribution. Consequently, in such a situation the calculation of the Mandel parameter fails and Q_{M} can indeed become negative for an entirely classical field [94]. In the following, we will introduce an alternative measure utilizing clicks from on-off detectors only. To this end, we will employ multiplexing of the incoming light field into N modes, each impinging on a separate detector. In particular, an incoming state of light is uniformly distributed among the N detectors and each photon will be detected by a certain detector with probability $1/N$. Further, two photons will be detected in different channels with a probability of $1 - 1/N$. Hence, if one photon is detected, the probability to find the other in any other channel is $N - 1$ times greater than to be found in the same one, and thus, being missed. By implication, the scheme becomes more efficient the higher the number of channels and converges to the genuine photon number statistics for very large N. Nevertheless, it applies conveniently for a finite number of $N \geq 2$ detectors. Quite naturally, it does not matter in which degree of freedom the multiplexing occurs. Accordingly, also a time-multiplexing approach has been put forward in [95].

Since any quantum state described by its density matrix $\hat{\rho}$ can by expressed in the Glauber-Sudarshan P representation as $\hat{\rho} = \int \mathrm{d}^2\alpha\, P(\alpha)\, |\alpha\rangle\, \langle\alpha|$ [96, 97], it is necessary to take only coherent states $|\alpha\rangle$ into account (see Appendix A). As a consequence, for any quantum state the probability to contain exactly *n photons* is given by [93, 98],

$$p_n = \langle n|\hat{\rho}|n\rangle = \int \mathrm{d}^2\alpha\, P(\alpha) \frac{|\alpha|^{2n}}{n!} \mathrm{e}^{-|\alpha|^2} = \left\langle : \frac{\hat{n}^n}{n!} \mathrm{e}^{-\hat{n}} : \right\rangle , \tag{4.2}$$

where $: \ldots :$ denotes normal ordering, e.g., $: \hat{a}\, \hat{a}^\dagger : = \hat{a}^\dagger \hat{a}$ [99]. The above distribution built the basis for Mandel to develop his Q_M parameter. For better understanding, one can consider the case where ρ represents a coherent state $|\alpha'\rangle$. Then the P function is $P(\alpha') = \delta^{(2)}(\alpha' - \alpha)$ and Eq. 4.2 becomes the well-known Poisson photon distribution $p_n = \mathrm{e}^{-\langle n\rangle} \langle n\rangle^n / n!$ for coherent states.

As Sperling *et al.* have revealed [94], the situation changes when considering the actual photon counting distribution such that the probability of $k \leq N$ simultaneous *click events* between the N detectors is calculated as

$$c_k = \left\langle : \frac{N!}{k!(N-k)!} \left(\mathrm{e}^{-\frac{\hat{n}}{N}}\right)^{N-k} \left(\hat{1} - \mathrm{e}^{-\frac{\hat{n}}{N}}\right)^k : \right\rangle . \tag{4.3}$$

At this, the expectation value of the exponential term is related to the probability of zero clicks $c_0 = \langle : \mathrm{e}^{-\hat{n}} : \rangle$. Taking a more realistic scenario into account with a limited detector efficiency $\eta \leq 1$ and a dark count rate (or more generally an overall noise rate) ν the photon counting or click statistics becomes

$$c_k = \left\langle : \binom{N}{k} \hat{\pi}^k \left(\hat{1} - \hat{\pi}\right)^{N-k} : \right\rangle , \tag{4.4}$$

where the expectation value of $\hat{\pi} = : \hat{1} - \mathrm{e}^{-(\eta\hat{n}+\nu)/N} :$ determines the probability to register a click. In contrast to the Poissonian photon statistics p_n this distribution becomes binomial as $c_k = \left\langle \binom{N}{k} p^k (1-p)^{N-k} \right\rangle$, with $p = 1 - \mathrm{e}^{-(\eta|\alpha|^2+\nu)/N}$, for a coherent state $|\alpha\rangle$ (see Fig. 4.2(a)). Accordingly, classical and non-classical light fields will result in a super- and sub-binomial distribution, respectively, as illustrated in Fig. 4.2(b). In the same way Mandel defined a parameter based on

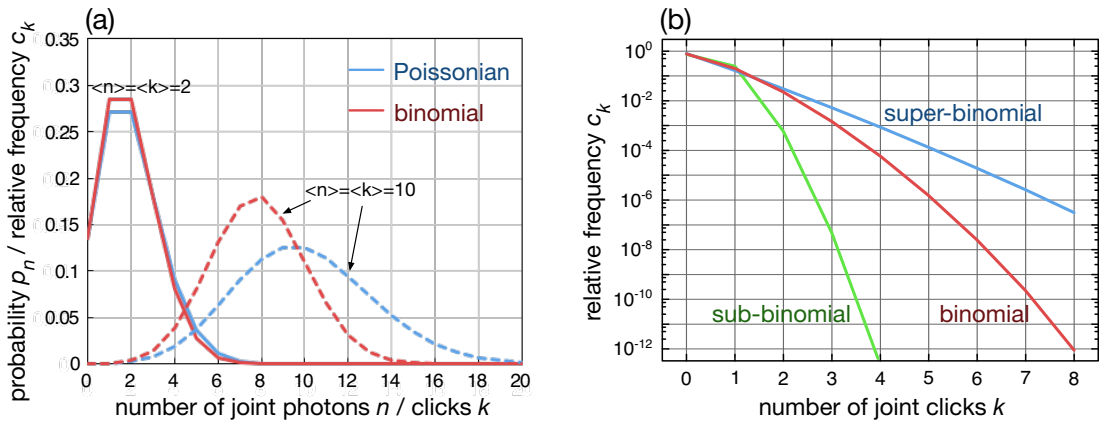

Figure 4.2.: Quantum statistics. (a) Difference between Poissonian and binomial statistics. Both distributions are quite similar for low mean values (average number of photons or clicks $\langle n\rangle = \langle k\rangle = 2$; solid lines), whereas they differ significantly for higher ($\langle n\rangle = \langle k\rangle = 10$; dashed lines). In all cases the number of detectors for registering clicks was set to $N = 20$. (b) Calculated different types of possible click statistics for the case of $N = 8$ and $\langle k\rangle = 0.25$ expected clicks per measurement in semilogarithmic plot. Associated to the super-, sub-, and binomial distributions are $Q_\mathrm{B} = +0.22, -0.22, 0$, respectively. Fig. 4.2(b) reproduced from [101].

photon statistics it is possible to define another parameter – Q_B – based on click statistics in order to quantify non-classical light [100]:

$$Q_\mathrm{B} = N\frac{\langle(\Delta k)^2\rangle}{\langle k\rangle(N-\langle k\rangle)} - 1 \begin{cases} > 0\,, & \text{for super-binomial click statistics} \\ = 0\,, & \text{for binomial click statistics} \\ < 0\,, & \text{for sub-binomial click statistics} \end{cases}, \tag{4.5}$$

where $\langle k\rangle = \sum_{k=0}^{N} k c_k$ and $\langle(\Delta k)^2\rangle = \langle k^2\rangle - \langle k\rangle^2$ are the mean number and variance, respectively, of the number of *joint* click events at the N detectors.

It is known and particularly demonstrated in this framework [94] that the binomial distribution converges to a Poissonian one for $N \to \infty$, meaning that for a large number of detectors the click statistics becomes the actual photon statistics. In accordance with that, Q_B becomes the Mandel parameter.* Moreover, in that limit any possible detector dead time can be overcome, since the probabil-

*For $N \to \infty$ one finds $\langle k\rangle \to \langle n\rangle$ and $N/(N - \langle k\rangle) \to 1$. Hence, comparing Eqs. 4.1 and 4.5 yields $Q_\mathrm{B} \overset{N\to\infty}{\longrightarrow} Q_\mathrm{M}$.

ity to miss another photon shortly after a detection event in the same detector converges to zero.

With the introduction of the Q_B parameter it is possible to evaluate the nature of any given state of light by means of the photon counting statistics recorded from N standard on-off detectors. Furthermore, real detectors with limited efficiency and noise are included and the experimental procedure will be presented and discussed in the next section.

4.2. Divide and conquer: characterization of light states by on-off detectors

The experimental demonstration of the applicability of the Q_B parameter to evaluate the non-classicality of an unknown state of light necessitates the uniform splitting of this state into N parts, each aligned to a detector. As revealed in Chapter 3, a QW on a discrete network of DCs ensures such an equal splitting. For that purpose, the very same waveguide structure for generating W-states $|W_8\rangle$ was exploited as multiplexer to distribute incoming light fields over $N = 8$ channels. On the detection side, standard click detectors based on avalanche photo diodes, as used for all experiments in this thesis, were applied. They are not photon number resolving, and thus, only provide click distributions. The measurement scheme works as follows: When launching light into the one-to-eight multiplexer, the absolute number of joint click events M_k is registered by the eight detectors, where k indicates again the number of detectors that clicked within a time window of 10 ns as it is exemplarily shown in Fig. 4.3. Hence, the probability of k joint detector events is given as the ratio of the absolute number of click events and the total number of time windows: $c_k = M_k / \sum_k M_k$. From that one can calculate the desired Q_B value. The approach is tested for two cases: First, attenuated laser light is used, and second, single photons from one arm of a down-conversion source are investigated. While the former case is theoretically best described by a coherent state, the latter one can be idealized as a single-photon Fock state.

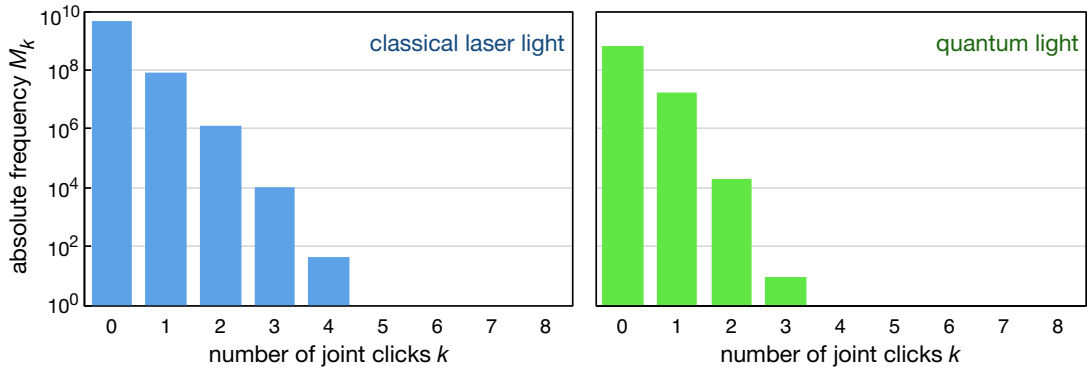

Figure 4.3.: Measured absolute frequency M_k of k simultaneous click events within a time window of 10 ns. On the left side for classical laser light compared to quantum light (heralded down-converted photons) on the right. Even though both distributions appear to be very similar on a first view, they differ significantly in the statistics they follow. It is super-binomial on the left but sub-binomial on the right, leading to a positive or negative Q_B value, respectively.

To this end classical laser light at 808 nm (provided by a laser diode) and with a maximum photon flux of two million (clicks) per second was launched into the multiplexer and detection events were recorded over 44 s. After the analysis just described above one finds $Q_B = (1.712 \pm 0.026) \times 10^{-2}$ verifying the super-binomial click statistics, and thus, the classical nature of coherent laser light. Note, although often denoted as a coherent state, laser light differs in its click (and also in its photon) statistics. Hence, for many purposes it is well approximated by a coherent state, but one should be aware of its inherent classical nature.

In a second experiment photons at 815 nm, provided from one arm of the SPDC source (see Fig. 2.9), were injected into the multiplexer. The other photon from the down converted pair is used to trigger the measurement (known as "herald") and was therefore directly send to another detector. In this way a heralding efficiency of 18% with 65,000 counts per second before the multiplexing device was achieved. Again, the relative frequencies c_k were obtained from the number of joint click events in one of the SPDC arms (triggered by the other). From that $Q_B = -(2.002 \pm 0.049) \times 10^{-2}$ was extracted, which clearly confirms the quantum nature of the single-photon states provided by the heralded SPDC

source. For clarification, considering pure single-photon Fock states and perfect detectors with detection efficiency $\eta = 1$ and vanishing noise rate $\nu = 0$ will result in $Q_B = -1$. However, in a realistic scenario, the brightness of a source is limited leading to many time bins with no click events such that Q_B features much smaller absolute values. It is important to mention, that not the absolute values are of interest, it is only the *sign* that matters in order to quantify the type of statistics, and hence, the genuine nature of a state of light.

The fidelity of the divide-and-conquer scheme with standard click detectors was additionally tested for different brightness levels of the two sources. To this end, both the classical laser light and the down converted single photon stream were attenuated by different neutral density filters. In all measurements the recording time was adjusted to collect a minimum of 100 million (non-zero) detection events. This corresponded to measurements times from 44 s up to 60 h. The results obtained in this way are presented in Fig. 4.4(a). Clearly, by attenuating the photon flux, more time bins will feature no-click events and $|Q_B|$ becomes smaller and finally converges to zero. This is natural since for strong damping the state to be detected is more or less the vacuum state, which of cause can be understood as a coherent state with mean photon number zero: $|\alpha = 0\rangle = |0\rangle$. However, as shown in the inset of Fig. 4.4(a), for all measurements, the Q_B parameter exhibits the correct sign indicating the type of input state.

The measurement uncertainties origin from two different issues. On the one side imperfections in the QW multiplexer influence the photon counting statistics leading to a systematic error. On the other side the limited measurement time, respectively, the number of detections itself, reduces the accuracy of the Q_B values. One can understand this as follows: It is quite unlikely to have very hight joint click events like for $k = 5 \ldots 8$. As consequence, even after 100 million clicks there were none fivefold or higher manifold events resulting in setting $c_{5,\ldots,8} = 0$, which does not perfectly match a (sub-/super-)binomial distribution (see Fig. 4.3). This increases the statistical error on the first and second moments of the click distribution c_k and thus, the resulting Q_B parameter. From that, it follows that the uncertainty of Q_B grows as the number of de-

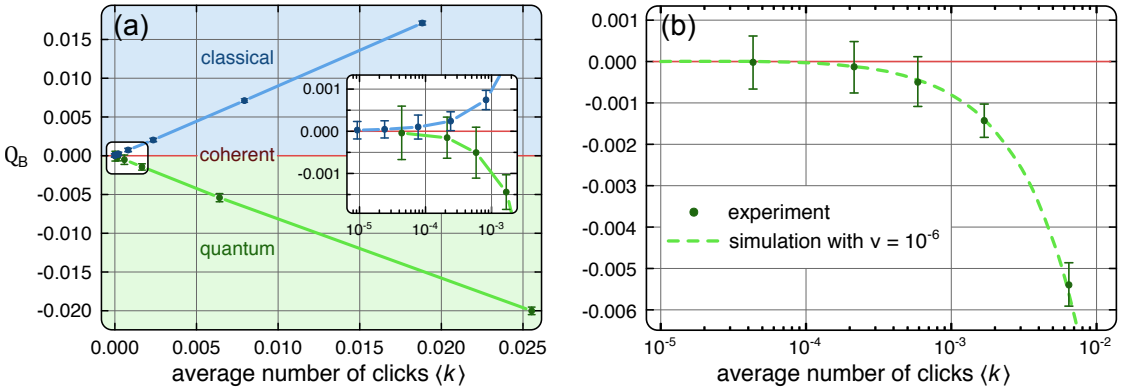

Figure 4.4.: Q_B parameter and characterization of light. (a) Experimentally obtained Q_B values for classical laser light and heralded single photons from SPDC at different attenuations, and thus, different average clicks per measurement $\langle k \rangle$. The inset is a semilogarithmic enlargement of the region with very high damping. Even for extreme low photon fluxes, when the uncertainties become larger than the absolute values, the sign of Q_B stays well defined, successfully denoting the type of light field. (b) Experimental Q_B values for different damping rates of the heralded single photons from the SPDC source compared to the theoretical curve of a pure single-photon Fock-state. From the results one can extract a noise rate $\nu = 10^{-6}$ as it is typical for a heralded photon source. Figure reproduced from [101].

tection events shrinks. Despite the fact that in Fig. 4.4(a) the uncertainties may exceed the absolute values, it is worth to mention again that the sign of Q_B stays well defined at all times. Besides, count rates of standard quantum sources are sharply higher than in this low-yield regime.

Harnessing this procedure, it becomes possible to characterize single-photon sources such as the SPDC source used here. It is supposed to provide single-photon Fock states, for which one can find an analytical expression for the average click number $\langle k \rangle = N(1 - e^{-\nu}) + \eta e^{-\nu}$ and of the Q_B parameter as [101]

$$Q_B = \left(\frac{N-1}{N-\eta} \right) \frac{-\eta e^{-\nu}}{N(1-e^{-\nu}) + \eta e^{-\nu}}, \tag{4.6}$$

only depending on the detection efficiency η and the noise count rate ν of the complete system. Accordingly, one can extract the dark count rate from the measured click statistics. For the quantum source used here, it is found to be $\nu = 10^{-6}$ (see Fig. 4.4(b)), and thus, very low as in agreement with a heralded source. This way, an efficient verification that the photons generated by the

down-conversion process can be idealized as single-photon Fock states is feasible.

In essence, the photon counting statistics provided by standard on-off detectors differs from the photon number distribution. This becomes crucial for many detection issues, in particular for the determination whether a light field is non-classical or not. Nevertheless, by virtue the Q_B parameter one can evaluate the recorded click distribution without any data post-processing and decide for the non-classicality of light even in case of extreme low photon fluxes. The scheme has been verified in various experiments and its applicability to characterize single-photon sources has been demonstrated. The results discussed in this chapter are also presented in [101] in a condensed form.

CHAPTER 5

Bloch oscillations of N00N states

In his seminal work from 1929 Felix Bloch considered the behavior of an electron wavefunction in a solid state lattice that is subjected to an external homogeneous electric field [102]. He predicted a periodic spreading and re-localization of the electronic wavefunction, which is nowadays known as *Bloch oscillation* (BO). This work conduced to the model of the electronic band structure that became a fundamental concept in solid state physics. Nevertheless, since electrons strongly interact with each other and their environment, electronic BOs are hardly observable. Although originally conceived for electrons in solid states, the idea of BOs holds for any wave-like propagation in all kind of lattices. Hence, the evolution of light or the QW of photons, in e.g., photonic waveguide lattices with a linear potential gradient, obeys the same principles and allows the observation of BOs [103–105]. So far, all experiments on BOs have been limited to single-particle dynamics. Bromberg *et al.* discussed theoretically the behavior of maximally entangled two-photon N00N states in a photonic Bloch oscillator lattice [106]. They spend particular interest on the evolution of the two-photon correlation function and predicted a cyclic change during evolution. As part of this thesis, BOs of path-entangled photon pairs

have been experimentally implemented and investigated as QWs in waveguide lattices. The correlation cycle could be experimentally confirmed and the correlations reveal a strong dependence on the mode-exchange symmetry of the path-entangled states. Those input states were efficiently generated by detuned DCs that are the subject of the first section of this chapter. This is followed by a section about the implementation of N00N state BOs and the experimental results.

5.1. On-chip generation of path-entangled states with tailored symmetry

In order to observe QWs of two-photon N00N states with a tailored mode-exchange symmetry in a Bloch oscillator lattice it is crucial to efficiently generate these states in an integrated manner. As it was shown in Sec. 2.3 (in particular by Eq. 2.14) two indistinguishable photons are transformed by a 50:50 DC into the path-entangled state (with the freedom of a global phase) $\frac{1}{2}\left[(\hat{a}_1^\dagger)^2 + (\hat{a}_2^\dagger)^2\right]|0\rangle$, which is symmetric under exchange of the waveguide modes. In order to achieve any other exchange phase between the two path possibilities one can introduce a phase shift in one of the arms at the output side. However, this would go hand in hand with adding an extra section to the DC, which may also exhibit additional losses when being curved [107]. A more elegant way is to make use of a degree of freedom the DCs offer. In fact, the propagation constants of the waveguides can be tuned. To describe a system of two evanescently coupled waveguides with a difference in their propagation constants of $\Delta\beta$ (see Fig. 5.1(a)) Eq. 2.1 becomes (see also Eqs. 2.9 & 2.10)

$$\frac{\mathrm{d}}{\mathrm{d}z}\begin{pmatrix}\hat{a}_1^\dagger(z)\\ \hat{a}_2^\dagger(z)\end{pmatrix} = \mathrm{i}\begin{pmatrix}\beta_0+\Delta\beta & \kappa\\ \kappa & \beta_0\end{pmatrix}\begin{pmatrix}\hat{a}_1^\dagger(z)\\ \hat{a}_2^\dagger(z)\end{pmatrix}. \tag{5.1}$$

The solution in a moving reference frame ($\hat{a}_q^\dagger(z) \rightarrow \hat{a}_q^\dagger(z)\mathrm{e}^{\mathrm{i}\beta_0 z}$) is

$$\begin{pmatrix} \hat{a}_1^\dagger(z) \\ \hat{a}_2^\dagger(z) \end{pmatrix} = \mathrm{e}^{\mathrm{i}\frac{\Delta\beta}{2}} \begin{pmatrix} \cos(\tilde{\kappa}z) + \mathrm{i}\frac{\Delta\beta}{2\tilde{\kappa}}\sin(\tilde{\kappa}z) & \mathrm{i}\frac{\kappa}{\tilde{\kappa}}\sin(\tilde{\kappa}z) \\ \mathrm{i}\frac{\kappa}{\tilde{\kappa}}\sin(\tilde{\kappa}z) & \cos(\tilde{\kappa}z) - \mathrm{i}\frac{\Delta\beta}{2\tilde{\kappa}}\sin(\tilde{\kappa}z) \end{pmatrix} \begin{pmatrix} \hat{a}_1^\dagger(0) \\ \hat{a}_2^\dagger(0) \end{pmatrix}, \tag{5.2}$$

with the effective coupling constant $\tilde{\kappa} = \sqrt{(\Delta\beta/2)^2 + \kappa^2}$. This detuned DC features a 50:50 splitting ratio for the length $z = \arcsin(\tilde{\kappa}/\sqrt{2}\kappa)/\tilde{\kappa}$. Accordingly, this allows a maximum detuning of $\Delta\beta = 2\kappa$. The intensity or photon density oscillation when injecting coherent light or a single photon into one channel is displayed in Fig. 5.1(b) for the detuning strengths $\Delta\beta = 0, \kappa, 2\kappa$. Also from there it becomes clear that equal splitting is only feasible up to the detuning threshold $\Delta\beta = 2\kappa$. Additionally shown is the z-dependence of the phase difference between the two channels

$$\Delta\varphi_m := \varphi_2 - \varphi_1 = (-1)^{m-1}\frac{\pi}{2} - \arctan\left[\frac{\Delta\beta}{2\tilde{\kappa}}\tan(\tilde{\kappa}z)\right], \tag{5.3}$$

when exciting waveguide $m = 1, 2$. In this vein a single photon input state is transformed into a path-entangled state according to

$$\hat{a}_m^\dagger|0\rangle \overset{\text{detuned DC}}{\longrightarrow} \frac{1}{\sqrt{2}}\left(\hat{a}_1^\dagger + \mathrm{e}^{\mathrm{i}\Delta\varphi_m}\hat{a}_2^\dagger\right)|0\rangle . \tag{5.4}$$

Accordingly, in the case of identical guides ($\Delta\beta = 0$) one finds $\tilde{\kappa} = \kappa$ and a 50:50 splitting ratio at $z = \pi/4\kappa$ as well as $\Delta\varphi_{1,2} = \pi/2$ as already known from Sec. 2.1. In contrast, for maximum detuning ($\Delta\beta = 2\kappa$) one finds $\tilde{\kappa} = \sqrt{2}\kappa$ and equal splitting at $z = \sqrt{2}\pi/4\kappa$. Further, at this z-position reflection and transmission channel are either in phase (when exciting waveguide $m = 1$) or they are out of phase by $\Delta\varphi_2 = \pi$ (when exciting waveguide $m = 2$). Interestingly, in that particular case the device will act as a Hadamard gate for path-encoded photonic qubits, which is another potential application.

For the experimental implementation of this scheme three detuned DCs with the detunings $\Delta\beta = 0, \kappa, 2\kappa$ were fabricated and tested for their 50:50 splitting ratio. Their detuning was controlled via the inscription velocity (changed at the

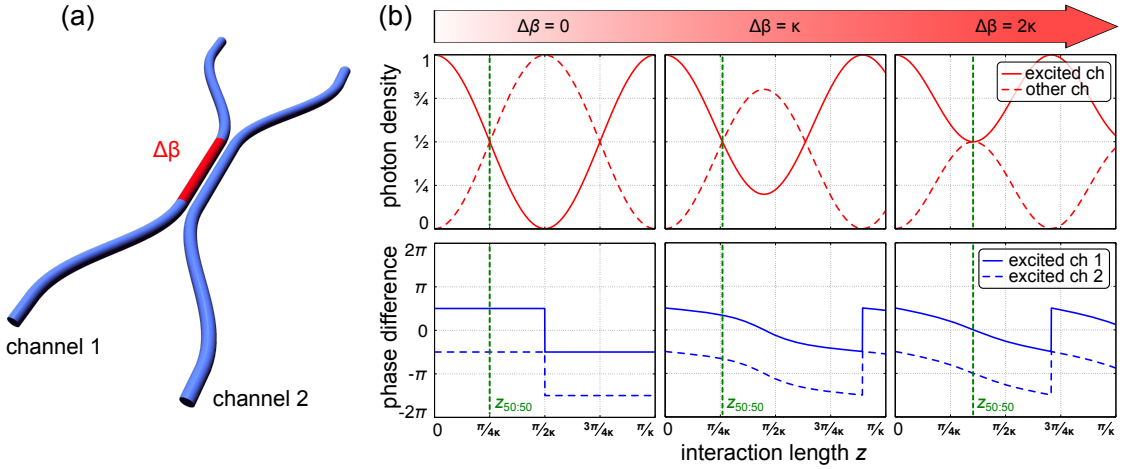

Figure 5.1.: Detuned directional coupler. (a) Scheme of a detuned DC where one of the straight parts exhibits a difference in its propagation constant of $\Delta\beta$ with respect to the other. (b) Photon density (top row) and phase difference (bottom row) over the interaction length (straight section) for detunings $\Delta\beta = 0, \kappa, 2\kappa$. The phase difference also depends on the excited channel. The z-position of an balanced splitting ratio is marked by green dashed lines and labeled with $z_{50:50}$. Figure reproduced from [108].

straight sections only). The minimum inter-waveguide distance was chosen to be rather large (24.7 µm) and the bending region as short as feasible in order to confine coupling dynamics to the straight region. The pertinent experimental parameters are summarized in Tab. 5.1. Uncertainties arise due to the limited positioning precision and some minimized but not completely vanishing coupling within the bended regions. However, the deviations are negligible for the experimental realization as one can see by testing the correct 50:50 splitting operation. In doing so, single photons were sent into one of the input ports and their output probabilities were measured. Fig. 5.2 presents the results for the three detuned DC devices. One can clearly notice the almost perfectly balanced splitting ratio in all settings. The data reveal an average transmission rate of $(50.4 \pm 0.8)\%$.

In addition to the equal splitting ratio one can verify the correct operation principle of the detuned DCs by sending their output directly into another well-known (non-detuned) standard DC. In this vein for $\Delta\beta = 0$ the complete setting becomes a balanced Mach-Zehnder interferometer, such that all light emerges

Table 5.1.: Detuned directional coupler. The straight section of channel 1 is detuned via its inscription velocity (all other parts including complete channel 2 were inscribed with 60.0 mm/min). Accordingly, to obtain a balanced splitting ratio the lengths have to be adjusted.

detuning $\Delta\beta$	inscription velocity	length of straight section
0	60.0 mm/min	17.2 mm
κ	61.5 mm/min	17.8 mm
2κ	63.0 mm/min	24.3 mm

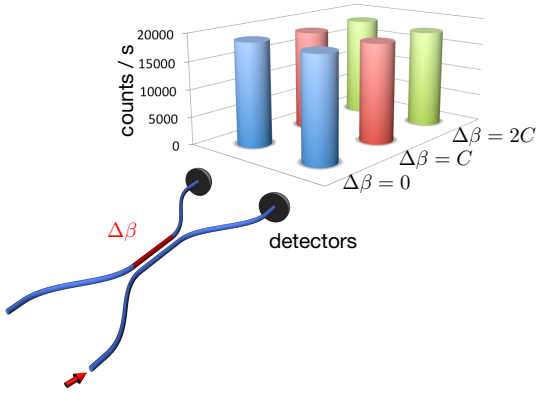

Figure 5.2.: Balanced splitting ratio of detuned directional couplers. Single photons were injected into detuned DCs with tailored detunings $\Delta\beta$ and their output statistics were recorded revealing an uniform distribution.

from one channel at the end of the second DC. In contrast, the output state of the detuned DC with maximum detuning is not altered by the second standard DC and thus, photons should leave the verification device with equal probability in both outputs. For the case of intermediate detuning of $\Delta\beta = \kappa$ one can expect a 1:3 probability distribution after the second DC. This verification scheme was implemented by writing another non-detuned DC directly behind the detuned ones (see Fig. 5.3(a)). Again, single photons were launched into one channel and the output statistics was recorded. The results shown in Fig. 5.3(a) demonstrate a very good agreement with the theoretical predictions proving the correct operation of the detuned DCs.

Now, turning from the single-photon scenario towards the case where a separable two-photon state impinges on a detuned DC. Based on Eq. 5.2 such states

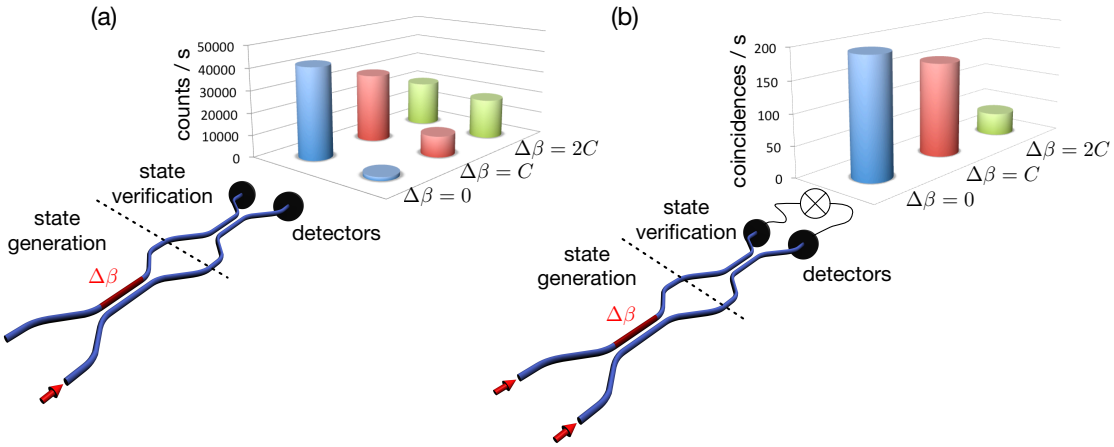

Figure 5.3.: Verification of detuned directional couplers. A standard non-detuned DC serves as a verification device directly connected to the detuned DCs. (a) Single-photon input into the detuned DCs yields the theoretically predicted outcome statistics after the verification stage. (b) Two photons launched into the detuned DCs giving certain coincidence rates after the verification DC. Hence, they confirm the successful generation of path-entangled states with various mode-exchange symmetry by the detuned DCs. Figure reproduced from [108].

will be transformed to path-entangled states of the form

$$\hat{a}_1^\dagger \hat{a}_2^\dagger |0\rangle \overset{\text{detuned DC}}{\longrightarrow} \frac{1}{2}\left[\left(\hat{a}_1^\dagger\right)^2 + \mathrm{e}^{\mathrm{i}\theta}\left(\hat{a}_2^\dagger\right)^2\right]|0\rangle =: |\psi^{(\theta)}\rangle \ . \tag{5.5}$$

Here the phase $\theta = \pi - 2\arctan\sqrt{(2\kappa/\Delta\beta)^2 - 1}$ defines the mode-exchange phase of the obtained state. Naturally, zero detuning causes a vanishing phase as already known for the standard DC, which yields a path-entangled state with even parity. Opposed to this, maximum detuning leads to the anti-symmetric path-entangled state with $\theta = \pi$, whereas $\theta = \pi/3$ follows from $\Delta\beta = \kappa$. Intriguingly, depending on their parity – even, odd, or intermediate – these path-entangled two-photon states can mimic the QW behavior of fermions (anti-bunching), bosons (bunching), or anyons (mixed), respectively [31, 109]. All three particle types differ in their particle exchange statistics $\hat{a}_m^\dagger \hat{a}_n^\dagger = \mathrm{e}^{\mathrm{i}\phi}\, \hat{a}_n^\dagger \hat{a}_m^\dagger$ ($m \neq n$): While fermions and bosons are characterized by odd ($\phi = \pi$), respectively, even ($\phi = 0$) particle exchange statistics anyons exhibit a mixed one ($0 < \phi < \pi$) [110, 111]. Since anyons are quasi-particles that only exist in even-dimensional spaces it is hard to study them. Therefore detuned DCs

may be an elegant expedient, in particular for the investigation of anyonic QWs by providing two-photon states capable of the same QW characteristics. Note, all detunings $0 < \Delta\beta < 2\kappa$ lead to an intermediate parity.

In accordance with the single-photon scenario one can additionally check the correct performance in the two-photon regime when a second non-detuned DC is added. Measuring the coincidences determines the phase shift of the entangled states. Along these lines the symmetric output state from the non-detuned DC will be transformed back into the separable two-photon state by the verification DC such that maximum coincidences are expected. On the contrary the DC with maximum detuning provides the state $|\psi^{(\pi)}\rangle$, which is not changed by the verification device leading to vanishing coincidences, or more realistically a minimum rate. Finally, for the state $|\psi^{(\pi/3)}\rangle$, when $\Delta\beta = \kappa$, the expected coincidence rate is $3/4$ of the one from the non-detuned case. This was experimentally tested by sending two indistinguishable photons into the same waveguide structures as used in the single-photon verification approach. The measured coincidence rates can be found in Fig. 5.3(b)). To account for different input and output coupling efficiencies for each of the three structures the joint clicks are weighted by the single-photon count rates. The results clearly reveal a maximum rate for vanishing detuning and 0.80 ± 0.01 of that for the mixed case with $\Delta\beta = \kappa$. For maximum detuning the coincidence rate does not vanish completely, but drops to a minimum. The deviations of the two latter cases from an ideal scenario are caused by the non-perfect indistinguishability (partial distinguishability) of the single photons provided by the SPDC source. In particular, the deviation from zero of the coincidences when $\Delta\beta = 2\kappa$ directly corresponds to the difference of the HOM-dip visibility from one, which was approximately 80% at the non-detuned DC in this setting.

In this way, an innovative scheme for the on-chip generation of two-photon path-entangled states with different mode-exchange symmetry was introduced theoretically as well as experimentally. Moreover, detuned DCs may become a useful tool as Hadamard gate for path-entangled photonic qubits as well as state provider for studies on fermionic, bosonic, and anyonic QWs.

5.2. Two-photon N00N states in a photonic Bloch oscillator lattices

In the solid state system considered by Felix Bloch electrons are supposed to exhibit BOs under the influence of an external constant electric field leading to a linearly tilted potential. Consequently, in the photonic regime, BOs occur when light fields traverse a waveguide lattices with a linear potential gradient, that is, a ramp in the propagation constant distribution as depicted in Fig. 5.4(a) & (b). Hence, the Heisenberg equation of motion becomes (see Eq. 2.10):

$$-\mathrm{i}\frac{\mathrm{d}\,\hat{a}_q^\dagger}{\mathrm{d}z} = q\mathcal{B}\,\hat{a}_q^\dagger(z) + \kappa\left(\hat{a}_{q-1}^\dagger + \hat{a}_{q+1}^\dagger\right). \tag{5.6}$$

Here, κ denotes the nearest-neighbor coupling strength and $\mathcal{B}$ is the propagation constant difference between adjacent modes. Accordingly, the propagation length for a revival is given by the Bloch period $\lambda_\mathrm{B} = 2\pi/\mathcal{B}$ [104]. The potential ramp can be realized by inscribing the waveguides with different power or velocity. However, to observe BOs over a large number of sites the propagation constants cannot be tuned sufficiently strong without changing the inter-waveguide coupling κ. Therefore, it is more convenient to adopt the work by Lenz *et al.* where it is derived that bending the whole waveguide array yields an effective potential ramp (see Fig. 5.5) [112]. In doing so, the ramping parameter $\mathcal{B}$ is determined by the bending radius R as $\mathcal{B} = 2\pi n_\mathrm{eff} d/\lambda R$ for a given wavelength λ, a fixed waveguide spacing d, and the refractive index n_eff of the glass the guides are inscribed into. Along these lines, the bending radius controls the potential tilt, which itself defines the Bloch period. This way it is possible to observe BOs at different fractions of λ_B while keeping the physical length of the arrays constant. Although this affects the Bloch amplitude as well, resulting in a wave function broadening nearly equal for all propagation points of interest, it does not change the dynamics of any two-photon correlation function regarding its rate of propagation or bunching and anti-bunching behavior. In this manner several differently curved waveguide arrays where fabricated allowing investigations at $(0.1 \ldots 1)\lambda_\mathrm{B}$ while having identical physical lengths

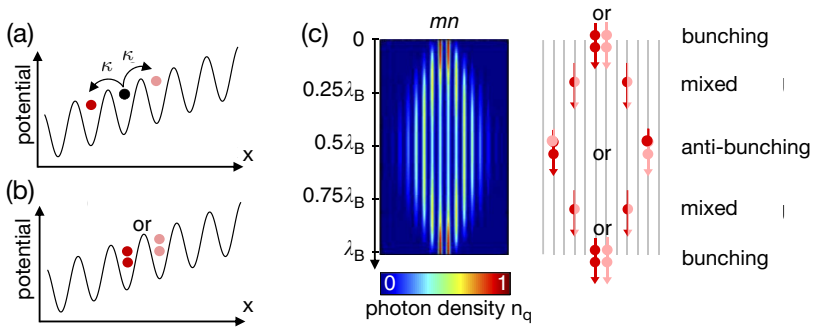

Figure 5.4.: Quantum Bloch oscillation. (a) Single-particle BO in a periodic lattice with external constant force. Due to coherent hopping to both sites path-entangled states occur. (b) BO of the entangled state $|\psi^{(\pi)}\rangle = \frac{1}{2}\left[(\hat{a}_m^\dagger)^2 - (\hat{a}_n^\dagger)^2\right]|0\rangle$ implying that both particles start in either of the adjacent excitation sites. (c) On the left side the evolution of the photon density for the symmetric state $|\psi^{(0)}\rangle$ shows the revival after one Bloch period. The right part depicts the correlation dynamics with transitions from bunching to anti-bunching during one Bloch period. Figure reproduced from [113].

of 6 cm.

A sketch of the complete setting for one lattice implementation is shown in Fig. 5.5. At the beginning a detuned DC provides the corresponding path-entangled input states $|\psi^{(\theta)}\rangle = \frac{1}{2}\left[(\hat{a}_0^\dagger)^2 + e^{i\theta}(\hat{a}_1^\dagger)^2\right]|0\rangle$ where θ determines the symmetry with respect to mode-exchange. In this work the focus is on symmetric ($\theta = 0$) and anti-symmetric ($\theta = \pi$) input states, which directly enter the curved Bloch oscillator lattice consisting of 16 waveguides. At the end a complex 3D fan-out segment ensures the interfacing with a fiber array attached to the chip and routing the emerging photons to detectors. As in Sec. 3.1 the intricate fan-out geometry originates from minimizing any further interaction between the waveguide modes in this section. In this vein the photon density and the two-photon correlation function at the end of the Bloch oscillator lattice can be obtained. The periodic spreading and in particular the re-localization after one Bloch cycle can be clearly seen by the photon density $n_q(z)$ at different fractions of the Bloch period in Fig. 5.6. Naturally, both input states yield the same dynamics, which coincides with the numerical simulations. The photon densities were extracted as the row sums of the correlation measurements as $n_q = \sum_r \Gamma_{q,r}$. The obtained revival probabilities at λ_B were 0.92 ± 0.02 for $|\psi^{(0)}\rangle$

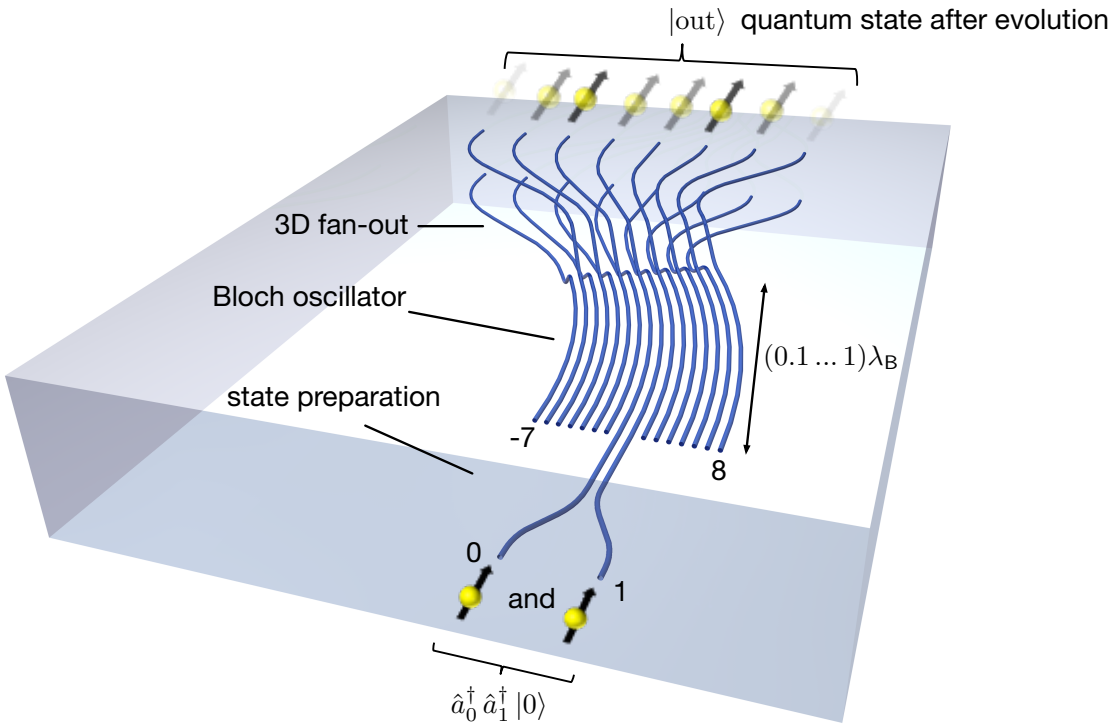

Figure 5.5.: Experimental implementation of Bloch oscillations of two-photon N00N states. The centerpiece is the curved Bloch oscillator lattice consisting of 16 evanescently coupled curved waveguides. It is connected to a detuned directional coupler for state preparation at its beginning and a fan-out section at its end. Figure reproduced from [113].

and 0.94 ± 0.01 for $|\psi^{(\pi)}\rangle$ demonstrating the capability of waveguide Bloch lattices to preserve coherence over an entire Bloch cycle.

As discussed in the theoretical work of Bromberg *et al.* the ramping potential is supposed to cause the photons to oscillate between bunched and antibunched states despite the fact that they are spatially separated during a Bloch cycle [106]. Hence, correlation turning points at particular propagation distances are predicted. The oscillations manifest themselves as a cyclic behavior of the two-photon correlation function and their period inversely scales with the number of photons N of the regarding N00N state. In order to obtain the first experimental results on this topic indistinguishable photon pairs were launched into the waveguide structures shown in Fig. 5.5 and their output correlations were measured. The structures differ in their effective propagation length as

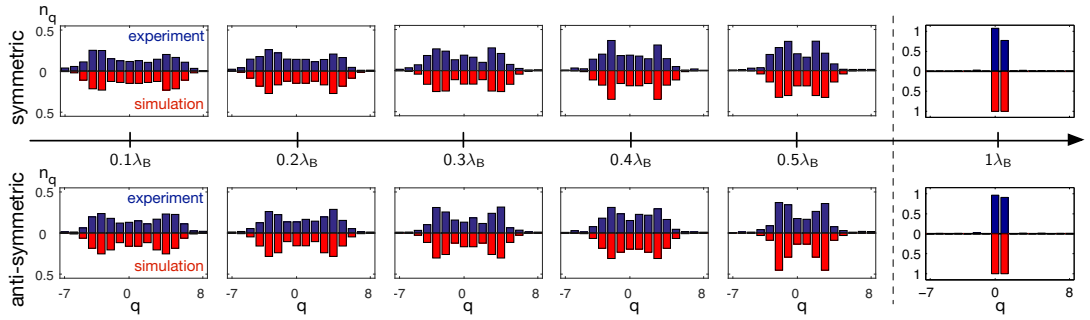

Figure 5.6.: Average photon number at different fraction of a Bloch cycle. Both, the symmetric (top row) and anti-symmetric (bottom row) input state yield the same distribution. Simulated (red) and measured (blue) results can be directly compared for propagation lengths of (0.1, 0.2, 0.3, 0.4, 0.5, 1)λ_B (left to right). Figure reproduced from [113].

well as in the input state preparation. The measurements were recorded over 15 min and have been corrected for slightly different detection efficiencies. Fig. 5.7 presents the experimental results for the symmetric two-photon N00N state $|\psi^{(0)}\rangle = \frac{1}{2}\left[(\hat{a}_0^\dagger)^2 + (\hat{a}_1^\dagger)^2\right]|0\rangle$ at various effective propagation lengths covering half a Bloch cycle. At a first glance, the correlation matrices unambiguously feature the predicted correlation cycle, thus, confirming theory. One can clearly notice the enhancement and reduction of certain quantum states during the BO. Taking a close look to the correlation evolution one notices that even though the input $|\psi^{(0)}\rangle$ is a highly-bunched state – both photons enter together either port "0" or "1"– they are suddenly split up and exhibit a distinct anti-bunching pattern at $0.1\lambda_B$. During further effective propagation this changes continuously crossing a correlation turning point between $0.2\lambda_B$ and $0.3\lambda_B$. Finally, at $0.5\lambda_B$ the photons are found most likely together (bunched), although the wave packet is spread over the entire lattice. Evidently, further effective propagation will reverse the dynamics and the two photons will inhabit their initial configuration at the full Bloch period $1\lambda_B$. The numerical simulations were performed as a best-fit scenario with $\kappa = 0.48\,\mathrm{cm}^{-1}$ and $\theta = (0.1 \pm 0.1)\pi$. Due to minor fabrication tolerances during the waveguide inscription the desired zero phase shift is slightly increased, yet very close to the ideal case. For getting a deeper insight into the correlation patterns, one can extract the inter-particle distance distribution describing the probability to find both photons within the distance

Δ of each other:

$$g(\Delta) = \frac{1}{\mathcal{N}} \sum_{q} \Gamma_{q,q+\Delta} \,. \tag{5.7}$$

Here, $\mathcal{N}$ are the number of matrix elements $\Gamma_{q,q+\Delta}$ satisfying $q + |\Delta| \leq 16$. As Fig. 5.7 reveals $g(\Delta)$ undergoes a transition from a double peak shape towards a distinct single peak form for growing effective propagation lengths. While the former one represents the situation to find the two photons maximally apart from another (anti-bunching) the latter one occurs when both photons are (very close) together (bunching). Thus, the inter-particle distance illustrates and also confirms the correlation cycle.

Turning now to the anti-symmetric input state $|\psi^{(\pi)}\rangle = \frac{1}{2}\left[(\hat{a}_0^\dagger)^2 - (\hat{a}_1^\dagger)^2\right]|0\rangle$ whose results are shown in Fig. 5.8. In contrast to the former case the correlation function starts with a bunching pattern. It also passes a turning point ending up with anti-bunching at $0.5\lambda_\mathrm{B}$. This behavior is also signalized by the inter-particle distance, whose evolution appears to be opposed as for the symmetric state. It starts with bunching and ends up with anti-bunching indicated by the single and double peak pattern, respectively. Simulations with $\kappa = 0.44\,\mathrm{cm}^{-1}$ and $\theta = (1.0 \pm 0.1)\pi$ gave the best-fit results highlighting the excellent state preparation via detuned DCs. It is worth to mention again, that bunching and anti-bunching are typical QW behaviors of separable states of two non-interacting bosons and fermions, respectively in a homogeneous lattice. Correspondingly, anyons will yield a mixed correlation pattern as found in the proximity of the turning points. In this way, it is possible to mimic QW statistics of bosons, fermions, and anyons by photons in a Bloch oscillator lattice with tailored propagation length.

For both, the symmetric and anti-symmetric input state one can quantify the conformity of the measured data $\Gamma_{q,r}^{(\mathrm{exp})}$ with the theoretical predictions $\Gamma_{q,r}^{(\mathrm{theory})}$

by the so-called similarity [36]

$$S = \frac{\left(\sum_{q,r} \sqrt{\Gamma_{q,r}^{(\mathrm{exp})} \Gamma_{q,r}^{(\mathrm{theory})}} \right)^2}{\sum_{q,r} \Gamma_{q,r}^{(\mathrm{exp})} \sum_{q,r} \Gamma_{q,r}^{(\mathrm{theory})}} . \tag{5.8}$$

The obtained values for both input states for the realized propagation lengths can be found in Tab. 5.2. They clearly show a very good agreement between theory and experiments.

Table 5.2.: Similarities for the two input state configurations and different propagation distances. Table reproduced from [113].

propagation length	$0.1\lambda_B$	$0.2\lambda_B$	$0.3\lambda_B$	$0.4\lambda_B$	$0.5\lambda_B$
symmetric state	0.950(4)	0.928(5)	0.924(2)	0.914(1)	0.907(1)
anti-symmetric state	0.931(3)	0.952(2)	0.939(6)	0.936(8)	0.833(2)

Additionally, one can have a look on the non-classicality of the two-photon correlations by calculating the violations of their Bell-like inequality (see Sec. 2.3). Fig. 5.9(top row) images two exemplary violation matrices $V_{q,r}$ for the symmetric and anti-symmetric input state after and before the correlation turning point at $0.4\lambda_B$ and $0.1\lambda_B$, respectively. Both show distinct violations of up to $23\sigma_{q,r}$ (standard deviations based on photon counting statistics), and thus, proving the genuine quantum nature of the correlations. Moreover, to unambiguously demonstrate that the origin of the quantum correlations lies in the indistinguishability of the photons, *distinguishable* photon pairs (obtained by temporal delay) were sent into the samples. Exemplarily, the measured correlation matrices for $\theta = (0.1 \pm 0.1)\pi$ at $0.4\lambda_B$ and $\theta = (1.0 \pm 0.1)\pi$ at $0.1\lambda_B$ are presented in Fig. 5.9(middle row). They clearly differ from the results with indistinguishable photon pairs in Figs. 5.7 & 5.8. As distinguishable photons remain separable during the evolution they have a similar probability to separate or gather leading to the four peaks in the correlation maps. Correspondingly, they show no violations of the Bell-like inequality.

Figure 5.7.: Experimental Bloch oscillations of symmetric N00N states. Measured and calculated correlation matrices together with the inter-particle distances (top to bottom) for propagation lengths $(0.1 \ldots 0.5)\lambda_B$ (left to right). The correlations clearly change from anti-bunching to bunching passing a correlation turning point at $0.25\lambda_B$. Figure reproduced from [113].

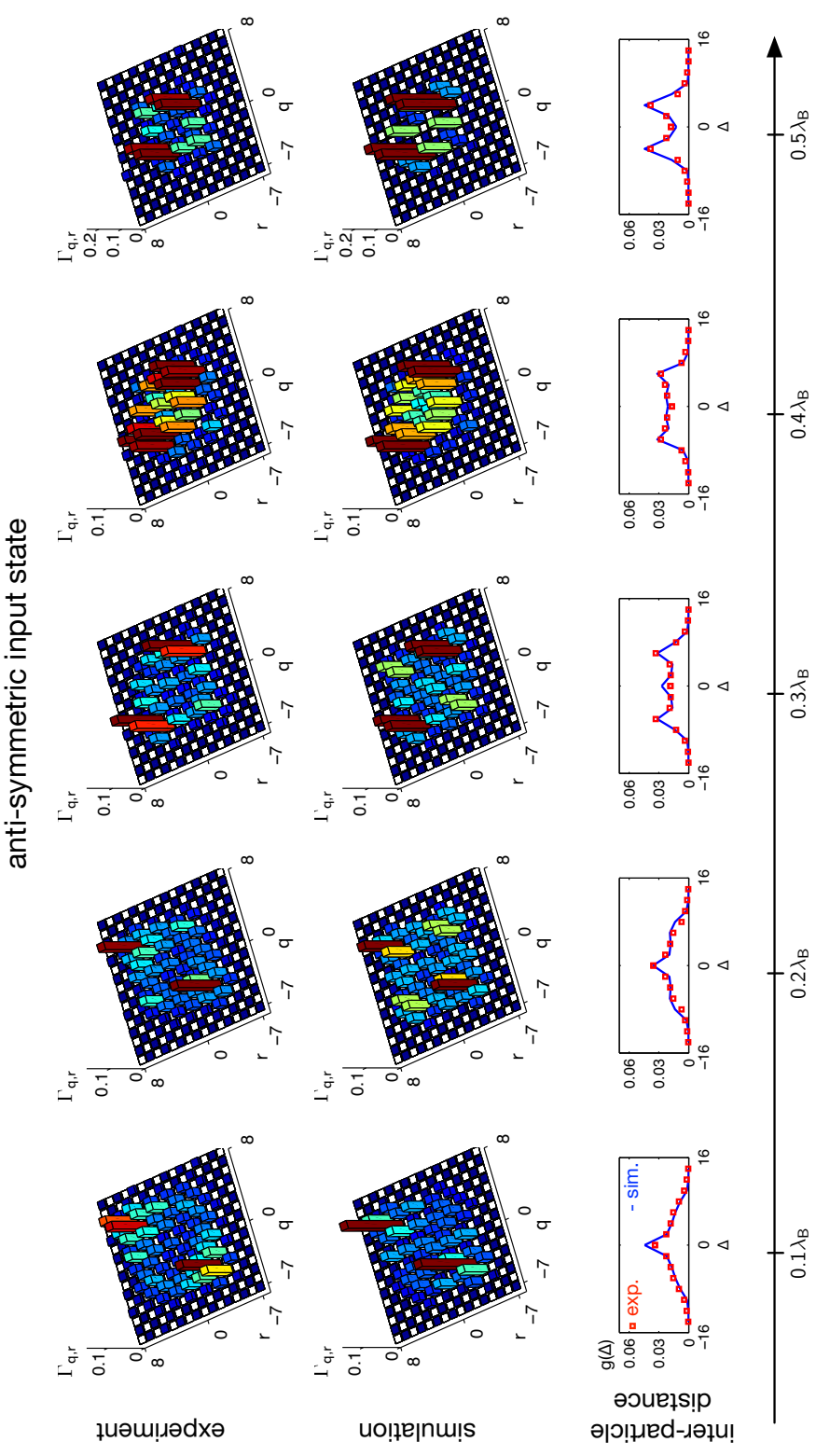

Figure 5.8.: Experimental Bloch oscillations of anti-symmetric N00N states. Measured and calculated correlation matrices together with the inter-particle distances (top to bottom) for propagation lengths $(0.1 \ldots 0.5)\lambda_B$ (left to right). The correlations clearly change from bunching to anti-bunching passing a correlation turning point at $0.25\lambda_B$. Figure reproduced from [113].

Finally, to complete the view on how the correlations depend on the mode-exchange symmetry of the state in a Bloch oscillator lattice, the case of a partially symmetric input state is considered. The state $|\psi^{(\theta)}\rangle$ was again provided by a detuned DC with a best-fit phase of $\theta = (0.8 \pm 0.1)\pi$. The experiments were carried out at $0.3\lambda_B$ and the two-photon correlation map can be found in Fig. 5.9(bottom row). For better comparison of the impact of the symmetry it is presented along with the results from the symmetric and anti-symmetric input state at the corresponding evolution length. One can see the distinct change from bunching ($\theta = (0.1 \pm 0.1)\pi$) to anti-bunching ($\theta = (1.0 \pm 0.1)\pi$) passing the case with concurrence of both ($\theta = (0.8 \pm 0.1)\pi$). Hence, it reveals the good control over the symmetry of the wavefunction, which causes an offset in the correlation cycle.

Summarized, in this chapter BOs of two-photon N00N states were investigated experimentally for the first time. Besides the re-localization after one Bloch cycle special attention was spent on the two-photon correlations that exhibit pure quantum features. The linear potential causes position depended phase shifts resulting in a correlation cycle. Here, the offset of the cycle is determined by the mode-exchange symmetry of the input state that is provided by detuned DCs. It turns out that BOs are capable of tailoring quantum correlations akin to those of bosons, fermions, and anyons, which may find application in topological quantum computing [114]. The results presented in this chapter can be also found in compressed form in [108] and [113].

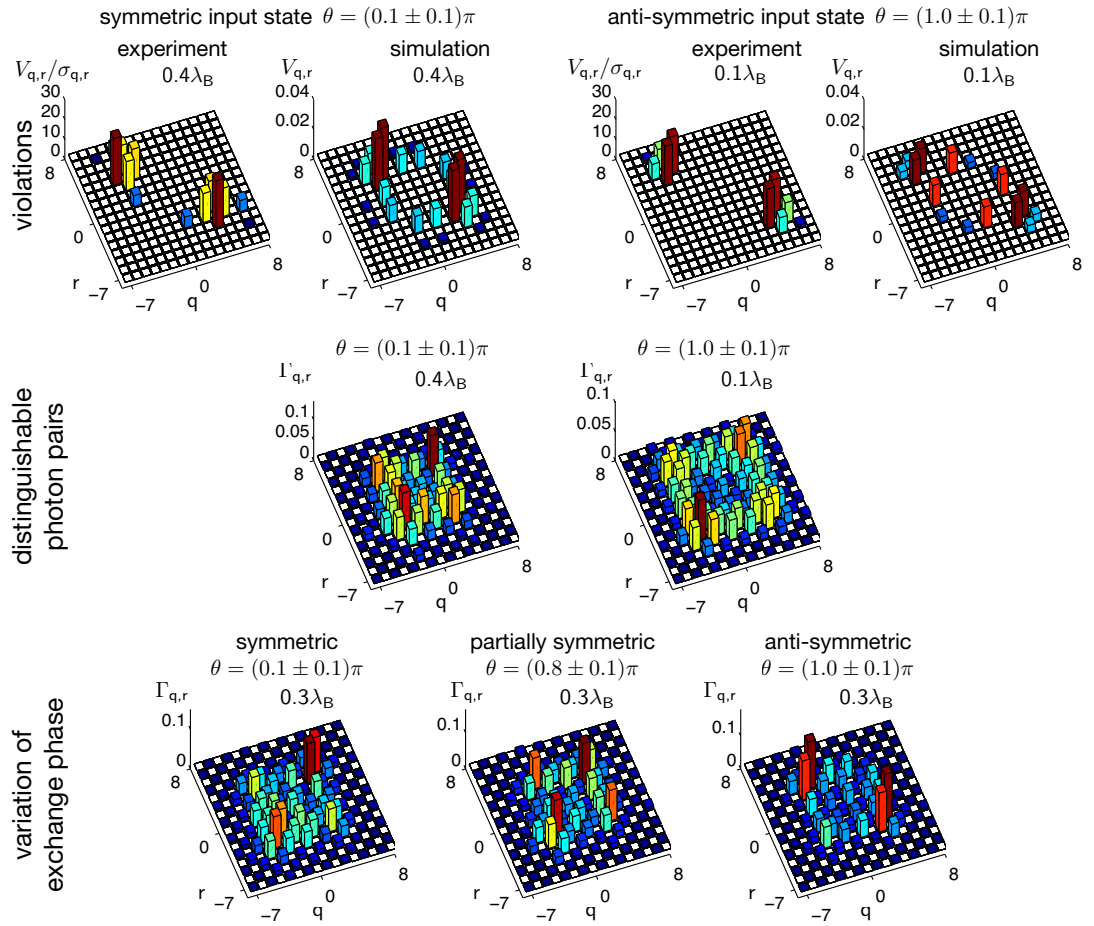

Figure 5.9.: Additional measurement data on N00N state Bloch oscillations. Violations $V_{q,r}$ are taken at $0.4\lambda_B$ for the symmetric input state and at $0.1\lambda_B$ for the anti-symmetric input state (top row). Both are compared with numerical simulations. For better illustration, negative values obeying the Bell-like inequality are set to zero. For comparison, correlation maps are recorded for distinguishable photon pairs at the same structures the violations are presented (middle row). Correlation maps for symmetric, partially symmetric and anti-symmetric input state at $0.3\lambda_B$ (bottom row) . One can clearly see the dependency of the correlation patterns on the mode exchange symmetry of the input state. Figure reproduced from [113].

CHAPTER 6

Conclusion & Outlook

Quantum walks feature, just as their classical counterparts, a variety of utilizations in both, understanding complex phenomena in nature and developing new trends in modern (quantum) technology. As such, single photons propagating through waveguide networks, monolithically embedded in a glass chip, are an excellent experimental platform to study QWs and, in doing so, gain a deeper understanding of related physical processes and develop new applications, especially in the field of quantum information processing.

The aim of this thesis was to extend the capabilities of fabrication technologies, implementation schemes, and applications for integrated-photonic QWs in the single- and two-photon regime. Along these lines, complex QWs under the influence of external forces were realized, multiple optical chips could be efficiently linked to extend their range, and advances in photon counting allowed for the characterization of the resulting quantum states of light.

Crucial to these efforts was the direct laser writing technique, since it allows the precise fabrication of tailored waveguide lattices and complex networks of

meticulously tuned directional couplers. In harnessing these unique capabilities, single-photon W-states spanning up to 16 entangled channels could be synthesized, distinctly exceeding the system size of such states realized on any competing platform. As evinced in Chapter 3, extended QWs were also instrumental in experimentally confirming this multipartite entanglement in a novel optical verification circuit. As possible application, the intrinsic quantum parallelism of W-states was shown to give rise to the generation of genuine random numbers without the need of any post-processing.

To fully describe the properties of a light field on the quantum level, detailed knowledge of its photon number distribution is indispensable. In this regard, photon number resolving detectors have been a subject of considerable attention. However, they have some intrinsic limits regarding dead time, high photon numbers and most importantly, they require enormous additional effort due to their need for cryogenic environments. Consequently *non*-number resolving on-off single-photon detectors are still widely used. Chapter 4 reveals and demonstrates a very different approach to solve this problem. To this end on-off detectors are employed in connection with a QW multiplexing device to, nonetheless, reliably infer whether a given state of light is of classical or quantum nature.

As last topic, quantum correlations of path-entangled N00N states undergoing Bloch oscillations, are the subject of Chapter 5. For this purpose, Bloch oscillator lattices with their characteristic linear potential have been implemented by curved waveguide arrays, which, compared to a physical gradient of the refractive index, offers the advantage of maintaining a strictly homogeneous coupling strength across the lattice. Particular attention is paid to the generation of entangled two-photon input states exhibiting different mode-exchange symmetry. As presented, they can be synthesized by detuned directional couplers where the detuning strength determines the exchange phase of the state. The two-photon correlation dynamics appears to be strongly dependent on the symmetry of the initial state. Generally the correlations undergo a cyclic transition within half a Bloch cycle from bunching to anti-bunching or vice versa, depending on the input state and hence, confirming theoretical predictions.

The obtained results in this thesis shed light upon certain aspects of photonic QWs. They clearly demonstrate that QWs of single photons and photon pairs in waveguide structures bear an enormous potential for applications in the fields of quantum computation and simulation. Progress in both research areas can be taken from the demonstration of chip-based multipartite entanglement verification, the coherent splitting of single photons with highest accuracy over multiple modes, and the introduction of assessing clicks for light state estimation. Moreover, QWs of two-photon N00N states in tailored Bloch oscillator lattices feature correlation patterns akin to two (non-interacting) bosons, fermions, or anyons evolving in standard homogeneous lattices. Therefore, they may be the tool of choice to get hands on anyonic QW dynamics leading to a deeper understanding of such exotic particles with fractional spin.

It should be emphasized that topics raised in this thesis offer a multitude on further research projects. While a select few have already been mentioned above as direct applications and implications of the results from this thesis, a number of further ones can be identified. So far, research was mainly limited to Hermitian systems, which by definition exhibit real eigenvalue spectra in their associated Hamiltonians. However, non-Hermitian systems offer a rich QW dynamics as well. In addition, in 1998 Bender and Boettcher revealed that Hamiltonians, which commute with the parity-time operator, can indeed exhibit completely real eigenvalues [115]. This observation was the starting point for the continuously growing field of PT-symmetry. The concept was carried over into the optical domain by introducing alternating gain-loss distributions [116–118]. As it was shown, such system dynamics does not change under a global loss transformation to lattices with alternating loss and no-loss sites, albeit they are not strictly PT-symmetric any more [119]. This is why they are often referred to as quasi-PT-symmetric. The question naturally arises as to how photon pairs will undergo QWs in such non-Hermitian lattices. A first attempt to answer this question was done by a theoretical investigation in [48]. There, a mathematical framework to efficiently calculate the propagation of two-photon correlations in waveguide lattices with arbitrary loss profile is given. It is applied to numerically determine the dynamics of various two-photon input states in quasi-PT-

symmetric arrays. Intriguing correlation patterns arise, which are very different from the Hermitian case. Of course, an experimental investigation would help to better understand these systems and may lead to a new field of non-Hermitian QWs with novel features and applications, especially in light of the fact that nature is usually not Hermitian. Yet, practical limits will be set due to losses, which will drastically lower any output photon count rates. A possible implementation of highly controllable losses in waveguides is presented in [120] by sinusoidal undulation of the guides along the propagation direction.

To overcome certain limits in photon detection caused by losses during the propagation in waveguides, several technical improvements suggest themselves. Waveguides in different glass types can be explored to minimize propagation losses. Further, as mentioned in Sec. 2.4, modifying the inscription process can lead to better mode matching with standard optical fibers and hence, reduce interfacing losses. A very effective alternative will be the application of a brighter source. Down-conversion sources arranged in a Sagnac setting with a periodically poled potassium titanyl phosphate crystal deliver collinear polarization-entangled photon pairs at very high rate [121–123]. Additionally, multi-photon events are considerably likely in the pulsed pump regime [124], drastically enlarging the Hilbert space of any associated QW.

The complexity of QWs can also be increased by extending them to higher dimensions. In the realm of waveguide lattices one spatial dimension is dedicated to the longitudinal evolution axis, leaving only two spatial transverse dimensions for QWs. Hence, another degree of freedom needs to be exploited and can be found in polarization [125]. Due to their inherent birefringence, laser-written waveguides exhibit distinct propagation constants for horizontally and vertically polarized light, respectively. This difference in the propagation constants is in the same order of magnitude as the hopping rates between adjacent guides and can be tuned by the inscription parameters (velocity and pulse power). Consequently, diagonally polarized light (representing a balanced superposition of horizontal and vertical polarization) will be transformed to anti-diagonally polarized light (π phase difference between horizontal and vertical polarization) after a characteristic propagation length. Doubling the length con-

verts the light back to its input configuration and so forth. By implication this introduces an additional dimension with two sites. In this vein, photonic QWs on various three-dimensional structures like on a cube or bi-layer graphene are possible and promise exceptional features [126]. The accompanied experimental efforts will grow strongly, since half-wave plates and polarizers or polarization dependent beam displacer have to be included – ideally on-chip. In spite of that, a manifold of new lattices can be implemented raising integrated photonic QWs to a whole new level.

Finally, it will be interesting to explore the rich physics that arise at the intersection of quantum optics and topology. Topological physics deals with geometrical properties of any mathematical space associated to a physical system. That properties are invariant to continuous deformations. For some time this field has attracted the attention of many research groups and prominent examples are the quantum hall effect [127] or topological insulators [128]. The latter one has also been realized in photonic waveguide structures [129]. There, edge states of photonic graphene have been demonstrated to be topologically immune to scattering at defects. Several questions arise: How does this work in the single-photon regime? Can entanglement be topologically protected? And what happens to an entangled photon pair, which is either prepared in the protected edge state or sent into the bulk? Recently, first attempts to address these issues have been made by [130] and [131].

In conclusion, this thesis yields new perspectives in the topic of photonic QWs. Novel application were introduced and sophisticated reliably-operating quantum networks are brought a step closer. The results pave the way for robust, scalable, and efficient on-chip quantum simulators that hopefully unravel some of nature's mysteries like fundamental biochemical transport processes.

APPENDIX A

Coherent states

This chapter briefly recaps the important points on the topic of coherent states with respect to understand its statistical properties that play an important role in Chapter 4. A complete and in-depth description can be found in [42] or [43].

While the number state (Fock state) is the eigenstate of the photon number operator ($\hat{n}\,|n\rangle = \hat{a}^\dagger \hat{a}\,|n\rangle = n\,|n\rangle$) the eigenstates of the annihilation operator is called coherent state:

$$\hat{a}\,|\alpha\rangle = \alpha\,|\alpha\rangle\ , \tag{A.1}$$

with the in general complex eigenvalue α (since $\hat{a}$ is non-Hermitian). Naturally, it can be expressed in terms of the number states such that the above eigenvalue equation becomes

$$\hat{a}\,|\alpha\rangle = \hat{a}\sum_{n=0}^{\infty} C_n\,|n\rangle = \sum_{n=0}^{\infty} C_n\sqrt{n}\,|n-1\rangle = \alpha\sum_{n=0}^{\infty} C_n\,|n\rangle\ . \tag{A.2}$$

From that follows $C_n\sqrt{n} = \alpha C_{n-1}$ or in other notation

$$C_n = \frac{\alpha}{\sqrt{n}} C_{n-1} = \frac{\alpha^2}{\sqrt{n(n-1)}} C_{n-2} = \ldots = \frac{\alpha^n}{\sqrt{n!}} C_0 \,. \tag{A.3}$$

Together with the normalization

$$1 = \langle \alpha | \alpha \rangle = |C_0|^2 \sum_{n=0}^{\infty} \sum_{n'=0}^{\infty} \frac{{\alpha^*}^n \alpha^{n'}}{\sqrt{n!n'!}} \langle n | n' \rangle = |C_0|^2 \sum_{n=0}^{\infty} \frac{|\alpha|^{2n}}{n!} = |C_0|^2 \mathrm{e}^{|\alpha|^2} \,, \tag{A.4}$$

one finds

$$|\alpha\rangle = \mathrm{e}^{-\frac{|\alpha|^2}{2}} \sum_{n=0}^{\infty} \frac{\alpha^n}{\sqrt{n!}} |n\rangle = \mathrm{e}^{-\frac{|\alpha|^2}{2}} \mathrm{e}^{\alpha\, \hat{a}^\dagger} |0\rangle \ . \tag{A.5}$$

Interestingly, the complex number α relates to the average number of photons in a light field prepared in a coherent state as $\langle n \rangle = \langle \alpha | \hat{n} | \alpha \rangle = |\alpha|^2$. In the same way, its fluctuation is given by $\langle (\Delta n)^2 \rangle = \langle n^2 \rangle - \langle n \rangle^2 = \langle n \rangle = |\alpha|^2$. Hence, the probability distribution to find n photons is (see main text below Eq. 4.2)

$$p_n = |\, \langle n | \alpha \rangle \,|^2 = \mathrm{e}^{-|\alpha|^2} \frac{|\alpha|^{2n}}{n!} = \mathrm{e}^{-\langle n \rangle} \frac{\langle n \rangle^n}{n!} \,, \tag{A.6}$$

which clearly is a Poissonian distribution and shown for $\langle n \rangle = 4$ in Fig. 4.1.

References

[1] P. Gupta, A. Goel, J. Lin, A. Sharma, D. Wang, and R. Zadeh, "WTF: The Who to Follow Service at Twitter," "Proceedings of the 22Nd International Conference on World Wide Web," WWW '13, 505–514, ACM, New York, NY, USA (2013).

[2] F. Bartumeus, M. G. E. da Luz, G. M. Viswanathan, and J. Catalan, "ANIMAL SEARCH STRATEGIES: A QUANTITATIVE RANDOM-WALK ANALYSIS," Ecology **86**, 3078 (2005).

[3] R. Engbert, K. Mergenthaler, P. Sinn, and A. Pikovsky, "An integrated model of fixational eye movements and microsaccades," Proceedings of the National Academy of Sciences **108**, E765 (2011).

[4] B. Hughes, *Random Walks and Random Environments: Random environments*, Oxford science publications, Clarendon Press (1996).

[5] K. Pearson, "The Problem of the Random Walk," Nature **72**, 294 (1905).

[6] J. W. S. Rayleigh, "The Problem of the Random Walk," Nature **72**, 318 (1905).

[7] A. Einstein, "Zur Theorie der Brownschen Bewegung," Ann. Phys. **17**, 549 (1905).

[8] A. Einstein, "Über die von der molekularkinetischen Theorie der Wärme geforderte Bewegung von in ruhenden Flüssigkeiten suspendierten Teilchen," Ann. Phys. **322**, 549 (1905).

[9] M. von Smoluchowski, "Zur kinetischen Theorie der Brownschen Molekularbewegung und der Suspensionen," Ann. Phys. **326**, 756 (1906).

[10] J. B. Perrin, "Mouvement brownien et réalité moléculaire," Ann. Chim. Phys. **18**, 5 (1909).

[11] Z. Bar-Yossef and M. Gurevich, "Random Sampling from a Search Engine's Index," J. ACM **55**, 24:1 (2008).

[12] A. Ariño and S. L. Pimm, "On the nature of population extremes," Evol. Ecol. **9**, 429 (1995).

[13] M. F. Shlesinger, "Random walks: Follow the money," Nature Phys. **2**, 69 (2006).

[14] Y. Aharonov, L. Davidovich, and N. Zagury, "Quantum random walks," Phys. Rev. A **48**, 1687 (1993).

[15] J. Kempe, "Quantum random walks: An introductory overview," Contemp. Phys. **44**, 307 (2003).

[16] R. P. Feynman and A. R. Hibbs, *Quantum Mechanics and Path Integrals*, McGraw-Hill, New-York (1965).

[17] L. K. Grover, "A fast quantum mechanical algorithm for database search," arXiv:quant-ph/9605043 (1996).

[18] A. M. Childs, "Universal Computation by Quantum Walk," Phys. Rev. Lett. **102**, 180501 (2009).

[19] A. M. Childs, D. Gosset, and Z. Webb, "Universal Computation by Multiparticle Quantum Walk," Science **339**, 791 (2013).

[20] G. S. Engel, T. R. Calhoun, E. L. Read, T.-K. Ahn, T. Mancal, Y.-C. Cheng, R. E. Blankenship, and G. R. Fleming, "Evidence for wavelike energy transfer through quantum coherence in photosynthetic systems," Nature **446**, 782 (2007).

[21] S. Lloyd, "A quantum of natural selection," Nature Phys. **5**, 164 (2009).

[22] M. Karski, L. Förster, J.-M. Choi, A. Steffen, W. Alt, D. Meschede, and A. Widera, "Quantum Walk in Position Space with Single Optically Trapped Atoms," Science **325**, 174 (2009).

[23] G. Summy and S. Wimberger, "Quantum random walk of a Bose-Einstein condensate in momentum space," Phys. Rev. A **93**, 023638 (2016).

[24] F. Zähringer, G. Kirchmair, R. Gerritsma, E. Solano, R. Blatt, and C. F. Roos, "Realization of a Quantum Walk with One and Two Trapped Ions," Phys. Rev. Lett. **104**, 100503 (2010).

[25] R. Blatt and C. F. Roos, "Quantum simulations with trapped ions," Nature Phys. **8**, 277 (2012).

[26] J. Du, H. Li, X. Xu, M. Shi, J. Wu, X. Zhou, and R. Han, "Experimental implementation of the quantum random-walk algorithm," Phys. Rev. A **67**, 042316 (2003).

[27] C. A. Ryan, M. Laforest, J. C. Boileau, and R. Laflamme, "Experimental implementation of a discrete-time quantum random walk on an NMR quantum-information processor," Phys. Rev. A **72**, 062317 (2005).

[28] M. W. Johnson, M. H. S. Amin, S. Gildert, T. Lanting, F. Hamze, N. Dickson, R. Harris, A. J. Berkley, J. Johansson, P. Bunyk, E. M. Chapple, C. Enderud, J. P. Hilton, K. Karimi, E. Ladizinsky, N. Ladizinsky, T. Oh, I. Perminov, C. Rich, M. C. Thom, E. Tolkacheva, C. J. S. Truncik, S. Uchaikin, J. Wang, B. Wilson, and G. Rose, "Quantum annealing with manufactured spins," Nature **473**, 194 (2011).

[29] A. Schreiber, K. N. Cassemiro, V. Potoček, A. Gábris, P. J. Mosley, E. Andersson, I. Jex, and C. Silberhorn, "Photons Walking the Line: A Quantum Walk with Adjustable Coin Operations," Phys. Rev. Lett. **104**, 050502 (2010).

[30] M. A. Broome, A. Fedrizzi, B. P. Lanyon, I. Kassal, A. Aspuru-Guzik, and A. G. White, "Discrete Single-Photon Quantum Walks with Tunable Decoherence," Phys. Rev. Lett. **104**, 153602 (2010).

[31] L. Sansoni, F. Sciarrino, G. Vallone, P. Mataloni, A. Crespi, R. Ramponi, and R. Osellame, "Two-Particle Bosonic-Fermionic Quantum Walk via Integrated Photonics," Phys. Rev. Lett. **108**, 010502 (2012).

[32] M. Gräfe, R. Heilmann, M. Lebugle, D. Guzman-Silva, A. Perez-Leija, and A. Szameit, "Integrated photonic quantum walks," J. Opt. **18**, 103002 (2016).

[33] K. M. Davis, K. Miura, N. Sugimoto, and K. Hirao, "Writing waveguides in glass with a femtosecond laser," Opt. Lett. **21**, 1729 (1996).

[34] T. Meany, M. Gräfe, R. Heilmann, A. Perez-Leija, S. Gross, M. J. Steel, M. J. Withford, and A. Szameit, "Laser written circuits for quantum photonics," Laser Photon. Rev. **9**, 363 (2015).

[35] Y. Bromberg, Y. Lahini, R. Morandotti, and Y. Silberberg, "Quantum and Classical Correlations in Waveguide Lattices," Phys. Rev. Lett. **102**, 253904 (2009).

[36] A. Peruzzo, M. Lobino, J. C. F. Matthews, N. Matsuda, A. Politi, K. Poulios, X.-Q. Zhou, Y. Lahini, N. Ismail, K. Wörhoff, Y. Bromberg, Y. Silberberg, M. Thompson, and J. O'Brien, "Quantum Walks of Correlated Photons," Science **329**, 1500 (2010).

[37] E. Martin-Lopez, A. Laing, T. Lawson, R. Alvarez, X.-Q. Zhou, and J. L. O'Brien, "Experimental realization of Shor's quantum factoring algorithm using qubit recycling," Nat. Photon. **6**, 773 (2012).

[38] B. J. Metcalf, J. B. Spring, P. C. Humphreys, N. Thomas-Peter, M. Barbieri, W. S. Kolthammer, X.-M. Jin, N. K. Langford, D. Kundys, J. C. Gates, B. J. Smith, P. G. R. Smith, and I. A. Walmsley, "Quantum teleportation on a photonic chip," Nat. Photon. **8**, 770 (2014).

[39] J. B. Spring, B. J. Metcalf, P. C. Humphreys, W. S. Kolthammer, X.-M. Jin, M. Barbieri, A. Datta, N. Thomas-Peter, N. K. Langford, D. Kundys, J. C. Gates, B. J. Smith, P. G. R. Smith, and I. A. Walmsley, "Boson Sampling on a Photonic Chip," Science **339**, 798 (2013).

[40] M. Tillmann, B. Dakic, R. Heilmann, S. Nolte, A. Szameit, and P. Walther, "Experimental boson sampling," Nat. Photon. **7**, 540 (2013).

[41] A. Crespi, R. Osellame, R. Ramponi, D. J. Brod, E. F. Galvao, N. Spagnolo, C. Vitelli, E. Maiorino, P. Mataloni, and F. Sciarrino, "Integrated multimode interferometers with arbitrary designs for photonic boson sampling," Nat. Photon. **7**, 545 (2013).

[42] L. Mandel and E. Wolf, *Optical Coherence and Quantum Optics*, Cambridge University Press (1995).

[43] C. C. Gerry and P. L. Knight, *Introductory Quantum Optics*, McGraw-Hill, New-York (2000).

[44] R. A. Campos, B. E. A. Saleh, and M. C. Teich, "Quantum-mechanical lossless beam splitter: SU(2) symmetry and photon statistics," Phys. Rev. A **40**, 1371 (1989).

[45] W. K. Lai, V. Buek, and P. L. Knight, "Nonclassical fields in a linear directional coupler," Phys. Rev. A **43**, 6323 (1991).

[46] A. L. Jones, "Coupling of Optical Fibers and Scattering in Fibers," J. Opt. Soc. Am. **55**, 261 (1965).

[47] D. N. Christodoulides, F. Lederer, and Y. Silberberg, "Discretizing light behaviour in linear and nonlinear waveguide lattices," Nature **424**, 817 (2003).

[48] M. Gräfe, R. Heilmann, R. Keil, T. Eichelkraut, M. Heinrich, S. Nolte, and A. Szameit, "Correlations of indistinguishable particles in non-Hermitian lattices," New J. Phys. **15**, 033008 (2013).

[49] H. S. Eisenberg, Y. Silberberg, R. Morandotti, A. R. Boyd, and J. S. Aitchison, "Discrete Spatial Optical Solitons in Waveguide Arrays," Phys. Rev. Lett. **81**, 3383 (1998).

[50] C. K. Hong, Z. Y. Ou, and L. Mandel, "Measurement of subpicosecond time intervals between two photons by interference," Phys. Rev. Lett. **59**, 2044 (1987).

[51] A. Politi, M. J. Cryan, J. G. Rarity, S. Yu, and J. L. O'Brien, "Silica-on-Silicon Waveguide Quantum Circuits," Science **320**, 646 (2008).

[52] R. Keil, *Quantum random walks in waveguide lattices Quantum random walks in waveguide lattices Quantum random walks in waveguide lattices Quantum random walks in waveguide lattices Quantum random walks in waveguide lattices*, Ph.D. thesis, Friedrich-Schiller-Universität Jena (2013).

[53] J. L. O'Brien, A. Furusawa, and J. Vuckovic, "Photonic quantum technologies," Nat. Photon. **3**, 687 (2009).

[54] A. Szameit and S. Nolte, "Discrete optics in femtosecond-laser-written photonic structures," J. Phys. B **43**, 163001 (2010).

[55] A. Yariv, *Quantum electronics*, Wiley (1989).

[56] Y. Shih, "Entangled biphoton source - property and preparation," Rep. Prog. Phys. **66**, 1009 (2003).

[57] D. Fukuda, G. Fujii, T. Numata, K. Amemiya, A. Yoshizawa, H. Tsuchida, H. Fujino, H. Ishii, T. Itatani, S. Inoue, and T. Zama, "Titanium-based transition-edge photon number resolving detector with 98% detection efficiency with index-matched small-gap fiber coupling," Opt. Express **19**, 870 (2011).

[58] B. Calkins, P. L. Mennea, A. E. Lita, B. J. Metcalf, W. S. Kolthammer, A. Lamas-Linares, J. B. Spring, P. C. Humphreys, R. P. Mirin, J. C. Gates, P. G. R. Smith, I. A. Walmsley, T. Gerrits, and S. W. Nam, "High quantum-efficiency photon-number-resolving detector for photonic on-chip information processing," Opt. Express **21**, 22657 (2013).

[59] R. H. Hadfield, "Single-photon detectors for optical quantum information applications," Nat. Photon. **3**, 696 (2009).

[60] H. A. Carteret, N. Linden, S. Popescu, and A. Sudbery, "Multiparticle Entanglement," Found. Phys. **29**, 527 (1999).

[61] I. Afek, O. Ambar, and Y. Silberberg, "High-NOON States by Mixing Quantum and Classical Light," Science **328**, 879 (2010).

[62] M. F. Riedel, P. Böhi, Y. Li, T. W. Hänsch, A. Sinatra, and P. Treutlein, "Atom-chip-based generation of entanglement for quantum metrology," Nature **464**, 1170 (2010).

[63] M. Walter, B. Doran, D. Gross, and M. Christandl, "Entanglement Polytopes: Multiparticle Entanglement from Single-Particle Information," Science **340**, 1205 (2013).

[64] W. Dür, G. Vidal, and J. I. Cirac, "Three qubits can be entangled in two inequivalent ways," Phys. Rev. A **62**, 062314 (2000).

[65] D. Bruß, D. P. DiVincenzo, A. Ekert, C. A. Fuchs, C. Macchiavello, and J. A. Smolin, "Optimal universal and state-dependent quantum cloning," Phys. Rev. A **57**, 2368 (1998).

[66] K. Banaszek and K. Wódkiewicz, "Testing Quantum Nonlocality in Phase Space," Phys. Rev. Lett. **82**, 2009 (1999).

[67] Y. Aharonov and L. Vaidman, "Nonlocal aspects of a quantum wave," Phys. Rev. A **61**, 052108 (2000).

[68] B.-S. Shi and A. Tomita, "Teleportation of an unknown state by W state," Phys. Lett. A **296**, 161 (2002).

[69] J. Joo, Y.-J. Park, S. Oh, and J. Kim, "Quantum teleportation via a W state," New J. Phys. **5**, 136 (2003).

[70] J. Dunningham and V. Vedral, "Nonlocality of a Single Particle," Phys. Rev. Lett. **99**, 180404 (2007).

[71] H. Yuan, J. Song, X.-Y. Liu, S. Cheng, K. Hou, and L.-F. Han, "Deterministic secure quantum communication with four-qubit W states," Int. J. Quantum Inf. **09**, 607 (2011).

[72] O. Morin, J.-D. Bancal, M. Ho, P. Sekatski, V. D'Auria, N. Gisin, J. Laurat, and N. Sangouard, "Witnessing Trustworthy Single-Photon Entanglement with Local Homodyne Measurements," Phys. Rev. Lett. **110**, 130401 (2013).

[73] J. B. Brask, R. Chaves, and N. Brunner, "Testing nonlocality of a single photon without a shared reference frame," Phys. Rev. A **88**, 012111 (2013).

[74] A. Rai and G. S. Agarwal, "Possibility of coherent phenomena such as Bloch oscillations with single photons via *W* states," Phys. Rev. A **79**, 053849 (2009).

[75] K. Fujii, H. Maeda, and K. Yamamoto, "Robust and scalable scheme to generate large-scale entanglement webs," Phys. Rev. A **83**, 050303 (2011).

[76] M. Eibl, N. Kiesel, M. Bourennane, C. Kurtsiefer, and H. Weinfurter, "Experimental Realization of a Three-Qubit Entangled *W* State," Phys. Rev. Lett. **92**, 077901 (2004).

[77] S. B. Papp, K. S. Choi, H. Deng, P. Lougovski, S. J. van Enk, and H. J. Kimble, "Characterization of Multipartite Entanglement for One Photon Shared Among Four Optical Modes," Science **324**, 764 (2009).

[78] K. S. Choi, A. Goban, S. B. Papp, S. J. van Enk, and H. J. Kimble, "Entanglement of spin waves among four quantum memories," Nature **468**, 412 (2010).

[79] S. Guha and J. H. Shapiro, "Reading boundless error-free bits using a single photon," Phys. Rev. A **87**, 062306 (2013).

[80] A. Perez-Leija, J. C. Hernandez-Herrejon, H. Moya-Cessa, A. Szameit, and D. N. Christodoulides, "Generating photon-encoded *W* states in multiport waveguide-array systems," Phys. Rev. A **87**, 013842 (2013).

[81] M. Gräfe, R. Heilmann, A. Perez-Leija, R. Keil, F. Dreisow, M. Heinrich, H. Moya-Cessa, S. Nolte, D. N. Christodoulides, and A. Szameit, "On-chip generation of high-order single-photon W-states," Nat. Photon. **8**, 791 (2014).

[82] P. Lougovski, S. J. van Enk, K. S. Choi, S. B. Papp, H. Deng, and H. J. Kimble, "Verifying multipartite mode entanglement of W states," New J. Phys. **11**, 063029 (2009).

[83] H. Nha, "Linear optical scheme to demonstrate genuine multipartite entanglement for single-particle *W* states," Phys. Rev. A **77**, 062328 (2008).

[84] O. Gühne and G. Tóth, "Entanglement detection," Phys. Rep. **474**, 1 (2009).

[85] C. Gabriel, C. Wittmann, D. Sych, R. Dong, W. Mauerer, U. L. Andersen, C. Marquardt, and G. Leuchs, "A generator for unique quantum random numbers based on vacuum states," Nat. Photon. **4**, 711 (2010).

[86] A. Figotin, I. Vitebskiy, V. Popovich, G. Stetsenko, S. Molchanov, A. Gordon, J. Quinn, and N. Stavrakas, "Random number generator based on the spontaneous alpha-decay," US Patent 6,745,217 (2004).

[87] H. Fürst, H. Weier, S. Nauerth, D. G. Marangon, C. Kurtsiefer, and H. Weinfurter, "High speed optical quantum random number generation," Opt. Express **18**, 13029 (2010).

[88] T. Jennewein, U. Achleitner, G. Weihs, H. Weinfurter, and A. Zeilinger, "A fast and compact quantum random number generator," Rev. Sci. Instrum. **71**, 1675 (2000).

[89] L. E. Bassham, A. L. Rukhin, J. Soto, J. R. Nechvatal, M. E. Smid, E. B. Barker, S. D. Leigh, M. Levenson, M. Vangel, D. L. Banks, N. A. Heckert, J. F. Dray, and S. Vo, "A statistical test suite for random and pseudorandom number generators for cryptographic applications," Technical report (2010).

[90] A. Predojević, S. Grabher, and G. Weihs, "Pulsed Sagnac source of polarization entangled photon pairs," Opt. Express **20**, 25022 (2012).

[91] F. Marsili, V. Verma, J. Stern, S. Harrington, A. E. Lita, T. Gerrits, I. Vayshenker, B. Baek, M. Shaw, R. Mirin, and S. Nam, "Detecting single infrared photons with 93% system efficiency," Nat. Photon. **7**, 210 (2013).

[92] F. E. Becerra, J. Fan, and A. Migdall, "Photon number resolution enables quantum receiver for realistic coherent optical communications," Nat. Photon. **9**, 48 (2015).

[93] L. Mandel, "Sub-Poissonian photon statistics in resonance fluorescence," Opt. Lett. **4**, 205 (1979).

[94] J. Sperling, W. Vogel, and G. S. Agarwal, "True photocounting statistics of multiple on-off detectors," Phys. Rev. A **85**, 023820 (2012).

[95] T. J. Bartley, G. Donati, X.-M. Jin, A. Datta, M. Barbieri, and I. A. Walmsley, "Direct Observation of Sub-Binomial Light," Phys. Rev. Lett. **110**, 173602 (2013).

[96] E. C. G. Sudarshan, "Equivalence of Semiclassical and Quantum Mechanical Descriptions of Statistical Light Beams," Phys. Rev. Lett. **10**, 277 (1963).

[97] R. J. Glauber, "Coherent and Incoherent States of the Radiation Field," Phys. Rev. **131**, 2766 (1963).

[98] P. L. Kelley and W. H. Kleiner, "Theory of Electromagnetic Field Measurement and Photoelectron Counting," Phys. Rev. **136**, A316 (1964).

[99] W. Vogel and D. Welsch, *Quantum Optics*, Wiley (2006).

[100] J. Sperling, W. Vogel, and G. S. Agarwal, "Sub-Binomial Light," Phys. Rev. Lett. **109**, 093601 (2012).

[101] R. Heilmann, J. Sperling, A. Perez-Leija, M. Gräfe, M. Heinrich, S. Nolte, W. Vogel, and A. Szameit, "Harnessing click detectors for the genuine characterization of light states," Sci. Rep. **6**, 19489 (2016).

[102] F. Bloch, "Über die Quantenmechanik der Elektronen in Kristallgittern," Z. Phys. **52**, 555 (1929).

[103] R. Morandotti, U. Peschel, J. Aitchison, H. Eisenberg, and Y. Silberberg, "Experimental observation of linear and nonlinear optical Bloch oscillations," Phys. Rev. Lett. **83**, 4756 (1999).

[104] T. Pertsch, P. Dannberg, W. Elflein, A. Bräuer, and F. Lederer, "Optical Bloch oscillations in temperature tuned waveguide arrays," Phys. Rev. Lett. **83**, 4752 (1999).

[105] F. Dreisow, A. Szameit, M. Heinrich, T. Pertsch, S. Nolte, A. Tünnermann, and S. Longhi, "Bloch-Zener oscillations in binary superlattices," Phys. Rev. Lett. **102**, 076802 (2009).

[106] Y. Bromberg, Y. Lahini, and Y. Silberberg, "Bloch oscillations of path-entangled photons," Phys. Rev. Lett. **105**, 263604 (2010).

[107] A. Crespi, R. Osellame, R. Ramponi, V. Giovannetti, R. Fazio, L. Sansoni, F. De Nicola, F. Sciarrino, and P. Mataloni, "Anderson localization of entangled photons in an integrated quantum walk," Nat. Photon. **7**, 322 (2013).

[108] M. Gräfe, R. Heilmann, S. Nolte, and A. Szameit, "On-chip generation of Einstein-Podolsky-Rosen states with arbitrary symmetry," Appl. Phys. Lett. **106**, 181106 (2015).

[109] J. C. F. Matthews, K. Poulios, J. D. A. Meinecke, A. Politi, A. Peruzzo, N. Ismail, K. Wörhoff, M. G. Thompson, and J. L. O'Brien, "Observing fermionic statistics with photons in arbitrary processes," Sci. Rep. **3** (2013).

[110] F. Wilczek, "Quantum Mechanics of Fractional-Spin Particles," Phys. Rev. Lett. **49**, 957 (1982).

[111] J. Myrheim, "Anyons," A. Comtet, T. Jolicœur, S. Ouvry, and F. David, editors, "Aspects topologiques de la physique en basse dimension. Topological aspects of low dimensional systems," volume 69 of *Les Houches - Ecole d'Ete de Physique Theorique*, 265, Springer Berlin Heidelberg (1999).

[112] G. Lenz, I. Talanina, and C. M. de Sterke, "Bloch Oscillations in an Array of Curved Optical Waveguides," Phys. Rev. Lett. **83**, 963 (1999).

[113] M. Lebugle, M. Gräfe, R. Heilmann, A. Perez-Leija, S. Nolte, and A. Szameit, "Experimental Observation of N00N States Bloch Oscillations," Nat. Commun. (2015).

[114] C. Nayak, S. H. Simon, A. Stern, M. Freedman, and S. Das Sarma, "Non-Abelian anyons and topological quantum computation," Rev. Mod. Phys. **80**, 1083 (2008).

[115] C. M. Bender and S. Boettcher, "Real Spectra in Non-Hermitian Hamiltonians Having PT Symmetry," Phys. Rev. Lett. **80**, 5243 (1998).

[116] R. El-Ganainy, K. G. Makris, D. N. Christodoulides, and Z. H. Musslimani, "Theory of coupled optical PT-symmetric structures," Opt. Lett. **32**, 2632 (2007).

[117] C. E. Ruter, K. G. Makris, R. El-Ganainy, D. N. Christodoulides, M. Segev, and D. Kip, "Observation of parity-time symmetry in optics," Nature Phys. **6**, 192 (2010).

[118] A. Regensburger, C. Bersch, M.-A. Miri, G. Onishchukov, D. N. Christodoulides, and U. Peschel, "Parity-time synthetic photonic lattices," Nature **488**, 167 (2012).

[119] M. Ornigotti and A. Szameit, "Quasi $\mathcal{PT}$ -symmetry in passive photonic lattices," J. Opt. **16**, 065501 (2014).

[120] T. Eichelkraut, S. Weimann, S. Stützer, S. Nolte, and A. Szameit, "Radiation-loss management in modulated waveguides," Opt. Lett. **39**, 6831 (2014).

[121] T. Kim, M. Fiorentino, and F. N. C. Wong, "Phase-stable source of polarization-entangled photons using a polarization Sagnac interferometer," Phys. Rev. A **73**, 012316 (2006).

[122] F. N. C. Wong, J. H. Shapiro, and T. Kim, "Efficient generation of polarization-entangled photons in a nonlinear crystal," Laser Phys. **16**, 1517 (2006).

[123] A. Fedrizzi, T. Herbst, A. Poppe, T. Jennewein, and A. Zeilinger, "A wavelength-tunable fiber-coupled source of narrowband entangled photons," Opt. Express **15**, 15377 (2007).

[124] O. Kuzucu and F. N. C. Wong, "Pulsed Sagnac source of narrow-band polarization-entangled photons," Phys. Rev. A **77**, 032314 (2008).

[125] O. Boada, A. Celi, J. I. Latorre, and M. Lewenstein, "Quantum Simulation of an Extra Dimension," Phys. Rev. Lett. **108**, 133001 (2012).

[126] C. Dittel, R. Keil, and G. Weihs, "Many-body quantum interference on hypercubes," Quantum Sci. Technol. **2**, 015003 (2017).

[127] K. von Klitzing, G. Dorda, and M. Pepper, "New Method for High-Accuracy Determination of the Fine-Structure Constant Based on Quantized Hall Resistance," Phys. Rev. Lett. **45**, 494 (1980).

[128] C. L. Kane and E. J. Mele, "Quantum Spin Hall Effect in Graphene," Phys. Rev. Lett. **95**, 226801 (2005).

[129] M. C. Rechtsman, J. M. Zeuner, Y. Plotnik, Y. Lumer, D. Podolsky, F. Dreisow, S. Nolte, M. Segev, and A. Szameit, "Photonic Floquet topological insulators," Nature **496**, 196 (2013).

[130] M. C. Rechtsman, Y. Lumer, Y. Plotnik, A. Perez-Leija, A. Szameit, and M. Segev, "Topological protection of photonic path entanglement," Optica **3**, 925 (2016).

[131] S. Mittal, V. V. Orre, and M. Hafezi, "Topologically robust transport of entangled photons in a 2D photonic system," Opt. Express **24**, 15631 (2016).

Acknowledgments

On the way towards the doctorate one encounters various ups and downs and hence, one can never achieve it without the help and understanding of other people. Therefore, I would like to give many thanks to all people whose support over the last few years has made this work possible.

First and foremost, it is a pleasure to express my deep gratitude to Prof. Dr. Alexander Szameit as he has not only been my supervisor but also mentor, advisor, idea generator, and most of all, friend. Numerous discussions about science and beyond as well as his exemplary enthusiasm when it comes to physics inspired me in many ways.

Further thanks go to Prof. Dr. Stefan Nolte who, as the head of the Ultrafast Optics department, enabled our subgroup to use the laser equipment in the lab and for fruitful discussions.

I am indebted to the people with whom I had the opportunity to cooperate during my work. In particular, Prof. Demetrios Christodoulides for bringing up the W-state topic as well as Prof. Dr. Werner Vogel and Dr. Jan Sperling for introducing the concept of the Q_B parameter.

In this regard, I owe many thanks to my (former) colleges and friends René Heilmann, whose exceptional lab skills still wow me; Dr. Armando Perez-Leija who is the smart theorist behind many of the projects from the last years; and Dr. Maxime Lebugle for pushing the quantum Bloch oscillations forward. In

this row I would like to add Dr. Robert Keil who brought me to the field of photonic quantum walks and whose critical feedback was very valuable for improving this thesis; Dr. Matthias Heinrich for very fruitful discussions and his linguistic corrections; and Dr. Felix Dreisow for teaching my the mysteries of the RegA system.

I am very thankful for the familial atmosphere provided by the Szameitonics and ultra fast optics group. I especially enjoyed all the moral-boosting funny moments with Klaus Bergner, Julia Zeuner, Daniel Richter, Christian Vetter aka "Vetti", and Lukas Maczewsky. And not to be forgotten, Tina Weichelt as additional member of the "Mittagsrunde".

Another note of thanks goes to the staff at the Institute of Applied Physics, in particular Christiane Otto for the meticulous and fast preparation of glass chips as well as towards Bodo Martin and his changing colleagues for taking care of the computers of the institute.

Despite not actively being a part of my work, I nevertheless want to say thank you to my family and friends for the countless joyful moments, which have always helped to free my mind and gain new motivation.

I am deeply grateful to my parents for their invaluable support on my way, for always believing in me, and for just being there when needed.

Lastly, but most importantly, I wish to thank my wife Christine from the depth of my heart, not only for her help, patience, and motivation, but for being the love of my life and making me every day notice what life is all about.

Zusammenfassung

Quantenzufallsbewegungen – sogenannte *Quantum Walks* (QWs) – sind das grundlegende Konzept hinter den Forschungsfeldern Quantencomputing und Quantensimulation. Als solche haben sie ein enormes Anwendungspotential in der Quanteninformationstechnologie. Auch die Natur bedient sich an QWs als grundlegenden Mechanismus für zahlreiche Phänomene. So basiert beispielsweise der hocheffiziente Energietransport in Lichtsammelkomplexen von Pflanzen während der Photosynthese auf QWs. Die vollständige Klärung dieses essentiellen Stoffwechselprozesses aus quantenphysikalischer Sicht ist nach wie vor ein offenes und stark beforschtes Gebiet.

Zum prinzipiellen Verständnis von QWs kann die quantenmechanische Version eines Galtonbretts dienen, bei dem das Kügelchen – der *Walker* – durch ein Quantenteilchen ersetzt wird. Im Gegensatz zum Kügelchen, welches an jedem Hindernis entweder nach links *oder* rechts springt, nimmt ein *Quantum Walker* einen Superpositionszustand aus links *und* rechts ein. Ermöglicht wird dies durch den Wellen-Teilchen-Dualismus, der eine kohärente Ausbreitung erlaubt und zu Interferenzeffekten führen kann. Hierbei sind QWs von ununterscheidbaren oder verschränkten Teilchen ebenso möglich und generieren aufgrund von Mehrteilcheninterferenz nicht-klassische Mehrteilchenkorrelationen.

Photonen sind aufgrund ihrer guten Kohärenzeigenschaft und Unempfindlichkeit gegenüber äußeren Einflüssen äußerst gut als Quantum Walker geeignet.

Kombiniert mit der Stabilität und Robustheit von Wellenleiterstrukturen, welche in einem kleinen monolithischen Glaschip eingebettet sind, steht ein vielseitiges System zur Untersuchung von QWs zur Verfügung. Hierbei können zahlreiche QW-Gitter in zwei Dimensionen realisiert werden (die dritte räumliche Dimension ist die longitudinale Ausbreitungsachse der Wellenleiter).

Das Ziel dieser Arbeit war, das Potential chip-basierter photonischer QWs auszubauen und neue Anwendungsmöglichkeiten zu erschließen. Hierbei wurden sowohl QWs einzelner als auch verschränkter Photonenpaare in komplexen Wellenleiternetzwerken untersucht. Mittels direktem Lasereinschreiben wurden verschiedene Wellenleiterstrukturen implementiert und ermöglichten damit QWs in Gittern mit externem Feld oder über zwei Chips hinweg, sowie die Weiterentwicklung der Photonendetektion.

W-Zustände sind vielteilig verschränkte Zustände und bieten äußerst interessante Anwendungsmöglichkeiten im Bereich abhörsicherer Kommunikation oder Teleportation. Sie sind nicht nur maximal-verschränkt, sondern zeigen auch eine intrinsische Robustheit gegenüber Verlusten. Kapitel 3 zeigt, wie mittels Netzwerken aus nahezu perfekten direktionalen 50:50 Kopplern als auch Wellenleitergittern mit maßgeschneiderten Koppelverteilungen experimentell Einzelphotonen-W-Zustände bis zur Ordnung 16 erzeugt werden können. Das heißt, ein einzelnes Photon ist kohärent über 16 Wellenleiter verteilt. Die damit verknüpfte vielteilige Verschränkung wird mit Hilfe eines QWs in einer Verifizierungsstruktur belegt. Die mit Einzelphotonen-W-Zuständen einhergehende Gleichverteilung der Wahrscheinlichkeit, in welchem der beteiligten Kanäle sich das Photon bei der Messung befindet, konnte zur effizienten Erzeugung von Zufallszahlen genutzt werden. Ströme von derart erzeugten Zufallszahlen bestanden ohne jegliche Nachbearbeitung alle Zufälligkeitstests des *National Institute of Standards and Technology*.

Die Natur eines Lichtfeldes – klassisch oder quantisch – ist eng mit seiner Photonenzahlstatistik verknüpft. Neuste photonenzahlauflösende Detektoren sind prinzipiell verfügbar, leiden allerdings an inhärenten Limitierungen in Bezug auf die Photonenzahl und Totzeit und sind aufgrund ihrer kryogenen Umge-

bung überaus kostspielig. Daher werden nach wie vor sehr häufig Klickdetektoren verwendet, welche *nicht* photonenzahlauflösend sind. Dementsprechend ist die Photonenstatistik mit solchen Detektoren nicht direkt zugänglich, sondern nur eine Photonenzähl- oder Klickverteilung. In Kapitel 4 wird experimentell dargelegt, wie nach Anwendung eines QW-Multiplexers diese Klickstatistik ausgewertet werden kann, um dennoch die Nicht-Klassizität eines Lichtfeldes festzustellen. Dies wird an zwei Lichtquellen – klassischem Laserlicht und Quantenlicht (getriggerte einzelne Photonen aus spontaner parametrischer Differenzfrequenzgenerierung) – demonstriert. Es zeigt sich, dass die Art des Lichtes selbst bei extrem geringen Photonenflüssen zuverlässig bestimmt werden kann. Überdies findet dieses Konzept Anwendung in der Charakterisierung von Photonenquellen, was ebenso erfolgreich getestet wurde.

Kapitel 5 behandelt Blochoszillationen von N00N-Zuständen. Blochoszillationen manifestieren sich als periodische Ausbreitung und Relokalisierung der Wellenfunktion während eines QWs in einem Gitter mit linearen Potentialgradienten. N00N-Zustände zweier Photonen wurden als pfadverschränkte Ausgangszustände eines direktionalen 50:50 Kopplers bereitgestellt (mit je einem von zwei ununterscheidbaren Photonen in den Eingängen). Mit der Einführung verstimmter direktionaler 50:50 Koppler kann die Modenaustauschsymmetrie der Eingangszustände effektiv gesteuert werden. Zwei-Photonen-Korrelationen nach QWs jener Zustände in Blochoszillatorgittern wurden gemessen und ausgewertet. In Übereinstimmung mit theoretischen Vorhersagen konnte ein zyklisches Verhalten von Bunching („Bündelung“) zu Anti-Bunching („Zerstreuung“), oder umgekehrt, experimentell nachgewiesen werden. Es zeigt sich eine direkte Abhängigkeit von der Symmetrie des Eingangszustandes. Auf diese Weise kann man durch den QW von N00N-Zuständen zweier Photonen nach einer bestimmten Länge in einem Blochoszillatorgitter Zwei-Photonen-Korrelationen ähnlich denen zweier (nicht-interagierenden) separabler Bosonen, Fermionen oder Anyonen in einem homogenen Gitter erhalten. Dies ermöglicht insbesondere die Untersuchung von Anyonen, welche als virtuelle Teilchen nur in geradzahligen Dimensionen existieren und somit experimentell nur schwer zugänglich sind.

Technische Verbesserungen wie modifizierte Wellenleiter mit Modengrößen, welche besser an deren optischer Fasern angepasst sind, sowie effizientere Photonenquellen (z. B. durch Verwendung eines periodisch gepolten Kaliumtitanylphosphatkristalls) ermöglichen bessere experimentelle Bedingungen und mehr Photonen als gleichzeitige Walker. Die Komplexität von QWs lässt sich nicht nur mit der Anzahl der beteiligten Photonen erhöhen, sondern auch mit der Anzahl der Dimensionen. Ein interessanter Ansatz wäre hier die Ausnutzung der intrinsischen Doppelbrechung direkt lasergeschriebener Wellenleiter, sodass als zusätzliche Dimension die Polarisation der Photonen genutzt werden kann, wenn auch nur als Freiheitsgrad mit zwei Werten. Ebenso wäre die Erweiterung auf nicht-hermitesche Systeme außerordentlich interessant und verspricht zahlreiche neue Erkenntnisse.

Die in dieser Arbeit erlangten Ergebnisse klären einige Aspekte photonischer QWs auf. Sie verdeutlichen das enorme Potential von QWs von einzelnen Photonen und Photonenpaaren in Wellenleiterstrukturen für Anwendungen im Bereich des Quantencomputings und der Quantensimulation. Durch den erfolgreichen chip-basierten Nachweis vielteiliger Verschränkung, die kohärente Verteilung einzelner Photonen über mehrere Moden mit höchster Genauigkeit und die Demonstration der Lichtfeldcharakterisierung basierend auf Klickstatistik können Forschritte in beiden Gebieten erzielt werden. Überdies hinaus erwiesen sich photonische Blochoszillatorgitter als mögliches Testsystem zur Erforschung anyonischer QWs, sodass ein tieferes und besseres Verständnis dieser exotischen Teilchen mit fraktionalem Spin erlangt werden kann.

List of own publications

[1] M. Gräfe*, R. Heilmann*, A. Perez-Leija*, R. Keil, F. Dreisow, M. Heinrich, H. Moya-Cessa, S. Nolte, D. N. Christodoulides, and A. Szameit, "On-chip generation of high-order single-photon W-states," Nat. Photon. **8**, 791 (2014).

[2] M. Gräfe and A. Szameit, "Two-particle quantum correlations at graphene edges." 2D Mater. **2**, 034005 (2015).

[3] M. Gräfe*, R. Heilmann*, R. Keil, T. Eichelkraut, M. Heinrich, S. Nolte, and A. Szameit, "Correlations of indistinguishable particles in non-hermitian lattices," New J. Phys. **15**, 059501 (2013).

[4] M. Gräfe, A. S. Solntsev, R. Keil, A. A. Sukhorukov, M. Heinrich, A. Tünnermann, S. Nolte, A. Szameit, and Y. S. Kivshar, "Biphoton generation in quadratic waveguide arrays: a classical optical simulation," Sci. Rep. **2**, 1 (2012).

[5] M. Gräfe, R. Heilmann, S. Nolte, and A. Szameit, "On-chip generation of Einstein-Podolsky-Rosen states with arbitrary symmetry," Appl. Phys. Lett. **106**, 181106 (2015).

[6] M. Gräfe, R. Heilmann, M. Lebugle, D. Guzman-Silva, A. Perez-Leija, and A. Szameit, Review on: "Integrated photonic quantum walks," J. Opt. **18**, 103002 (2016).

[7] M. Lebugle, M. Gräfe, R. Heilmann, A. Perez-Leija, S. Nolte, D. N. Christodoulides, and A. Szameit, "Experimental observation of N00N state Bloch oscillations," Nat. Commun. **6**, 8273 (2015).

[8] T. Meany, M. Gräfe, R. Heilmann, A. Perez-Leija, S. Gross, M. J. Steel, J. Withford, and A. Szameit, Review on: "Laser written circuits for quantum photonics," Laser Photon. Rev. **9**, 363 (2015).

[9] R. Heilmann, M. Gräfe, S. Nolte, and A. Szameit, "Arbitrary photonic wave plate operations on chip: Realizing hadamard, pauli-x, and rotation gates for polarisation qubits," Sci. Rep. **4**, 4118 (2014).

[10] R. Heilmann*, M. Gräfe*, S. Nolte, and A. Szameit, "A novel integrated quantum circuit for high-order W-state generation and its highly precise characterization," Sci. Bull. **60**, 96 (2015).

[11] R. Heilmann*, J. Sperling*, A. Perez-Leija*, M. Gräfe, M. Heinrich, S. Nolte, W. Vogel, and A. Szameit, "Harnessing click detectors for the genuine characterization of light states," Sci. Rep. **6**, 19489 (2016).

[12] R. Keil, B. Pressl, R. Heilmann, M. Gräfe, G. Weihs, and A. Szameit, "Direct measurement of second-order coupling in a waveguide lattice," Appl. Phys. Lett. **107**, 241104 (2015).

[13] D. N. Biggerstaff, R. Heilmann, A. A. Zecevik, M. Gräfe, M. A. Broome, A. Fedrizzi, S. Nolte, A. Szameit, A. G. White, and I. Kassal, "Enhancing coherent transport in a photonic network using controllable decoherence," Nat. Commun. **7**, 11282 (2016).

[14] R. Heilmann, R. Keil, M. Gräfe, S. Nolte, and A. Szameit, "Ultraprecise phase manipulation in integrated photonic quantum circuits with generalized directional couplers," Appl. Phys. Lett. **105**, 061111 (2014).

[15] S. Weimann*, A. Perez-Leija*, M. Lebugle*, R. Keil, M. Tichy, M. Gräfe, R. Heilmann, S. Nolte, H. Moya-Cessa, G. Weihs, D. N. Christodoulides, and A. Szameit, "Implementation of quantum and classical discrete fractional Fourier transforms," Nat. Commun. **7**, 11027 (2016).

[16] D. Guzman-Silva, R. Brüning, F. Zimmermann, C. Vetter, M. Gräfe, M. Heinrich, S. Nolte, M. Duparré, A. Aiello, M. Ornigotti, and A. Szameit, "Demonstration of local teleportation using classical entanglement," Laser Photon. Rev. **10**, 317 (2016).

[17] U. Alvarez-Rodriguez, A. Perez-Leija, I. L. Egusquiza, M. Gräfe, M. Sanz, L. Lamata, A. Szameit, and E. Solano, "Advanced-Retarded Differential Equations in Quantum Photonic Systems," Sci. Rep. **7**, 42933 (2017).

[18] K. Poulios, R. Keil, D. Fry, J. D. A. Meinecke, J. C. F. Matthews, A. Politi, M. Lobino, M. Gräfe, M. Heinrich, S. Nolte, A. Szameit, and J. L. O'Brien, "Quantum walks of correlated photon pairs in two-dimensional waveguide arrays," Phys. Rev. Lett. **112**, 143604 (2014).

[19] S. Minardi, F. Dreisow, M. Gräfe, S. Nolte, and T. Pertsch,"Three-dimensional photonic component for multichannel coherence measurements," Opt. Lett. **37**, 3030 (2012).

[20] A. Perez-Leija*, D. Guzman-Silva*, R. de J. León-Montiel*, M. Gräfe, M. Heinrich, H. Moya-Cessa, K. Busch, and A. Szameit, "Endurance of Quantum Coherence in Born-Markov Open Quantum Systems," in preparation (2017).

[21] M. Gräfe, D. A. Antonosyan, A. S. Solntsev, A Szameit, and A. A. Sukhorukov, "Optical emulation of photon-pair generation in nonlinear lossy waveguides," in preparation (2017).

[22] A. Perez-Leija, M. Gräfe, K. Busch, and A. Szameit, "Evolution equation and density matrix of two-photon light in tight-binding waveguide lattices," in preparation (2017).

[23] M. Gräfe and A. Szameit, "Quantum Correlations of N Indistinguishable Particles," in preparation (2017).

[24] J. Titchener, M. Gräfe, R. Heilmann, A. S. Solntsev, A Szameit, and A. A. Sukhorukov, "Scalable on-chip quantum state tomography," in preparation (2017).

*equally contributed

Conference contributions

Invited contributions

[1] M. Gräfe, A. Perez-Leija, M. Lebugle, S. Weimann, R. Heilmann, and A. Szameit, "Photonic Quantum Walks in Waveguide Lattices," PIERS, Shanghai, China, (2016)

[2] M. Gräfe, R. Heilmann, A. Perez-Leija, M. Lebugle, D. Guzman-Silva, M. Heinrich, S. Nolte, A. Szameit, "Integrated laser-written quantum photonics," SPIE Optics + Photonics, San Diego, USA, (2015)

[3] M. Gräfe, R. Heilmann, A. Perez-Leija, M. Lebugle, R. Keil, M. Heinrich, S. Nolte, D. N. Christodoulides, and A. Szameit, "Quantum Random Walks in Photonic Lattices," workshop on Quantum Simulations, Benasque, Spain, (2015)

[4] M. Gräfe, R. Heilmann, A. Perez-Leija, S. Nolte, and A. Szameit, "Fs-laser-written integrated photonic quantum circuits," 23rd Congress of the International Commission for Optics (ICO 23), Santiago de Compostela, Spain, (2014)

Regular contributions

[5–7] M. Gräfe, A. Perez-Leija, M. Lebugle, S. Weimann, R. Heilmann, D. Guzman-Silva, M. Heinrich, R. Keil, R. de J. León-Montiel, K. Busch, S. Nolte, G. Weihs, D. N. Christodoulides, and A. Szameit, "Quantum Walks in Laser-written

Integrated Photonic Structures: Part I - III," PIERS, St. Petersburg, Russia, (2017)

[8] M. Gräfe, M. Lebugle, A. Perez-Leija, R. Heilmann, S. Nolte, and A. Szameit, "Quantum Bloch Oscillations of N00N states," Discrete, Nonlinear and Disordered Optics (DINDOS), Dresden, Germany (2017)

[9] M. Gräfe, M. Lebugle, A. Perez-Leija, R. Heilmann, S. Nolte, and A. Szameit, "Quantum Bloch Oscillations of N00N states," Quantum Information and Measurement (QIM) - IV: Quantum Technologies, paper QF6C.4, Paris, France (2017)

[10] M. Gräfe, S. Weimann, A. Perez-Leija, M. Lebugle, R. Keil, R. Heilmann, S. Nolte, G. Weihs, D. N. Christodoulides, and A. Szameit, "Implementation of quantum discrete fractional Fourier transform," Quantum Information and Measurement (QIM) - IV: Quantum Technologies, paper QW6B.4, Paris, France (2017)

[11] M. Gräfe, R. Heilmann, J. Sperling, A. Perez-Leija, M. Heinrich, S. Nolte, W. Vogel, and A. Szameit, "Divide & Conquer: genuine characterization of light states by click detectors," Quantum Information and Measurement (QIM) - IV: Quantum Technologies, paper QT6A.6, Paris, France (2017)

[12] M. Gräfe, D. A. Antonosyan, A. S. Solntsev, A. Szameit, A. A. Sukhorukov, "Photon-pair generation in nonlinear lossy waveguides: An optical emulation," CLEO QELS Conference, paper FTh4A.2, San Jose, USA (2016)

[13] M. Gräfe, R. Heilmann, S. Nolte, and A. Szameit, "Integrated-photonic generation of general EPR-states," CLEO QELS Conference, paper JW2A.14, San Jose, USA (2015)

[14] M. Lebugle, M. Gräfe, A. Perez-Leija, R. Heilmann, S. Nolte, and A. Szameit, "Bloch Oscillations of Einstein-Podolsky-Rosen States," CLEO QELS Conference, paper FTh4D.2, San Jose, USA (2015)

[15] M. Gräfe, R. Heilmann, A. Perez-Leija, R. Keil, F. Dreisow, M. Heinrich, S. Nolte, D. N. Christodoulides, and A. Szameit, "High-order W-states for

random number generation," CLEO EUROPE/IQEC, paper EA_1_3, Munich, Germany (2015)

[16] M. Gräfe, R. Heilmann, R. Keil, S. Nolte, and A. Szameit, "Generation of general EPR-states on-chip ," CLEO EUROPE/IQEC, paper EB_P_1, Munich, Germany (2015)

[17] M. Lebugle, M. Gräfe, A. Perez-Leija, R. Heilmann, S. Nolte, and A. Szameit, "Bloch Oscillations of Einstein-Podolsky-Rosen States," CLEO EUROPE/IQEC, paper JSV_3_3, Munich, Germany (2015)

[18] M. Gräfe, M. Lebugle, R. Heilmann, A. Perez-Leija, S. Nolte, and A. Szameit, "Bloch Oscillations of two-photon EPR States with arbitrary exchange symmetry," 586. WE-Heraeus-Seminar on Quantum Correlations beyond Entanglement, Bad Honnef, Germany, (2015)

[19] M. Gräfe, R. Heilmann, A. Perez-Leija, R. Keil, F. Dreisow, M. Heinrich, S. Nolte, D. N. Christodoulides, and A. Szameit, "Single-Photon W-states of High-Order for Random Number Generation," Quantum Information and Measurement (QIM), paper QTh1A.4, Berlin, Germany (2014)

[20] M. Gräfe, R. Heilmann, A. Perez-Leija, R. Keil, F. Dreisow, M. Heinrich, S. Nolte, D. N. Christodoulides, and A. Szameit, "High-Order Photonic W-states for Random Number Generation," 45th Annual Meeting of the APS Division of Atomic, Molecular and Optical Physics (DAMOP), Madison, USA (2014)

[21] M. Gräfe, R. Heilmann, A. Perez-Leija, R. Keil, F. Dreisow, M. Heinrich, S. Nolte, D. N. Christodoulides, and A. Szameit, "High-Order Single-Photon W-states for Random Number Generation," CLEO QELS Conference, paper JTu4A.36, San Jose, USA (2014)

[22] M. Gräfe, R. Heilmann, A. Perez-Leija, R. Keil, F. Dreisow, M. Heinrich, S. Nolte, D. N. Christodoulides, and A. Szameit, "High-Order Single-Photon W-states for Random Number Generation," 553. WE-Heraeus-Seminar on Discrete and Analogue Quantum Simulators, Bad Honnef, Germany, (2014)

[23] M. Gräfe, R. Heilmann, R. Keil, T. Eichelkraut, M. Heinrich, S. Nolte, and A. Szameit, "Indistinguishable particles and their correlations in non-Hermitian lattices," CLEO QELS Conference, paper JTh2A.74, San Jose, USA (2013)

[24] A. Perez-Leija, M. Gräfe, J. C. Hernandez-Herrejon, H. Moya-Cessa, A. Szameit, and D. N. Christodoulides, "Generation of multipartite single photon W states in waveguide lattices," CLEO QELS Conference, paper QM1E.6, San Jose, USA (2013)

[25] M. Gräfe, A. S. Solntsev, R. Keil, A. Tünnermann, S. Nolte, A. A. Sukhorukov, Y. S. Kivshar, and A. Szameit, "Photon pair generation in quadratic waveguide arrays: A classical optical simulation," CLEO EUROPE/IQEC, Munich, paper IA_P_13, Germany (2013)

[26] M. Gräfe, R. Heilmann, R. Keil, T. Eichelkraut, M. Heinrich, S. Nolte, and A. Szameit, "Indistinguishable particles in non-Hermitian lattices and their correlations," CLEO EUROPE/IQEC, paper IA_P_24, Munich, Germany (2013)

[27] M. Gräfe, A. S. Solntsev, R. Keil, A. Tünnermann, S. Nolte, A. A. Sukhorukov, Y. S. Kivshar, and A. Szameit, "Classical Optical Simulation of Bi-Photon Generation in Quadratic Waveguide Arrays," CLEO QELS Conference, paper NW2D.2, San Jose, USA (2012)

[28] M. Gräfe, A. S. Solntsev, R. Keil, A. Tünnermann, S. Nolte, A. A. Sukhorukov, Y. S. Kivshar, and A. Szameit, "Biphoton generation in quadratic waveguide arrays: A classical optical simulation," 518. WE-Heraeus-Seminar on Quantum Optical Analogies: a Bridge between Classical and Quantum Physics, Bad Honnef, Germany, (2012)

Ehrenwörtliche Erklärung

Ich erkläre hiermit ehrenwörtlich, dass ich die vorliegende Arbeit selbständig, ohne unzulässige Hilfe Dritter und ohne Benutzung anderer als der angegebenen Hilfsmittel und Literatur angefertigt habe. Die aus anderen Quellen direkt oder indirekt übernommenen Daten und Konzepte sind unter Angabe der Quellen gekennzeichnet.

Bei der Auswahl und Auswertung des folgenden Materials haben mir die nachstehend aufgeführten Personen in der jeweils beschriebenen Weise unentgeltlich geholfen:

1. Die Auswertung der statistischen Test des *National Institute of Standards and Technology* in Tab. 3.1 wurde von Armando Perez-Leija, Friedrich-Schiller-Universität Jena, durchgeführt.

2. Das theoretische Modell des Q_B-Parameters wurde von Jan Sperling, Universität Rostock, eingeführt und die Aufnahme der experimentellen Daten für Abb. 4.4 wurden zusammen mit René Heilmann, Friedrich-Schiller-Universität Jena, gewonnen.

3. Die Messungen der Photonen-Koinzidenzen in Abb. 5.7, 5.8 & 5.9 wurden zusammen mit Maxime Lebugle, Friedrich-Schiller-Universität Jena, vorgenommen.

Weitere Personen waren an der inhaltlich-materiellen Erstellung der vorliegenden Arbeit nicht beteiligt. Insbesondere habe ich hierfür nicht die entgeltliche

Hilfe von Vermittlungs bzw. Beratungsdiensten (Promotionsberater oder anderen Personen) in Anspruch genommen. Niemand hat von mir unmittelbar oder mittelbar geldwerte Leistungen für Arbeiten erhalten, die im Zusammenhang mit dem Inhalt der vorgelegten Dissertation stehen.

Teile dieser Arbeit wurden aus Prioritätsgründen bereits veröffentlicht oder zur Veröffentlichung eingereicht [32, 34, 81, 101, 108, 113].

Die Arbeit wurde bisher weder im In- noch im Ausland in gleicher oder ähnlicher Form einer anderen Prüfungsbehörde vorgelegt.

Die geltende Promotionsordnung der Physikalisch-Astronomischen Fakultät ist mir bekannt.

Ich versichere ehrenwörtlich, dass ich nach bestem Wissen die reine Wahrheit gesagt und nichts verschwiegen habe.

Jena, den 27.07.2017 Markus Gräfe